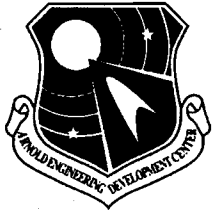


**AEDC TR-95-28**



## **Arc Heater Manifold Evaluation**

D. D. Horn, W. E. Bruce, III, E. J. Felderman, and G. R. Beitel  
Micro Craft Technology/AEDC Operations

May 1996

Final Report for Period August 1993 — September 1995

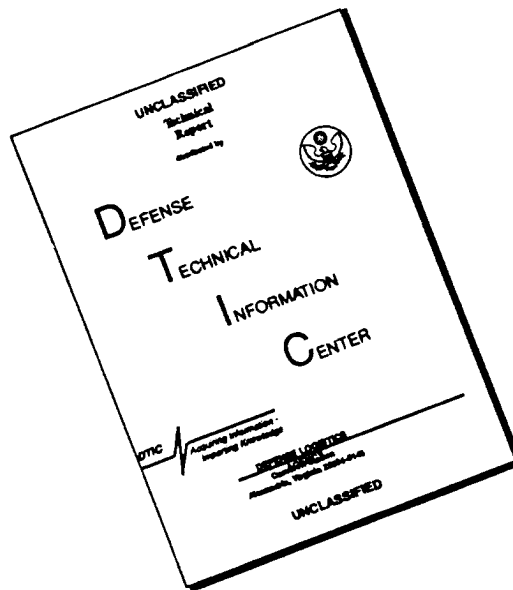
Approved for public release; distribution is unlimited.

19960607 131

**ARNOLD ENGINEERING DEVELOPMENT CENTER  
ARNOLD AIR FORCE BASE, TENNESSEE  
AIR FORCE MATERIEL COMMAND  
UNITED STATES AIR FORCE**

**DTIC QUALITY INSPECTED 3**

# DISCLAIMER NOTICE



THIS DOCUMENT IS BEST QUALITY AVAILABLE. THE COPY FURNISHED TO DTIC CONTAINED A SIGNIFICANT NUMBER OF PAGES WHICH DO NOT REPRODUCE LEGIBLY.

## NOTICES

When U. S. Government drawings, specifications, or other data are used for any purpose other than a definitely related Government procurement operation, the Government thereby incurs no responsibility nor any obligation whatsoever, and the fact that the Government may have formulated, furnished, or in any way supplied the said drawings, specifications, or other data, is not to be regarded by implication or otherwise, or in any manner licensing the holder or any other person or corporation, or conveying any rights or permission to manufacture, use, or sell any patented invention that may in any way be related thereto.

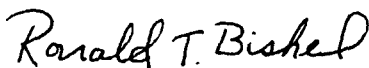
Qualified users may obtain copies of this report from the Defense Technical Information Center.

References to named commercial products in this report are not to be considered in any sense as an endorsement of the product by the United States Air Force or the Government.

This report has been reviewed by the Office of Public Affairs (PA) and is releasable to the National Technical Information Service (NTIS). At NTIS, it will be available to the general public, including foreign nations.

## APPROVAL STATEMENT

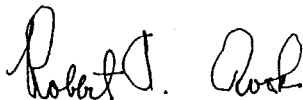
This report has been reviewed and approved.



RONALD T. BISHEL  
Facility Dynamics Technology  
Applied Technology Division  
Test Operations Directorate

Approved for publication:

FOR THE COMMANDER



ROBERT T. CROOK  
Asst. Chief, Applied Technology Division  
Test Operations Directorate

REPORT DOCUMENTATION PAGE			Form Approved OMB No. 0704-0188	
Public reporting burden for this collection of information is estimated to average 1 hour per response, including the time for reviewing instructions, searching existing data sources, gathering and maintaining the data needed, and completing and reviewing the collection of information. Send comments regarding this burden estimate or any other aspect of this collection of information, including suggestions for reducing this burden, to Washington Headquarters Services, Directorate for Information Operations and Reports, 1215 Jefferson Davis Highway, Suite 1204, Arlington, VA 22202-4302, and to the Office of Management and Budget, Paperwork Reduction Project (0704-0188), Washington, DC 20503.				
1. AGENCY USE ONLY (Leave blank)		2. REPORT DATE May 1996		3. REPORT TYPE AND DATES COVERED Final Report for Period August 1993 - September 1995
4. TITLE AND SUBTITLE Arc Heater Manifold Evaluation			5. FUNDING NUMBERS PN - 1613 PE - 65807F	
6. AUTHOR(S) Horn, D. D., Bruce, W. E., III, Felderman, E. J., and Beitel, G. R., Micro Craft Technology/AEDC Operations				
7. PERFORMING ORGANIZATION NAME(S) AND ADDRESS(ES) Arnold Engineering Development Center/DOT Air Force Materiel Command Arnold Air Force Base, TN 37389-9011			8. PERFORMING ORGANIZATION (REPORT NUMBER) AEDC-TR-95-28	
9. SPONSORING/MONITORING AGENCY NAME(S) AND ADDRESS(ES) Arnold Engineering Development Center/DOT Air Force Materiel Command Arnold Air Force Base, TN 37389-9011			10. SPONSORING/MONITORING AGENCY REPORT NUMBER	
11. SUPPLEMENTARY NOTES Available in Defense Technical Information Center (DTIC).				
12A. DISTRIBUTION/AVAILABILITY STATEMENT Approved for public release; distribution is unlimited.			12B. DISTRIBUTION CODE	
13. ABSTRACT (Maximum 200 words)  Arc heaters are required to provide the high pressure and temperature test conditions necessary to meet critical testing needs for propulsion, materials, and structures. Two configurations can produce the high-power arc heater capability required: a single large arc or a multi-arc configuration based on manifolding a number of smaller heaters into a common plenum. Such multi-arc configurations can be a convenient route to high-power heaters (on the order of 200-300 MW), but at the cost of reduced performance because of additional wall cooling losses. A multi-arc configuration may be an effective way to improve flow uniformity of both enthalpy and pressure. The mixing of effluents of separate arc heaters in a single plenum may dampen flow-field fluctuations because oscillations in the individual arc units will probably be totally independent. Experiments were performed to assess the effect of manifolding arc heaters into a single plenum on flow quality and heater efficiency. A reduction in enthalpy of approximately 7 percent was attributed to the manifold. The reduction in enthalpy is caused by the additional wall losses in the manifold. Fluctuations in the flow were slightly better for the multi-arc configuration (compared to a single heater), primarily because of smaller fluctuations in the pressure. Heat flux fluctuations for the multi-arc system were nearly the same as for a single-arc heater.				
14. SUBJECT TERMS arc heaters, high enthalpy, manifold, test facilities, high pressure, plasma arc heater			15. NUMBER OF PAGES 104	
			16. PRICE CODE	
17. SECURITY CLASSIFICATION OF REPORT UNCLASSIFIED	18. SECURITY CLASSIFICATION OF THIS PAGE UNCLASSIFIED	19. SECURITY CLASSIFICATION OF ABSTRACT UNCLASSIFIED	20. LIMITATION OF ABSTRACT SAME AS REPORT	

## PREFACE

The work reported herein was performed by Arnold Engineering Development Center (AEDC), Air Force Materiel Command (AFMC), under Program Element 65807F. The Air Force Program Managers were Capt. P. L. Zeman and R. T. Bishel, DOT. The work was performed by Micro Craft Technology, technical services contractor for the aerospace flight dynamics testing effort at AEDC, AFMC, Arnold Air Force Base, TN. The work was performed in the Technology and Development Facility, Facility Technology Department, under AEDC Project Number 1613. The work was sponsored by the Foreign Comparative Testing (FCT) Program under Program Element 65130D for the period August 30, 1993 through September 30, 1995. The arc heater manifold tests were performed at Aerospatiale, Aquitaine Plant, Plasma Test Laboratory, located in Saint-Medard-en-Jalles (northwest of Bordeaux), France.

The authors gratefully acknowledge the cooperation and support of the Aerospatiale test team, including Mr. Yves Valy, Mr. Jean Boitaud, Mr. Rene Leroux, Ms. Martine Cadre, Mr. Maxime Labrot, Mr. Jean-Paul Spieldenner, Mr. Philippe Pradet, Mr. Christian Pitt, Mr. Jean Louis Maubert, Mr. Dominique Conte, Mr. Philippe Donnart, Mr. Alain Gerbeau, Mr. Philippe Plet, Mr. Marcel Vincent, and Mr. Daniel Loubet.

## CONTENTS

	<u>Page</u>
1.0 INTRODUCTION .....	7
2.0 APPARATUS .....	8
2.1 HP Facility .....	8
2.2 JP-200 Facility .....	10
2.3 Arc Heater Comparison .....	14
3.0 TEST SUMMARY .....	14
3.1 HP Test Entry .....	14
3.2 JP-200 Test Entry .....	15
4.0 JP-200 OPERATIONAL OBSERVATIONS .....	17
5.0 PERFORMANCE AND THERMAL EFFICIENCY .....	18
5.1 Arc Heater .....	19
5.2 Manifold .....	19
5.3 Nozzle .....	20
5.4 Overall Performance .....	21
6.0 FLOW QUALITY EVALUATION .....	21
6.1 Data Validation .....	22
6.2 Flow Quality .....	23
7.0 CONCLUSIONS .....	26
REFERENCES .....	28

## ILLUSTRATIONS

<u>Figure</u>	<u>Page</u>
1. HP Arc Heater Facility .....	29
2. HP Arc Heater .....	30
3. HP and JP-200 Magnetic Coil Design .....	31
4. HP and JP-200 Magnetic Coil Axial Location .....	32
5. HP Air Injector Locations and Diameters .....	32
6. Details of the Nozzle-Pressure Ring-Cathode Interfaces .....	33
7. HP Nozzle, $A^* = 1.25 \text{ cm}^2$ .....	34
8. Pitot Pressure Probe .....	35
9. Heat Flux Probe .....	35
10. Schematic of HP Cooling Water System .....	36
11. JP-200 Arc Heater Facility .....	37
12. JP-200 Heater Locations .....	38
13. JP-200 Arc Heater .....	39
14. JP-200 Air Injector Locations and Diameters .....	40
15. Assembly View of Arc Heater, Manifold, Pressure Ring, and Nozzle .....	41
16. JP-200 Nozzle, $A^* = 5.0 \text{ cm}^2$ .....	42

<u>Figure</u>	<u>Page</u>
17. JP-200 Nozzle, $A^* = 2.5 \text{ cm}^2$ . . . . .	43
18. Manifold Liner Dimensions . . . . .	44
19. JP-200 Water Cooling System for Runs 1506 and 1507 . . . . .	47
20. JP-200 Cooling Water System for Runs 1508 through 1517 . . . . .	48
21. JP-200 High-Pressure Air System . . . . .	49
22. Heater Geometry Comparison . . . . .	50
23. Individual Arc Heater Performance at Cathode Exit . . . . .	51
24. JP-200 Manifold Thermal Loss Relative to the Total Loss . . . . .	52
25. JP-200 Manifold Thermal Loss Relative to the Power in the Gas Entering the Manifold . . . . .	53
26. JP-200 Percent Reduction in Enthalpy Attributed to the Manifold (And Other Related Hardware) . . . . .	54
27. Nozzle Thermal Loss Relative to the Total Loss . . . . .	55
28. Nozzle Thermal Loss Relative to the Power in the Gas Entering the Nozzle . . . . .	56
29. Percent Reduction in Enthalpy Attributed to the Nozzle . . . . .	57
30. Pitot Pressure Probe Data for HP Run 430 . . . . .	58
31. Pitot Pressure Probe Data for JP-200 Run 1513 . . . . .	59
32. Heat Flux Probe Data for HP Run 430 . . . . .	60
33. Heat Flux Probe Data for JP-200 Run 1513 . . . . .	61
34. Typical Pressure and Heat Flux Profiles . . . . .	62
35. Ratios of Integrated Probe Data Quantities to Measured Bulk Data Quantities (Solid Symbols Include Bluntness Correction) . . . . .	64
36. The Effect of a Flattened Nose on Stagnation Point Heat Transfer . . . . .	65
37. Profiles for Run HP430, Reverse Sweep; Mean Value $\pm$ One Standard Deviation Shown (Computed over $r = \pm 8 \text{ mm}$ ) . . . . .	66
38. Profiles for Run HP430, Reverse Sweep; Mean Value $\pm$ One Standard Deviation Shown (Computed over $r = \pm 20 \text{ mm}$ ) . . . . .	71
39. Standard Deviation Expressed as a Fraction of the Parameter; Pressure, $\sigma_p/P_o$ , and Heat Flux, $\sigma Q/Q$ . . . . .	76
40. Velocity Fluctuations (Standard Deviation) Compared with the Implied Turbulence Based on the Measured Enthalpy Enhancement . . . . .	77
41. Velocity Profile in the Multi-Arc Configuration . . . . .	78
42. Heat Flux/Voltage Comparison . . . . .	79
43. Heat Flux/Total Voltage Comparison . . . . .	83
44. Fast Fourier Transform of Pitot Pressure Data . . . . .	84
45. Pitot Pressure Signal Processing . . . . .	85
46. Pitot Pressure/Arc Voltage Comparison . . . . .	86
47. Heat Flux Profile, Run 1509, Forward Sweep; Heaters 1,3,4 Hot, Heater 2 Cold . . . . .	91
48. Heat Flux Profile, Run 1512, Forward Sweep; Heaters 1,3 Hot, Heaters 2,4 Cold . . . . .	92

## TABLES

<u>Table</u>	<u>Page</u>
1. HP Instrumentation .....	93
2. JP-200 Instrumentation .....	94
3. Surface Area of HP and JP-200 Arc Heater Facilities Exposed to Hot Gas .....	95
4. HP and JP-200 Run Matrix .....	95
5. Anode Arc Attachment Locations .....	96
6. Electrode Mass Loss.....	96
7. Analysis of Individual Arc Heater Performance (At End of Cathode) .....	97
8. JP-200 Manifold Performance and Thermal Efficiency .....	98
9. Nozzle Performance and Thermal Efficiency .....	98
10. Overall Arc Heater Performance and Thermal Loss .....	99

## APPENDIX

A. SURFACE AREA OF HP AND JP-200 ARC HEATER FACILITIES EXPOSED TO HOT GAS .....	101
--	-----



## 1.0 INTRODUCTION

Critical needs for propulsion, materials, and structures testing dictate high pressures and temperatures not attainable by conventional means. Arc heaters are required to provide the extreme test conditions necessary to meet these critical testing needs. Two configurations can produce the high-power arc heater capability required: a single large arc or a multi-arc configuration based on manifolding a number of smaller heaters into a common plenum. Such multi-arc configurations can be a convenient route to high-power heaters (approximately 200 to 400 MW), but at the cost of reduced performance because of additional wall cooling losses. A multi-arc configuration may be an effective way to improve flow uniformity of both enthalpy and pressure. The mixing of the effluents of separate arc heaters in a single plenum may dampen flow-field fluctuations because oscillations in the individual arc units will probably be totally independent.

Experiments were performed to assess the effect of manifolding arc heaters into a single plenum on flow quality and heater efficiency. The flow-field steadiness and pressure and heat flux profiles were quantified for various arc heater manifold configurations. The overall heater and manifold thermal efficiency, along with the manifold mixing efficiency, were also evaluated. The acquired data were necessary to determine if manifolding arc heaters is a viable option for a driver of a large hypersonic facility.

The manifold experiments were performed at the Aerospatiale test facilities located near Bordeaux, France. Aerospatiale has a state-of-the-art arc heater manifold system which has been in operation since 1979 and is the only manifold arc heater facility currently in operation. The JP-200 system comprises four 5-MW Huels-type arc heaters manifolded into a single plenum. The Aerospatiale facility is very attractive to use for manifold experiments because the JP-200 is a mature system with a history of reliable operation. A single-arc heater, similar to one of the JP-200 arc heaters, is also available at Aerospatiale. The single heater was used to establish baseline flow-field and heater performance. The multi-arc system performance was then compared to the single-arc heater performance to evaluate the improvement in flow-field fluctuations and profile. The overall performance of the single-arc and the multi-arc systems was also evaluated, along with the mixing efficiency of the manifold system.

## 2.0 APPARATUS

Aerospatiale Aquitaine is located in Saint-Medard-en-Jalles, France, 15 km northwest of Bordeaux. The Aquitaine plant employs approximately 1,700 people whose primary activities are devoted to the development of missile systems for the French Strategic Nuclear Force and European Space Agency programs. The plant specializes in developing high-temperature composite materials and providing test facilities to evaluate the materials.

Four large arc facilities (5-20 MW) are located in the Aquitaine plant's plasma test laboratory. Three of these facilities utilize Huels-type heaters, and the remaining facility uses the segmented-type heater. The two heaters used in the manifold evaluation test effort are the HP single-arc heater and the JP-200 multi-arc system. Each of these two facilities is described in detail below.

## 2.1 HP FACILITY

The HP facility (Fig. 1) uses a single 9-MW Huels-type arc heater to heat air and expand the flow to a supersonic free jet in the atmospheric environment of the test building. The HP facility is primarily used for high-pressure testing, generating plasma flows with a total pressure up to 130 bar with run times up to 60 sec. It has been in operation for approximately 6 years, mainly supporting military programs.

### 2.1.1 Arc Heater

The HP arc heater is shown in Fig. 2. The 9-MW Huels-type arc heater consists of two tubular electrodes separated by an air injection chamber. A coil is installed around the upstream electrode to enhance arc rotation and attachment location.

**Upstream Electrode:** The upstream electrode is a 50-mm-ID, 450-mm-long anode. The electrode liner is made of copper and is backside water cooled.

**Magnetic Coil:** The magnetic coil around the upstream electrode is shown in Fig. 3. The coil consists of six rings with each ring consisting of two axial spirals and twenty radial spirals. Only the upstream three rings are powered. The inside diameter of the coil is 216 mm, and the outside diameter is 600 mm. The coil is positioned axially on the anode so that the upstream ring is 450 mm from the downstream lip of the electrode liner, as shown in Fig. 4.

**Air Injection Chamber:** The air injection chamber consists of 32 sonic air injection holes located on four axial rows around the outer wall of the chamber. The air injection hole locations are shown in Fig. 5. The holes are drilled at an angle to produce a swirl in the heater in a clockwise direction looking downstream. Twenty-six of the holes have a minimum injection diameter of 0.7 mm, and 6 holes have an injection diameter of 0.8 mm, giving a total air injection area of  $13.02 \text{ mm}^2$ . All of the 0.8-mm holes are located on the upstream row.

**Downstream Electrode:** The downstream electrode is the cathode which has an inside diameter of 35 mm and a inside length of 689 mm. The electrode liner is made of copper and is backside water cooled. The cathode is electrically grounded.

### 2.1.2 Pressure Ring and Nozzle

**Static Pressure Ring:** A ring is installed between the arc heater downstream electrode and the nozzle to permit a static pressure measurement, as shown in Figs. 2 and 6. The internal dimensions of the pressure ring are 70 mm in diameter and 12 mm long. Since the pressure ring diameter is twice the diameter of the cathode, there is a step change from the cathode to the pressure ring. Between the pressure ring and the nozzle is another step change to a larger diameter of 82 mm for a length of only 2 mm, as shown in Fig. 6. This space is machined into the upstream nozzle flange to create this gap. The purpose of this gap is unknown. The pressure ring cross-sectional area is 30.8 times the throat area, which should produce a low velocity at the pressure ring and provide a pressure measurement very close to the total pressure.

**Nozzle:** The HP nozzle was specially designed and fabricated for this test and is shown in Fig. 7. The detailed design specifications are presented in Ref. 1. The nozzle has a throat diameter of 12.6 mm and an exit diameter of 24.4 mm, which gives a Mach number of approximately 2.6 at the exit. The entrance diameter to the contoured portion of the nozzle is 40 mm.

### 2.1.3 Support Systems

**Model Injection System:** The HP facility has a rotary model injection system which can accommodate up to 8 probes or models. The three probes used for this test were installed on arms 2, 3, and 4 and were swept across the flow field at a rate of 1 m/sec. The radius of the arms (from the center of the probe to the model injection system axis of rotation) is 395 mm.

**Probes:** Three probes were used to evaluate the HP flow field; two pitot pressure probes and one heat flux probe. The two pressure probes were installed on the model injection system arms 2 and 4 while the heat flux probe was installed between the two pressure probes on arm 3. The probes are swept through the flow twice during the run, forward and then reverse. The first probe enters the flow on arm 2 approximately 9 sec after start-up, with the probes on arms 3 and 4 being swept through the flow at 12 and 15 sec, respectively. The reverse sweep starts with the probe on arm 4 entering the flow at 22 sec into the run, followed by the probes on arms 3 and 2 at 25 and 27 sec, respectively. The probes were swept through the center of the nozzle flow at an axial location no more than 5 mm downstream from the nozzle exit.

The two pressure probes provided by Aerospatiale are designed as shown in Fig. 8 and use Kistler® 601-A piezoelectric transducers. A tube 1 mm in diameter and 72 mm long leads from the probe tip to a cavity with a volume of 24 mm<sup>3</sup> in front of the transducer. Aerospatiale calculated the frequency response of the probe to be 450 Hz. Pressure probe response and instrumentation details are available in Refs. 2 and 3.

The heat flux probe is a sphere-cone null point calorimeter with a nose radius of 3.8 mm and a cone half-angle of 15 deg as shown in Fig. 9. The probe was fabricated at AEDC to Aerospatiale specifications using a Chromel®-Alumel (type K) thermocouple. The measured time response of the probe was between 1 and 2 msec. Two parameters are recorded versus time from the heat flux probe: (1) temperature, using a fifth-order polynomial for type K thermocouples, and (2) heat flux, using an analog signal processor which solves the one-dimensional heat conduction equation for the measured temperature history of the probe.

**Cooling Water System:** Each component of the HP arc heater is individually water cooled by a closed-loop cooling water system. The water flow rate and temperature rise for each component are recorded, which allows the calculation of an energy loss for each component. There are five separate cooling water circuits on the HP heater: upstream electrode, coil, air injection chamber, downstream electrode, and nozzle, as shown in Fig. 10. The pressure ring does not have a separate circuit, but is included with the downstream electrode.

The inlet water pressure is maintained around 70 to 80 bar with a total flow rate through the heater, not including the coil, of 54.1 l/sec. The coil water flow rate and temperature rise were

not recorded for this study, since the coil is powered by a separate power supply and was not included in the energy balance. The inlet pressure for each circuit is measured downstream of the valve (see Fig. 10).

The water flow rate is determined using an orifice plate located on the downstream side of the heater. The pressure differential is measured across the orifice, and the water flow rate is calculated from knowledge of the orifice geometry.

The water temperature rise is determined using copper-constantan thermocouples configured for a temperature difference measurement. The thermocouples are located on the inlet and outlet sides of each flow circuit and electrically connected to measure the water temperature rise.

**High-Pressure Air System:** A 400-bar high-pressure air system is used to supply approximately 440 gm/sec of air to the HP heater to achieve the desired test conditions. A pressure of 120 bar at the heater air injectors is required to meet sonic flow conditions through the injectors. The air flow rate is determined using an orifice plate and measuring the differential pressure across the orifice. The air temperature and pressure are also measured to use in the flow rate calculation.

**Instrumentation:** Instrumentation used on the HP test is presented in Table 1. Reference 3 provides additional information on the types of sensors used to make each measurement, along with signal conditioning requirements, calibration, and instrumentation accuracy.

**Data Acquisition:** Data were recorded at two different rates, 10 Hz and 5 kHz. All of the data were recorded versus time with time equal to zero set approximately 3 sec prior to arc initiation. The parameters recorded at a rate of 10 Hz (data point every 0.1 sec) are arc voltage, arc current, chamber pressure (anode location), static pressure (pressure ring location), upstream electrode cooling water temperature rise, downstream electrode cooling water temperature rise, air injection chamber cooling water temperature rise, nozzle cooling water temperature rise, upstream electrode water flow rate, downstream electrode water flow rate, air injection chamber water flow rate, nozzle water flow rate, air flow rate, and aerodynamic (calculated) total enthalpy. The parameters recorded at 5 kHz (data point every 0.0002 sec) are arc voltage, chamber pressure (anode location), static pressure (pressure ring location), pitot pressure probe on arm 2, pitot pressure probe on arm 4, temperature of the heat flux probe, heat flux evaluated by the analog signal processor, and location of the model injection system. The data were delivered to AEDC on a floppy disk in ASCII format and are plotted and summarized in Ref. 2.

## 2.2 JP-200 FACILITY

The JP-200 facility uses four 5-MW, Huels-type arc heaters manifolded into a single plenum to create high-enthalpy mass flows up to 2 kg/sec. The four heaters are located 90 deg apart so as to look like a vertical cross, with the flow exiting through a single nozzle perpendicular to the plane of the arc heaters. Pressures up to 60 bar with run times up to 60 sec are possible. The JP-200 facility is shown during a run, without the model injection system installed, in Fig. 11. This facility has been used since 1979, mainly for military programs.

The four arc heaters are each assigned a number for reference purposes. The numbering sequence for the heaters is shown in Fig. 12a, with heater number one located at the top and continuing in a counterclockwise direction, looking upstream, to heater number four on the right.

Each heater is powered by a separate module of the power supply with the cathodes of each heater grounded. The coils located around the anode of each heater are powered by a separate power supply.

### 2.2.1 Arc Heaters

The four arc heaters used in the JP-200 facility are identical and are very close in geometry to the HP arc heater. As shown in Fig. 13, a typical heater consists of two tubular electrodes separated by an air injection chamber with a coil installed around the upstream electrode to enhance arc rotation and attachment location.

**Upstream Electrode:** The upstream electrode is the anode which has an inside diameter of 68 mm and a length of 420 mm. The electrode liner is made of copper and is backside water cooled.

**Magnetic Coil:** The magnetic coil around the upstream electrode is shown in Fig. 3. The coil consists of four rings, with each ring consisting of two axial spirals and twenty radial spirals. Only the upstream three rings are powered. The inside diameter of the coil is 216 mm and the outside diameter is 600 mm. Only the three upstream coils are powered. The coil is positioned axially on the anode so that the upstream ring is 450 mm from the downstream lip of the electrode liner, as shown in Fig. 4.

**Air Injection Chamber:** The air injection chamber consists of 31 sonic air injection holes located on four axial rows around the outer wall of the chamber, as shown in Fig. 14. The holes are drilled at an angle to produce a swirl in the clockwise direction looking downstream. Twenty of the holes have a minimum injection diameter of 0.8 mm, and 11 holes have an injection diameter of 1.0 mm giving a total air injection area of  $18.69 \text{ mm}^2$ . One air injector is plugged because of a machining problem during fabrication.

**Downstream Electrode:** The downstream electrode is the cathode which has an inside diameter of 35 mm and a inside length of 650 mm. The electrode liner is made of copper and is backside water cooled. The cathode is electrically grounded.

### 2.2.2 Pressure Ring and Nozzle

**Static Pressure Ring:** A ring is installed between the manifold and the nozzle to permit a static pressure measurement as shown in Fig. 15. The internal dimensions of the pressure ring are 58 mm in diameter and 38 mm long, and its cross-sectional area ( $A = 26.42 \text{ cm}^2$ ) is only 5.3 times the throat area of the large nozzle ( $A^* = 5.0 \text{ cm}^2$ ) and 10.6 times the throat area of the small nozzle ( $A^* = 2.5 \text{ cm}^2$ ). This means that the velocity through the pressure ring will be too high to produce a static pressure measurement which will accurately represent the total pressure.

**Nozzle:** The two nozzles shown in Fig. 16 and 17 were specially designed and fabricated for the JP-200 arc heater for this test. The detailed design specifications are presented in Ref. 1. The larger nozzle (Fig. 16) has a throat diameter of 25.20 mm ( $A^* = 5.0 \text{ cm}^2$ ) with an exit diameter of 48.80 mm and an entrance diameter of 58 mm. The smaller nozzle has a throat diameter of 17.84 mm ( $A^* = 2.5 \text{ cm}^2$ ) with an exit diameter of 34.56 mm and an entrance diameter of 58 mm. Both nozzles have a Mach number of approximately 2.6 at the exit.

### 2.2.3 Manifold

The manifold is used to channel the flow from the four arc heaters to a single nozzle. The manifold liner is shown in an assembly view in Fig. 15 with one of the four arc heaters, the pressure ring, and nozzle. The manifold liner dimensions are presented in Fig. 18. The manifold is made of copper which is backside water cooled and contained in a stainless steel cubical housing. All of the water connections are made from the rear of the housing (opposite of the nozzle). A pressure port is also available at the rear of the manifold but is not used because of operational problems with contamination obstructing the pressure port. The cooling water scheme for the manifold and the water blocks was not provided.

Compared to the nozzle throat, the cross-sectional area of the nozzle tube in the manifold is relatively small. The nozzle tube cross-sectional area is  $20.43 \text{ cm}^2$ , which is only four times the nozzle throat area of the large nozzle ( $A^* = 5 \text{ cm}^2$ ). The combined cross-sectional area of the four arc heater tubes is  $53.32 \text{ cm}^2$  (a single arc heater tube is  $13.33 \text{ cm}^2$ ). The nozzle tube diameter is made as small as possible, it appears, to reduce wall losses since the nozzle tube dictates the size of the manifold central sphere, as can be seen in Fig. 18. This manifold is designed to produce a high-enthalpy flow by minimizing wall losses. There is no attempt to provide a stilling chamber effect to dampen flow fluctuations by creating a large cavity at the central sphere because this would increase the wall losses and reduce the total enthalpy.

### 2.2.4 Support Systems

**Model Injection System:** The JP-200 facility uses a linear model injection system which can expose three probes to the flow. The model injection system has a sweep speed up to 1 m/sec, which was the sweep speed used for this test. However, the sweep speed is not constant because the carriage is accelerating slightly as the first probe enters the flow, and then slows down slightly as the probes traverse the flow field. This change in sweep speed is very slight and should have no effect on the data or results. The carriage's position is measured versus time and recorded on the high-speed data system. The model injection system sweeps horizontally across the flow field in front of the nozzle. The direction of the first sweep across the flow field (forward sweep) is from the heater 2 side (see Fig. 12) to the heater 4 side. The reverse sweep is in the direction from heater 4 to heater 2.

**Probes:** Three probes, which are the same probes that were used on the HP test, were used to evaluate the JP-200 flow field: two pitot pressure probes and one heat flux probe. The two pressure probes were installed on the model injection system positions 1 and 3, and the heat flux probe was installed between the two pressure probes on position 2. The probes are swept through

the flow twice during the run, forward and then reverse. The probes are positioned to sweep through the center of the nozzle flow at an axial location no more than 5 mm downstream from the nozzle exit. The probes are more fully detailed in the HP facility description in Section 2.1.3.

**Cooling Water System:** Each component of the JP-200 arc heater system is individually water cooled by a closed-loop cooling water system. The water flow rate and temperature rise for each component are recorded, which allows the calculation of an energy loss for each component. There are 12 separate cooling water circuits on the JP-200 system plus separate cooling water circuits for the coils from which data were not recorded for this test. The 12 circuits are four upstream electrode circuits, four downstream electrode circuits, two air injection chamber circuits (heaters 2 and 4 are in series and heaters 1 and 3 are in series), the manifold, and the nozzle. The pressure ring does not have a separate circuit, but is in series with the nozzle. Two different configurations on the manifold outlet were used, as shown in Figs. 19 and 20. The original configuration (Fig. 19) was used only for runs 1506 and 1507. After problems were discovered with the manifold temperature difference measurement, the water outlet configuration on the manifold was reconfigured for the remainder of the runs (Fig. 20) to improve response time and accuracy. For Run 1517, heaters 2 and 4 were disconnected and flanges were placed over the manifold where the heaters were connected. The cooling water, which would have been used for the air injection chambers on heaters 2 and 4, was used to cool the two flanges, F2 and F4, shown in Fig. 20.

The water flow rate through each circuit is determined using an orifice plate located on the downstream side of the heater. The pressure differential is measured across the orifice and the water flow rate is calculated through knowledge of the orifice geometry.

The water temperature rise is determined using platinum resistance probes configured for a temperature difference measurement. A resistance probe is located on the inlet and outlet side of each circuit, and they are electrically connected to measure the water temperature rise directly.

**High-Pressure Air System:** A 420-bar high-pressure air system is used to supply air to all four heaters, as shown in Fig. 21. A separate pressure regulator controls the flow rate to each heater. The air flow rate to each heater is determined by measuring the differential pressure across an orifice plate. The air temperature and pressure are also measured for use in the flow rate calculation.

**Instrumentation:** Instrumentation used on the JP-200 test is presented in Table 2. Reference 4 provides additional information on the types of sensors used to make each measurement, along with signal conditioning requirements, calibration, and accuracy of the instrumentation.

**Data Acquisition:** Data were recorded at two different rates, 10 Hz and 5 kHz. All of the data are recorded versus time, with time equals zero set approximately 3 sec prior to arc initiation. The parameters recorded at the 10-Hz rate (data point every 0.1 sec) for each heater are arc voltage, arc current, chamber pressure (anode location), upstream electrode cooling water temperature rise, downstream electrode cooling water temperature rise, air injection chamber cooling water temperature rise (heaters 2 and 4 in series and heaters 1 and 3 in series), upstream elec-

trode water flow rate, downstream electrode water flow rate, air injection chamber water flow rate, and air flow rate. Additional parameters recorded at 10 Hz are manifold cooling water temperature rise, nozzle and pressure ring cooling water temperature rise, manifold cooling water flow rate, nozzle and pressure ring cooling water flow rate, static pressure (pressure ring location), and aerodynamic (calculated) total enthalpy.

The parameters recorded at a rate of 5 kHz (data point every 0.0002 sec) are arc voltage - each heater, chamber pressure - each heater (anode location), static pressure (pressure ring location), pitot pressure probe on position 2, pitot pressure probe on position 4, temperature of the heat flux probe, heat flux evaluated by the analog signal processor, and location of the model injection system. The data were delivered to AEDC on floppy disks in ASCII format and are plotted and summarized in Refs. 5, 6, and 7.

## 2.3 ARC HEATER COMPARISON

The HP arc heater is very close in design to the JP-200 heaters. Ideally, the heaters in the two facilities would be identical to eliminate any geometry variables. Although the heater geometries are similar, they are not identical. A schematic showing a comparison of the heater internal dimensions is presented in Fig. 22. From an inspection of Fig. 22 it is evident that the only dimension that is identical is the downstream electrode diameter. The coil geometries, locations relative to the anode, and field intensities are also identical (see Figs. 3 and 4). Although most of the dimensions are different, they are relatively minor and should not appreciably alter the results. The surface areas exposed to hot gas for the HP and JP-200 facilities are presented in Table 3, and the calculation methodology is presented in Appendix A.

## 3.0 TEST SUMMARY

Tests were performed in two arc facilities: the single-arc HP facility and the multi-arc JP-200 facility. The objectives of the tests were to evaluate heater and flow-field performance with a single arc heater, and then, using the same type heater, to compare the performance with a multi-arc manifold system. Tests were first performed in the single-arc HP facility to evaluate heater performance for a chamber pressure of  $60 \pm 2.5$  bar and a reduced enthalpy of  $74 \pm 10$  percent. Once an acceptable condition was achieved with the HP heater, the same condition was selected for all of the JP-200 runs. All of the data are presented in plot format in Refs. 2, 5, 6, and 7.

### 3.1 HP TEST ENTRY

Four runs were performed in the HP facility: three to evaluate heater performance (runs 429, 430, and 432), and one to evaluate heat flux probe performance (Run 431). The four runs were performed June 2 - June 6, 1994. AEDC representatives were not present to witness the HP test series. The HP test matrix is presented in Table 4.

The HP heater was operated at three different arc currents while the air mass flow was held constant at 440 gm/sec to evaluate heater performance. Run 429 was operated at a current of 1,446 amp, which produced a chamber pressure of 65.6 bar and an overall enthalpy,  $H/RT_0$  of



90, which were too high. The arc was blowing out the nozzle on Run 432 at a current of 863 amp, which was not acceptable. Run 430 met the pressure and enthalpy requirements at a current of 1,077 amp. Run 431 was performed at the same conditions as Run 430 to evaluate another heat-flux probe. Run 430 was used as the standard run by which all of the JP-200 data were compared.

The electrodes were inspected following the test series to determine the axial arc attachment location. The electrodes were also measured to determine the mass loss. Results of these measurements are presented in Tables 5 and 6. Arc attachment measurements were not made on the downstream electrode because it was hard to determine a location where the arc was predominantly running. From observations of the cathode, it appears that the arc was attaching primarily near the downstream end.

### 3.2 JP-200 TEST ENTRY

Twelve runs were performed in the JP-200 facility: six full-length runs and six short check runs. The runs were numbered sequentially from 1506 through 1517. The 12 runs were performed from October 4 through October 19, 1994. AEDC personnel witnessed all of the JP-200 runs and participated in pre-run planning and post-run analysis with Aerospatiale personnel. The JP-200 run matrix is presented in Table 4. The run matrix consists of five "matrix" runs which include runs with all four heaters hot, three heaters hot and one heater flowing cold air, two heaters hot and two heaters flowing cold air, two heaters hot and two heaters inactive, and two heaters hot and two heaters removed. Heaters 1 and 3 (see Fig. 12a) were hot for all runs with no configuration changes while changes were made on heaters 2 and 4. All of the changes were made to heaters 2 and 4 because the probes swept horizontally across the flow field in the direction from heater 2 to 4 and then from heater 4 to 2. If any asymmetry existed in the flow field from poor mixing during runs with cold air flow, inactive heaters, or heaters removed, then limiting the configuration changes to heaters 2 and 4 presented the best opportunity for the probes to detect any effect of these changes.

A check run of approximately 15 sec was performed prior to each "matrix" run except Run 1513 to evaluate the heater performance and setup. If the heater performance and setup were acceptable, a full-length energy balance run was performed.

Run 1507 was a full-length, 35-sec run with all four heaters operating. Problems were noticed on the manifold cooling water temperature difference measurement. The water temperature rise appeared to be too low. Following this run, the manifold cooling water configuration on the outlet side was modified to improve the temperature difference measurement (see Fig. 20). Run 1507, with the four heaters hot, was repeated as Run 1513.

Run 1509 was performed with heaters 1, 3, and 4 hot and heater 2 flowing cold air (no arc), which lowered the flow-field enthalpy. A "ringing" in the pitot pressure measurements was noticed on the data plots following the run. This phenomenon persisted for the remainder of the test series. During one of the check runs, the entrance tube on pitot probe number 2 was plugged to see if the ringing was caused by mechanical vibration. Probe 2 did not respond as it traversed

the flow field, and no oscillations or “ringing” were observed while pitot probe number 1 (tube not plugged) continued to exhibit the ringing characteristic. This experiment ruled out the possibility that the oscillations were vibration induced. The ringing appears to be related to the natural frequency of the probe cavity at lower flow-field enthalpies. The ringing was not severe and did not affect data analysis.

From an examination of the data on Run 1509, it appeared that the water temperature rise data were just reaching steady state at arc shutdown (35 sec). The run time was extended to 40 sec for the remainder of the energy balance runs (Runs 1512, 1513, 1515, and 1517) to ensure that the water temperature rise was complete.

Run 1512 was performed with heaters 1 and 3 hot and heaters 2 and 4 flowing cold air. The flow field was very dim and hard to see (could only see the flow field for approximately 10 cm downstream of the nozzle) compared to runs 1507 and 1513, where the flow field was bright and observable for approximately 2.5 m downstream (observed 8 Mach disks in the flow). The light reflecting off the inside of the nozzle wall on Run 1512 from the flow field appeared to flicker, indicating a larger fluctuation in the flow-field enthalpy compared to Runs 1507 and 1513, which appeared relatively steady. The flow-field intensity on Run 1509 was only slightly less than runs 1507 and 1513 with all four heaters hot. Approximately 7 Mach disks were observed in the flow on Run 1509.

Run 1515 was performed with heaters 1 and 3 hot and heaters 2 and 4 inactive. Heaters 2 and 4 were connected to the manifold, but no air was flowing through these heaters. The small nozzle ( $A^* = 2.5 \text{ cm}^2$ ) was installed for Runs 1515 through 1517. The flow-field intensity appeared the same as the runs with all four heaters hot, with 8 Mach disks observed in the flow. A low-frequency acoustic rumble not heard during the previous runs was evident during Run 1515. The flow field also appeared to have a slight pulsing or flickering. From an examination of Run 1515 data, it was observed that the time required to pressurize the heaters was slower than previous runs.

Following Run 1515, the model injection system was removed to work on the facility (remove heaters 2 and 4 and cap the manifold). During this operation an inspection of the heat flux probe revealed that the null point sensor in the probe tip had recessed slightly into the probe body, creating a small cavity on the nose tip. It is not known when the sensor slipped into the probe body; however, a close inspection of the data suggests this may have occurred at the end of Run 1512 or the beginning of Run 1513. The heat flux data were adjusted numerically and the subject is addressed in detail in Section 6.0.

During heater maintenance between Runs 1515 and 1516 it was possible to observe the inside surface of the manifold. The heater and nozzle tubes were very lightly coated with soot and small granules (approximately 1 mm in diameter) which were easily removed with a paper towel. The largest concentration of slag or residue was noticed on the subsonic section of the nozzle. The rear of the manifold, where the pressure port is located (see Fig. 18a), appeared clean and shiny.

The final run, 1517, was performed with heaters 1 and 3 hot and heaters 2 and 4 removed and the manifold entrance ports plugged with special water-cooled flanges. The flanges are basically flat copper disks with backside water cooling which were bolted to the manifold where the arc heater downstream electrode was connected. The flow field appeared the same as in Run 1515 with 8 Mach disks. The low-frequency acoustic resonance and flow-field flicker were also evident during this run.

Following the test series, heater 1 was disassembled to inspect the electrodes to determine an arc attachment location and measure the mass loss. Results of these measurements are presented in Tables 5 and 6. Arc attachment measurements were not made on the cathode because of difficulty in determining an exact location; however, it appears that the arc was attaching near the downstream end of the electrode.

#### **4.0 JP-200 OPERATIONAL OBSERVATIONS**

AEDC personnel witnessed all of the JP-200 runs and were able to observe operations approximately 10 min before and after each run. Additionally, an AEDC employee was permitted to observe operations personnel make hardware configuration changes between Runs 1515 and 1516 when heaters 2 and 4 were removed from the manifold in preparation for the runs with two heaters hot and two heaters removed.

Pre-run operations appeared smooth, efficient, and trouble-free. Prior to each run (approximately 15 to 20 min) a cold flow was performed to check out hardware and the computer program which controls the entire facility. A key interlock system is used to set up systems prior to the run (power switches, manual water valves, etc.). A computer system controls the entire run sequence, which appeared to operate as follows: One button is pushed on the computer control panel to initiate the program which starts all the systems and operates the entire facility from approximately 2 to 3 min before arc initiation until all systems are shut down. The computer system first starts the cooling water flow. Once the cooling water flow reaches steady-state conditions, the air flow is started. When the air flow is steady, the striker rods initiate the arcs in the heaters to start the run. The models are swept and the run is terminated at the programmed times. The computer system then terminates the air and water flows.

High- and low-speed data are downloaded from the data acquisition system by a hardwire connection to a personal computer in the control room, where they are available for inspection on the computer screen immediately following the run. Data manipulation, including plot scale changes, enlarging specific sections of plots, data overlays (for example, plotting all the probe sweeps on one plot), etc., are all performed in the control room. Hard copies of the data are made (waiting on the printer appeared to be the most time-consuming step in the data reduction process) and can be presented to the user within approximately 30 min after the run. Additionally, the data are stored on a standard 3.5-in. floppy disk and delivered to the user.

All of the control and pre-run setup is performed on a 486 personal computer using color graphic displays. For example, to set the desired air flow rate for each heater, a schematic of the air system, similar to Fig. 21, is displayed on the screen, and the requested flow is entered over a

graphical representation of a pressure regulator. A schematic of the power system is displayed in which the desired current for each heater is entered on the screen. All electrically operated systems (valves, switches, model injection system, etc.) are controlled from this computer. Basically, all of the control room operations are performed by a single computer.

Hardware changes by the operations crew were observed between Runs 1515 and 1516 while heaters 2 and 4 were removed from the manifold and the entrance ports on the manifold were capped with special flanges. A crew of three people, two craftsmen and one engineer, worked on the JP-200 facility. The design and layout of the facility appeared to be efficient and well planned as work proceeded smoothly and at a faster pace than expected. The model injection system was first removed with an overhead crane and placed on the floor beside the heater. Two floor panels in front of heater 3 (below the nozzle) were automatically pivoted out of the way with pneumatic actuators to allow heater 3 to clear the floor level. The entire arc heater system was then pivoted about heaters 2 and 4 with a hydraulic system so that all four heaters were horizontal to the floor with the nozzle pointing towards the ceiling. The floor panels beneath heater 3 were then rotated back into place. The heaters are mounted and bolted to a grooved track. Heaters 2 and 4 were unbolted from the track and the manifold and were slid back, away from the manifold. The flanges were then bolted to the manifold, and water lines were rerouted from the air injection chambers of heaters 2 and 4 to the manifold flanges. Work around the manifold area was very tight because of limited space from the heaters and the cooling water lines. The anode on heater 3 was unbolted and slid back from the air injection chamber to permit cleaning. Since heater 3 is at the bottom of the system, any foreign material that is not expelled through the nozzle usually ends up in the bottom (anode) of heater 3. The anode was cleaned with a paper towel and compressed air and reconnected to the air injection chamber. The heaters were rotated vertically, and air and water flow checks were performed. This entire operation was performed in a 3-1/2-hr period in the morning. The model injection system was reinstalled and the probes were aligned in the afternoon, which required an additional 3 hr.

Aerospatiale personnel commented that if a new manifolded arc heater system were ever designed, they would probably align the heaters in a horizontal plane because of the additional complexity of rotating the arc heaters with all of the hose connections. Also, the bottom heater tends to have more operational problems than the other heaters because of foreign material settling there. It was also observed that facility operations and maintenance with a multi-arc system is more complex than with a single-arc heater (based on AEDC experience with single-arc heater operations). This added complexity is caused by the additional hardware and the close proximity of the components.

## **5.0 PERFORMANCE AND THERMAL EFFICIENCY**

A major objective of this test program was to compare the facility performance and thermal efficiency of a single-arc heater with manifolded arc heaters. Even if the flow quality of a manifolded multi-arc heated facility is improved over a single-arc heater, the magnitude of the thermal penalty incurred from the additional hardware required to manifold the flow must be measured. Also of interest was the amount of variation in performance of the individual arc heat-

ers while they were operated simultaneously in a manifolded arrangement. The nozzle losses and the overall performance must also be evaluated.

## 5.1 ARC HEATER

The performance of the individual arc heaters for the longer-duration energy balance runs is shown in Table 7 and in Fig. 23 for both the HP and JP-200 arc heater tests. The enthalpy and efficiency values include only arc heater thermal losses and not the losses from the manifold or nozzle and thus represent the enthalpy and efficiency at the end of the cathode for each individual arc heater. The target input values for each arc heater on each run were an air mass flow rate of 440 gm/sec, an arc current of 1,075 amp, and a nozzle throat diameter installed that would produce an arc heater pressure of about 60 bar. Thus, the heater voltage, power, enthalpy, and efficiency should be approximately the same for all heaters and for all runs. To account for the small difference in geometry between the HP and the JP-200 arc heaters, an adjustment in the arc current for the HP heater was planned if the enthalpy at the end of the cathode for two facilities differed by more than 8 percent. That proved not to be necessary, as seen by comparing  $H/RT_0$  for Runs 1507 and 1513 with Runs 430 and 431 in Table 7.

The variation in each global parameter and the percent deviation of each parameter from the mean for each heater for each run is shown in Table 7, along with average values of the parameters for each run, the overall average for all runs, and the overall variation for all runs. Also, a plot of the variation in each parameter for each arc heater on each run is shown in Fig. 23, along with overall average, maximum, and minimum values of each parameter for all runs. The largest overall variation was in the electrical power (+8.17 to -7.28 percent) caused largely by the variation in mass flow (+1.66 to -4.5 percent) and voltage (+7.21 to -6.19 percent) which in turn resulted in an enthalpy variation of +5.64 to -5.58 percent. The enthalpy variation was well within the  $\pm 8$ -percent target. The maximum power level occurred in arc heater 2 on Run 1513, and the minimum occurred in arc heater 4 on Run 1509, both primarily the result of the air regulator not providing the target mass flow of 440 gm/sec. In addition to the variation in input variables (mass flow and current), a significant part of the observed heater parameter variation can be attributed to the nature of a Huels-type arc heater where the arc length is free to vary over a wide range. The lower efficiency for the HP arc heater relative to the JP-200 arc heaters shown in Fig. 23 is probably caused by the longer heater geometry for the HP arc heater relative to the JP-200 arc heaters, the longer length thus causing more thermal losses.

## 5.2 MANIFOLD

The flow from each JP-200 arc heater is combined in the manifold and then exits to the nozzle. The manifold is a critical component of a multi-arc facility, a component which is not required in a single-arc heater facility. Therefore, the magnitude of the thermal loss associated with the manifold and the accompanying reduction in enthalpy is important in determining the overall performance of such a facility. The thermal performance of the manifold is presented in Table 8 and plotted in Figs. 24-26 as a function of aerodynamic enthalpy. The aerodynamic enthalpy is calculated from the continuity equation for equilibrium sonic flow. Figure 24 shows the manifold thermal loss as a percent of the total loss in all of the arc heater hardware for each

run with the JP-200 facility. Run 1507, the first run with all four arc heaters operating hot, produced a low thermal loss in the manifold. This result was questioned after comparing this loss with the manifold loss obtained on Runs 1509 and 1512 with cold air added to reduce the enthalpy. Run 1507 was repeated on Run 1513, which resulted in a higher manifold thermal loss of 8.1 percent of the total loss. This result seems reasonable when compared to a manifold loss of 7.3 percent on Run 1509 with cold air flowing in one heater and 6.7-percent loss on Run 1512 with cold air flowing in two heaters. Runs 1515 and 1517 with only two heaters operating and no cold air introduced, produced manifold losses between 11 and 12 percent of the total. The relative increase was caused by a nearly 50-percent reduction in the surface area of the arc heaters, where most of the thermal losses occurred while the manifold area remained constant. The manifold thermal loss as a percent of the power in the gas at the entrance to the manifold is plotted in Fig. 25, and the overall reduction in bulk enthalpy attributed to the presence of the manifold is shown in Fig. 26. Both of these figures show the same trend as discussed in Fig. 24. The percent reduction in enthalpy caused by the manifold with all four arc heaters hot was 7.1 percent (Run 1513) and was down to 5.2 percent with two heaters flowing cold air (Run 1512). These thermal losses are quite reasonable and would not be considered a significant penalty for choosing the manifolded concept.

### 5.3 NOZZLE

Thermal losses occurring in the nozzle are presented in Table 9 and Figs. 27-29. The nozzle loss as a percent of the total thermal loss is shown in Fig. 27. The nozzle loss with all four JP-200 arc heaters operating is 4.5 percent of the total loss, and the loss decreases with cold air added (Runs 1509 and 1512). With only two heaters operating and no cold air added (Runs 1515 and 1517), the nozzle loss increased to 6.0 percent. These losses are similar in trend to the manifold losses (see Section 5.2). Note that the nozzle loss in Fig. 27 for Runs 1507 and 1513 is essentially the same, which substantiates the likelihood that the lower-than-expected manifold heat loss level on Run 1507 is incorrect.

The nozzle loss as a percent of the total loss for the HP arc heater is higher than for the JP-200 manifolded arc heaters. The higher nozzle loss for the HP arc heater was attributed to the design of the nozzle which contains more surface area exposed to the hot gas relative to the exposed surface area for the entire HP arc heater than does the JP-200 nozzle and the pressure measuring station (see Figs. 6 and 15 and Table 3). Figure 27 shows a reduction in the ratio of the HP nozzle loss to total loss as the arc current and aerodynamic enthalpy are increased while holding the mass flow constant. The higher current shortens the arc length and results in higher thermal losses in the cathode relative to the nozzle for the higher enthalpy runs.

The nozzle loss relative to the power to the gas at the nozzle entrance is shown in Fig. 28, and the reduction in enthalpy attributed to the nozzle is plotted in Fig. 29 as a function of aerodynamic enthalpy. The results are similar to those previously presented.

## 5.4 OVERALL PERFORMANCE

The overall performance of the HP and the JP-200 arc heater facilities are shown in Table 10. The aerodynamic enthalpy is based on the equilibrium sonic flow calculation with gas properties obtained from the Mollier chart. The calorimetric or energy balance enthalpies are also shown in Table 10 calculated four different ways: total enthalpy with all losses included, enthalpy excluding nozzle loss, enthalpy excluding only the manifold loss, and the enthalpy excluding both the manifold and nozzle losses. The aerodynamic enthalpy agrees extremely well with the calorimetric enthalpy, if the nozzle loss is excluded, for all runs for both the HP and the JP-200 arc facilities. Also note that for those same enthalpy measurements (aerodynamic enthalpy and calorimetric enthalpy excluding nozzle loss), the JP-200 enthalpy is about 7 percent lower than the HP enthalpy. However, the thermal losses in the HP nozzle are relatively high because of its design compared to the nozzle loss for the JP-200 facility. Therefore, the overall calorimetric enthalpy with all losses included is only about 4 percent lower for the JP-200 facility than for the HP facility.

A comparison of probe data for the HP and JP-200 facilities is shown for pitot pressure in Figs. 30-31 and for heat flux in Figs. 32-33. For pitot pressure, the levels and profiles are essentially the same for the HP and JP-200 facilities. However, the heat flux for the JP-200 averaged only  $40 \text{ MW/m}^2$ , compared to  $60 \text{ MW/m}^2$  for the HP arc heater. Most of this difference is attributed to heat flux enhancement from free-stream turbulence which has been largely removed by the manifold in the JP-200 facility. This heat transfer enhancement which occurs in a single-arc heater is often used to great advantage for materials testing where extremely high rates are required. Certainly the 7-8 percent thermal loss in the manifold is not enough to account for this large difference in flow-field heat flux. The heat flux profiles from both facilities are generally flat (not peaked in the center) although the HP heat flux is somewhat lower on one side of the flow than on the opposite side. This phenomenon is believed to be caused by a probe measurement problem because the low heat flux was always measured on the side of the flow that the probe entered, regardless of the probe sweep direction. It was surprising that the heat flux profiles for the HP arc heater were generally flat. Usually, with a single-arc heater the heat flux is considerably higher on centerline because of the swirl and cored flow generated in the arc heater. The only explanation that could be found for the flat profiles obtained with the HP arc heater was the presence of the short, but large-diameter cavity between the downstream end of the cathode and the entrance to the nozzle. This cavity is used as a pressure measuring station (see Fig. 6), but it may also have caused the flow to recirculate and allow the hot core to mix with the cooler surrounding flow.

## 6.0 FLOW QUALITY EVALUATION

The flow field was probed to evaluate flow-field conditions. Two pitot probes and one heat flux probe were used. Data were taken for a forward sweep and a reverse sweep through the flow for each matrix run.

## 6.1 DATA VALIDATION

Since probe data were used to characterize the flow field, certain checks were done to assess the validity of the probe data.

### 6.1.1 Heat Flux and Pitot Pressure Data Reduction

The Aerospatiale heat flux data were output directly as a result of inputting the time-temperature data into an analog heat flux network. The analog network does a reasonably good job, but the result is slightly low when compared with a numerical integration, as shown in Fig. 34. Data for Run 430 are shown in Fig. 34a and for Run 1513 in Fig. 34b. In light of these data, the heat flux derived at AEDC from a numerical integration of the time-temperature data was used for the flow-field evaluations. The pitot pressure data (also shown in Fig. 34) shows that the two Aerospatiale pressure probes give essentially the same answer.

### 6.1.2 Derived Parameters

Given swept probe data (pitot pressure,  $P_o'$ , and heat flux,  $Q$ ) as a function of radial position, other parameters were derived on a point-by-point basis to give profiles of enthalpy,  $H$ , velocity,  $V$ , Mach number,  $M$ , and density,  $\rho$ . An inferred enthalpy can be computed from Fay and Riddell (Ref. 8) heat-transfer theory, and then the remaining parameters can be obtained by solving a reverse shock crossing problem using equilibrium air properties.

### 6.1.3 Profile Integrations

Once the profiles of  $H$ ,  $V$ ,  $M$ , and  $\rho$  are known, integrations across the flow field can be performed to obtain the total mass flow and the mass average enthalpy. The mass average enthalpy computed from an integration of probe data has historically been observed to exceed the heat balance enthalpy by an amount that has been dubbed the "enhancement." This "enhancement" has been attributed to free-stream turbulence enhancing the heat transfer above the value predicted by the laminar theory of Fay and Riddell. The relationship between free-stream turbulence and heat-transfer enhancement can be predicted with the Wassel and Denny (Ref. 9) theory. Self-consistent data should then exhibit the following characteristics: (a) the Mach number profile should agree with the Mach number based on the geometric area ratio, (viscous effects are small in a high pressure, low Mach number nozzle); (b) the integrated mass flow should agree with the mass flow measured upstream of the arc heater; and (c) the integrated mass average enthalpy should exceed the heat balance enthalpy by some "enhancement" value which is reasonable for that configuration. An enhancement less than 1.0 generally indicates an error in some component of the data.

The ratio of the integrated parameter values derived from probe data to the measured value for each of these quantities is shown in Fig. 35. These results are plotted versus run number in chronological order to facilitate the detection of any changes that may have occurred in the instrumentation. For instance, it was observed that the null-point calorimeter slug slipped back into the



probe body at some point during the test. This would effectively cause the probe to appear more blunt, hence reducing the measured heat transfer.

To quantify the effect of the null-point slug slippage, a hemisphere with a flat spot the size of the slug was analyzed. This is a conservative model since the slug actually slipped deeper into the body. The effect is investigated by looking at the stagnation point velocity gradient, a critical component of the Fay and Riddell heat-transfer expression. The stagnation point velocity gradients for a sphere and for a sphere with a flat spot are compared in Fig. 36. The velocity gradient for a sphere is 0.64, and for a flattened sphere it is 0.46. Since the heat transfer is proportional to the square root of the velocity gradient, the blunting of the sphere reduces the heat transfer by the square root of the ratio of 0.46 to 0.64, i.e., a reduction of 15 percent. It is not known when in the run sequence the slug slipped; however, a 15-percent correction was applied to the last 3 runs, Runs 1513, 1515 and 1517, and the results are shown as a possible correction of the data (the solid symbols) in Fig. 35. This results in bringing all of the heat-transfer enhancements above 1.0 and improves the mass flow prediction for these last three runs. The mass flows calculated are then within  $\pm 10$  percent of the measured values, a good rule of thumb for acceptability.

#### **6.1.4 Evaluation of Probe Data Quality**

The agreement of the integrated probe data with heater measurements can be summarized as follows: (a) the Mach number agreement is within 2 percent; (b) the mass flow agreement is acceptable (within 10 percent); and (c) the enthalpy enhancement with the proposed adjustments is greater than 1.0, as it should be. The probe data are self-consistent with the adjustments used; however, the acceptance/rejection of the adjustments does not significantly affect the flow quality arguments that follow.

### **6.2 FLOW QUALITY**

The flow quality of the single-arc and multi-arc configurations will be examined to determine whether one configuration yields significantly better flow quality than the other. The flow quality will be characterized by: (a) the profile shape for parameters such as pressure, enthalpy, etc., (b) the magnitude of fluctuations of the various parameters, and finally (c) by the mixing efficiency in the multi-arc case.

#### **6.2.1 Profile Shapes**

Profiles for the measured and computed parameters are shown in Figs. 37a-e for the single HP arc heater, Run 430, and in Figs. 38a-e for the JP-200 multi-arc, Run 1513. The heat flux for the HP heater, Fig. 37b, is relatively flat, i.e., maximum values near the edge of the flow vary only a few percent from those at the centerline. It is not uncommon for the edge heat flux to be 50 percent lower than the centerline value for a heater closely coupled to the nozzle. A possible explanation for this uniform heat flux profile is that the enlarged pressure measurement station just before the nozzle is acting as a stilling chamber. The Mach number profile is uniform (Fig. 37d) indicating good flow from the nozzle. Finally, the inferred enthalpy profile (Fig. 37e) is relatively flat and reflects the fluctuations present in the heat flux profile.

The heat flux profile is flat for the JP-200 multi-arc configuration (Fig. 38b), as was expected. The Mach number profile is also flat (Fig. 38d), again indicating good flow from the nozzle. Again, the inferred enthalpy profile is flat and mirrors the fluctuations present in the heat flux profile.

### 6.2.2 Flow-Field Fluctuations

**Comparison Methodology:** Temporal (and spatial, as the probe is swept) fluctuations in amplitude of the flow parameters are characterized by computing a standard deviation,  $\sigma$ , over the center 85 percent of the core flow. This corresponds to  $r = \pm 8$  mm for the single-arc configuration and  $r = \pm 20$  mm for the multi-arc configuration. The frequency of fluctuations was compared qualitatively. Because of instrument response considerations and, in the case of heat transfer, the effect of the data reduction procedure, it was concluded that a formal frequency analysis would not be meaningful.

**Comparison of Various Configurations:** The mean core value and a band of  $\pm$  one standard deviation are shown for each parameter in Figs. 37 and 38 for Runs 430 and 1513, respectively. In Fig. 39, pressure and heat flux data for all runs are shown so that repeatability can be assessed. Fluctuations (quantified as a standard deviation) are shown in Fig. 39 as a percent of the mean value of the parameter for the measured quantities pitot pressure,  $P_o$ , and heat transfer,  $Q$ . The lines drawn through the heat flux data represent the average of the forward and reverse sweeps. It is noteworthy that the pressure fluctuations are consistently lower for the multi-arc configuration than for the single-arc configuration. Heat-transfer fluctuations are about the same; the fluctuations for the multi-arc configuration are no worse than for the single arc.

Velocity fluctuations are shown in Fig. 40 for all runs. Also shown are the turbulence levels required to produce the inferred enhancements from Fig. 35c, according to the Wassel and Denny theory. It should be cautioned that these two quantities are not defined in exactly the same way; hence, the magnitudes may not be directly comparable. Nevertheless, it is noted that for the single-arc runs (429 - 432) the velocity fluctuations and the Wassel and Denny turbulence agree quite well. This is also true for the multi-arc design point, Run 1513. It is also noteworthy that the levels for the multi-arc Run 1513 are significantly lower than the single-arc levels. This indicates a quieter, less turbulent flow with less heat-transfer enhancement.

**Heater Fluctuations Propagated to the Flow Field:** The effects of individual arc heater and total voltage fluctuations on stagnation-point heat flux and pitot pressure measurements at the nozzle exit were investigated. A lack of coupling between the voltages and flow-field measurements in the multi-arc configuration indicates that the mixing plenum is providing adequate damping of flow-field fluctuations. Direct comparison of the stagnation-point heat flux with arc heater voltage fluctuations requires a knowledge of the dwell time of a slug of air from the moment it is heated by the arc to the time it is sensed and processed by the heat flux probe/analog processor. The local velocities within the heater, manifold, pressure ring, and nozzle were determined from the respective geometries and heater conditions for Run 1513, and are presented in Fig. 41. The dwell time for a slug of air to transverse half the length of a heater, through the manifold, pressure ring, and nozzle to the probe (supersonic portion is assumed negligible) is

approximately 0.007 sec. The response times for the null-point calorimeter and analog processor add an additional 0.004 sec for a total lag time of 0.011 sec. A slug of air traveling the full length of the heater will require an additional 0.003 sec, while a slug just leaving the heater will require 0.003 sec less. Therefore, the heat flux given by the calorimeter will lag behind the heater voltage by 0.008-0.014 sec (i.e., the effect of an instantaneous voltage fluctuation on a slug of air within a given heater will not be detected in the heat flux until 0.008-0.014 sec later).

Figure 42 presents a comparison of individual and overall average voltages with heat flux for the forward sweep of Run 1513. The average lag time of 0.11 sec was used to adjust the time scales to make them consistent. If one assumes that an individual arc heater flow is restrained from mixing with the other heater flows and occupies a given quadrant, then voltage fluctuations for a given heater may be detected in the heat flux data as the probe sweeps through the appropriate quadrant. Assuming further that the overall flow through the nozzle does not rotate, then the forward sweep would first pass through the discharge from heater 2 and then heater 4. As seen in Figs. 42b and d, only a few heat flux points tend to follow the heater 2 and heater 4 voltage trends, respectively. The above assumption (sweep through heater 4, then heater 2 discharge) did not appear to hold in reverse sweep, either. Since the swirl in opposite heaters is in the opposite direction, all rotations should cancel if the flows mix, or remain local rotations if not mixed. If, however, we assume that the overall flow has a steady rotation, then the probe sweeps should show a trend toward a given flow orientation (i.e., if the heat flux trends follow the voltage trends for heater 1 for the first half of the forward sweep and heater 3 for the last half of the forward sweep, then the heat flux trends should follow the voltage trends for heater 3 for the first half of the reverse sweep and heater 1 for the last half of the reverse sweep). No coupling of this nature for any flow orientation was observed. If we now assume the heater flows are well mixed, it may still be possible to identify a coupling of the heat flux with the average voltage of all the heaters; however, as seen in Fig. 43, such a coupling does not appear to exist for the forward sweep, nor was it evident for the reverse sweep. The magnitude of fluctuations for the average voltage of the four heaters was smaller than the fluctuations in the individual arc voltages, indicating some cancellation.

A similar analysis can be performed to identify any coupling between the arc heater voltages and chamber, manifold, and pitot pressures. In several runs, including Run 1513, the pitot pressure exhibits 1,100- to 1,400-Hz ringing, possibly due to an acoustic phenomenon within the probe cavity. Since the ringing is not attributed to characteristics in the flow field, it is desirable to remove the oscillations from the pressure data prior to comparison to the voltage data. Fast Fourier transforms were applied to the pitot pressure data to verify the magnitude and level of the oscillations, an example of which is shown in Fig. 44. Application of a low-pass Butterworth filter tailored to remove oscillations greater than 1,000 Hz removed the ringing, but left lower-frequency response in the data. Figure 45 shows the improvement of the filtered pressure data over the original unfiltered data for the first pitot probe in the forward sweep on Run 1513.

Because of the short length of the passage between the pitot pressure port and the Kistler® piezoelectric transducers within the pitot probe, only a slight lag time exists between the pitot pressure response and the arc heater voltages. A conservative estimate is that the lag time is less than 0.001 sec, an order of magnitude less than the lag time between the heat flux and the volt-

age. Figure 46 presents the forward sweep no. 1 pitot probe response, along with the voltages from each of the four arc heaters. In addition, a comparison between pitot pressure and an overall average voltage of the four heaters is shown in Fig. 46e. Following the previous logic used in analyzing the heat flux data concerning arc heater flow quadrants, there does not appear to be any coupling between the pitot pressure response and the arc heater voltages. Similar results are observed with the no. 2 pitot pressure and the results from both probes in the reverse sweep. Figure 46 also includes the respective chamber pressure for each arc heater; however, the long lead tubing and slow response of the Druck<sup>®</sup> transducers used in the measurement of the chamber pressures and the static pressure at the inlet to the nozzle prevented observation of any oscillation.

### 6.2.3 JP-200 Mixing Efficiency

The JP-200 multi-arc configuration was operated at several off-design conditions in order to assess the flow-field behavior at these conditions, and to get some insight into the mixing efficiency. The off-design conditions may be summarized as:

- a. Run 1509: heaters 1, 3, 4 hot, heater 2 cold
- b. Run 1512: heaters 1, 3 hot, heaters 2, 4 cold
- c. Run 1515: heaters 1, 3 hot, heaters 2, 4 inactive
- d. Run 1517: heaters 1, 3 hot, heaters 2, 4 removed

The probes were swept in the plane of the off-design heaters so that the effects could be readily observed. The heat flux profile for Run 1509 (heater 2 cold) is shown in Fig. 47. The effect of the one cold heater is clearly evident in the reduced heat transfer in the quadrant where that heater is located. This is supported by the video for that run which shows a significantly less luminous flow on the side of the plume nearest the cold heater. When compared to the control, Run 1513, (see Fig. 38b) the average heat flux is lower. When there are two cold heaters in the probe sweep plane, Run 1512, the heat-transfer level is significantly lower, as shown in Fig. 48. Both Runs 1509 and 1512 show positive enthalpy enhancements, Fig. 35, which is somewhat surprising, considering that the probes were swept in the plane where the cold air was dominant. A plausible explanation is that the hot and cold streams have different velocities leading to shear layers, greater turbulence generation, and enhanced heat transfer.

## 7.0 CONCLUSIONS

AEDC does not plan to procure an arc heater manifold at this time. The requirement to obtain a large arc heater capability does not exist now. The arc heater manifold evaluation test was very productive, providing AEDC with important data to make an informed decision about manifold options if the opportunity to build a large arc-heated facility arises in the future. This test showed that manifolding arc heaters is a viable option to obtain a large arc heater capability. However, this test did not provide all of the information upon which a final decision to pursue the development of a multi-arc or single-arc system will be based. Further studies will be

required to make an informed decision between a multi-arc or single-arc system. The decision will be based on such factors as application-specific needs, development time requirements, financial constraints, available technology, etc.

The Aerospatiale personnel were very professional and extremely cooperative, providing AEDC with additional data and repeating a run at AEDC's request for which the data were in question. The Aerospatiale personnel also shared valuable information about their facilities and operation.

Based on the results and analysis of data from the Arc Heater Manifold Evaluation test performed at the Aerospatiale Plasma Laboratory Facilities in Saint-Medard-en-Jalles, France, the following conclusions were reached:

1. Facility operation and maintenance is more complex with a multi-arc system than with a single-arc heater.
2. Operational reliability of the JP-200 Huels-type multi-arc heater system appears to be very good.
3. The flow field, centerline heat flux was lower for the multi-arc facility than for the single-arc facility. The single-arc heater flow-field heat flux was approximately 60 to 65 MW/m<sup>2</sup> while the heat flux from the multi-arc facility was lower at approximately 40 to 44 MW/m<sup>2</sup>. The reduction in heat flux is attributed to the manifold system, which dampens the free-stream turbulence and reduces the heat flux. The manifold also contributes to the lower heat flux by lowering the enthalpy (see conclusion 4).
4. A reduction in enthalpy of approximately 7 percent was attributed to additional wall losses in the manifold (see Section 5.2).
5. Profile shapes for the multi-arc were flat, but only slightly more so than for the single heater. The single-arc profiles were flatter than expected, presumably because of the short but large-diameter pressure section upstream of the nozzle.
6. Fluctuations in the flow (as measured by standard deviation) were slightly better for the multi-arc configuration flow, primarily because of smaller fluctuations in the pressure (1.8 percent for the multi-arc configuration versus 2.2 percent for the single-arc). Heat flux fluctuations for the multi-arc (7.7 percent) were nearly the same as for the single arc (7.8 percent).
7. There is no evidence that individual heater fluctuations propagating through the manifold can be correlated with probe measurements in the effluent.
8. When one of the heaters flowed cold air, a significantly lower probe heat-transfer rate resulted in the corresponding quadrant. This indicates that complete mixing does not occur in the mixing chamber.

9. When two arc heaters were inactive, the time required to pressurize the heaters was slower, and an acoustic resonance was present.
10. With two arc heaters inactive or removed, the reduction in enthalpy attributed to the manifold increased to 10 - 12 percent.
11. Maximum deviation of individual arc heater conditions from the average value for all heaters on all runs was 3 percent for chamber pressure and 5.6 percent for reduced enthalpy.

## REFERENCES

1. "USAF Nozzles - Profiles Definition and Wall Heat Flux Evaluations." Aerospatiale Internal Report Number NT 30660/TA/PA/NC, March 9, 1994.
2. "USAF - Test Results on the HP Arc Heater." Aerospatiale Internal Report Number NT 31203 STB/L.AQ, July 20, 1994.
3. "USAF Test Campaigne - High Pressure Arc Heater, Measurement Lines - Definitions and Accuracy." Aerospatiale Internal Report Number NT 31521/STB/L-AQ, November 2, 1994.
4. "USAF Test Campaigne - JP200 Arc Heater, Measurement Lines - Definition and Accuracy." Aerospatiale Internal Report Number NT 31520/STB/L-AQ, November 2, 1994.
5. "USAF - Test Results on the JP200 Arc Heater, Tome (Volume) 1 of 3." Aerospatiale Internal Report Number NT 31562-STB/L.AQ, November 10, 1994.
6. "USAF - Test Results on the JP200 Arc Heater, Tome (Volume) 2 of 3." Aerospatiale Internal Report Number NT 31562-STB/L.AQ, November 10, 1994.
7. "USAF - Test Results on the JP200 Arc Heater, Tome (Volume) 3 of 3." Aerospatiale Internal Report Number NT 31562-STB/L.AQ, November 10, 1994.
8. Fay, J. A. and Riddell, F. R "Theory of Stagnation Point Heat Transfer in Dissociated Air." *Journal of the Aerospace Sciences*, Vol. 25, No.73, February 1958.
9. Wassel, A. T. and Denny, V. E. "Heat Transfer to Axisymmetric Bodies in Super and Hypersonic Turbulent Streams." *Journal of Spacecraft and Rockets*, Vol. 14, April 1977, pp. 212-218.

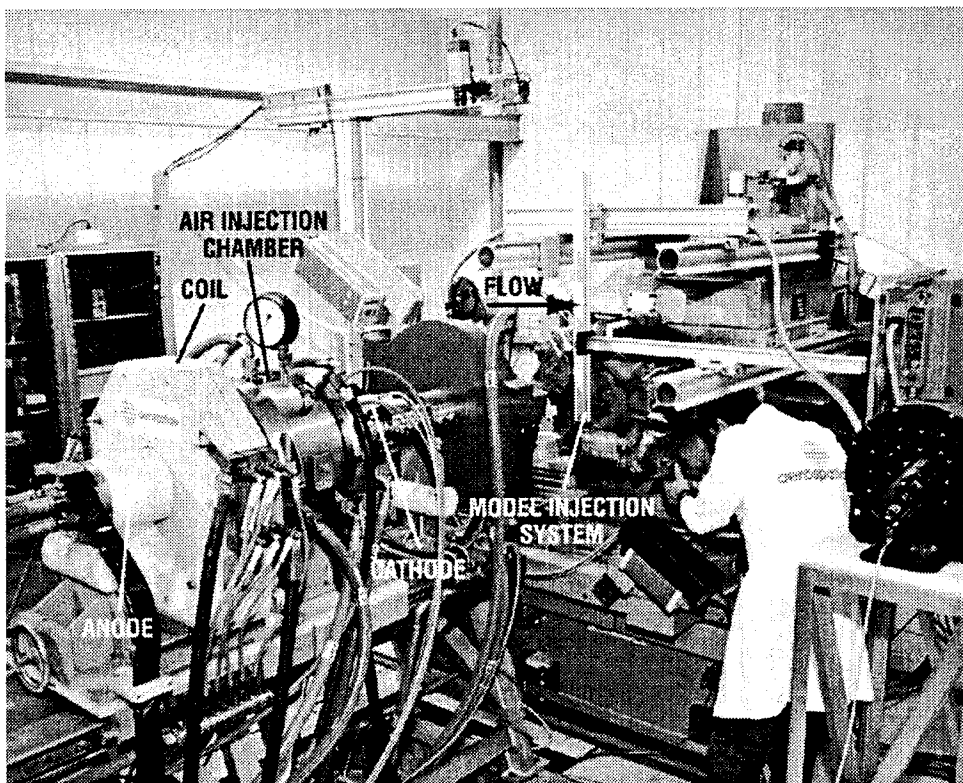


Figure 1. HP arc heater facility.

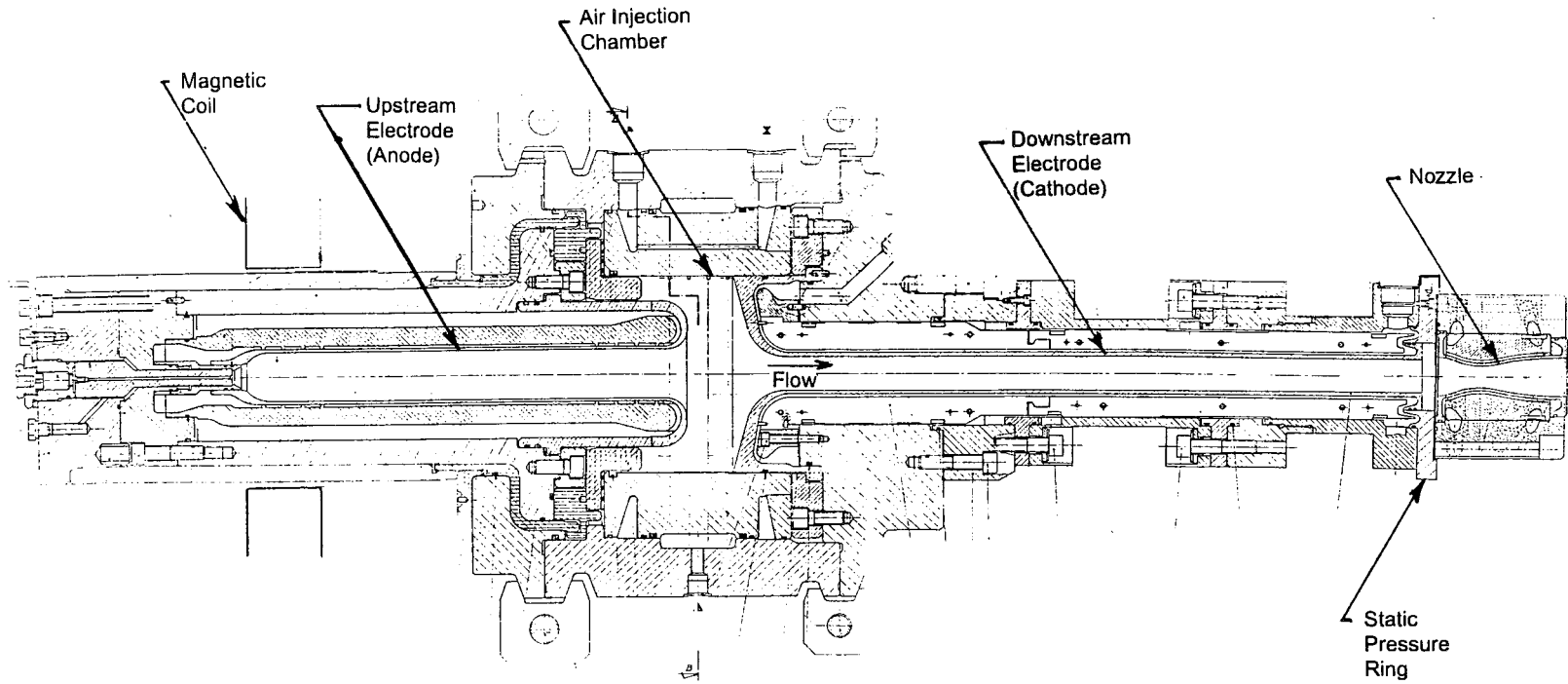
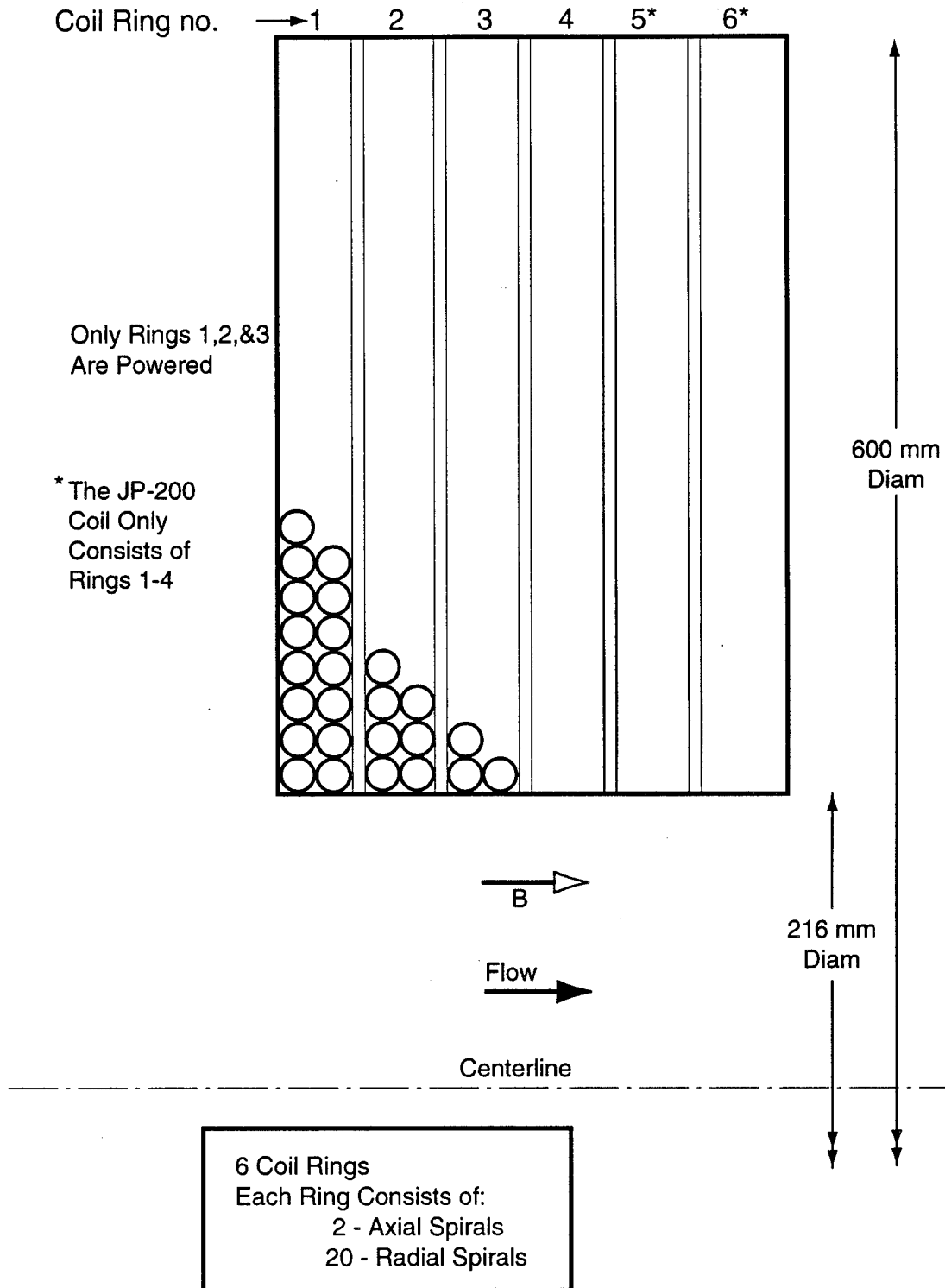


Figure 2. HP arc heater.





**Figure 3. HP and JP-200 magnetic coil design.**

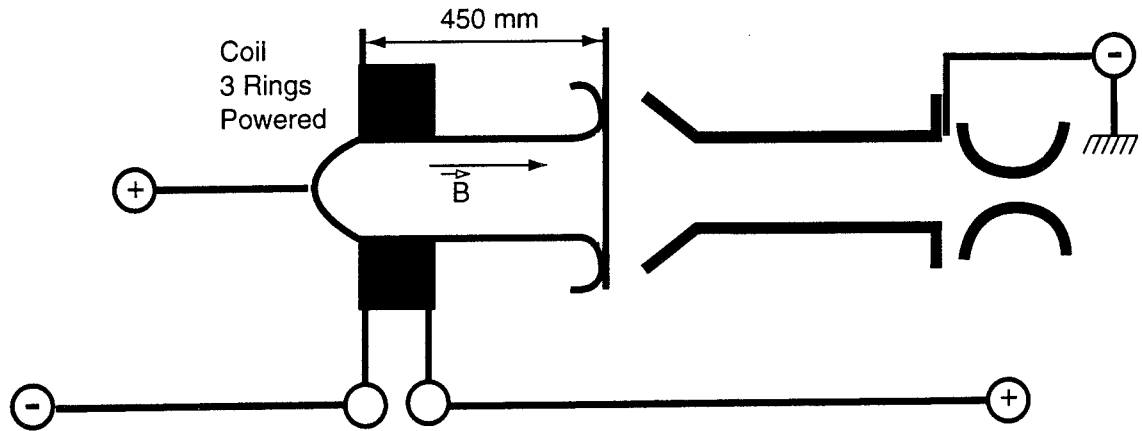


Figure 4. HP and JP-200 magnetic coil axial location.

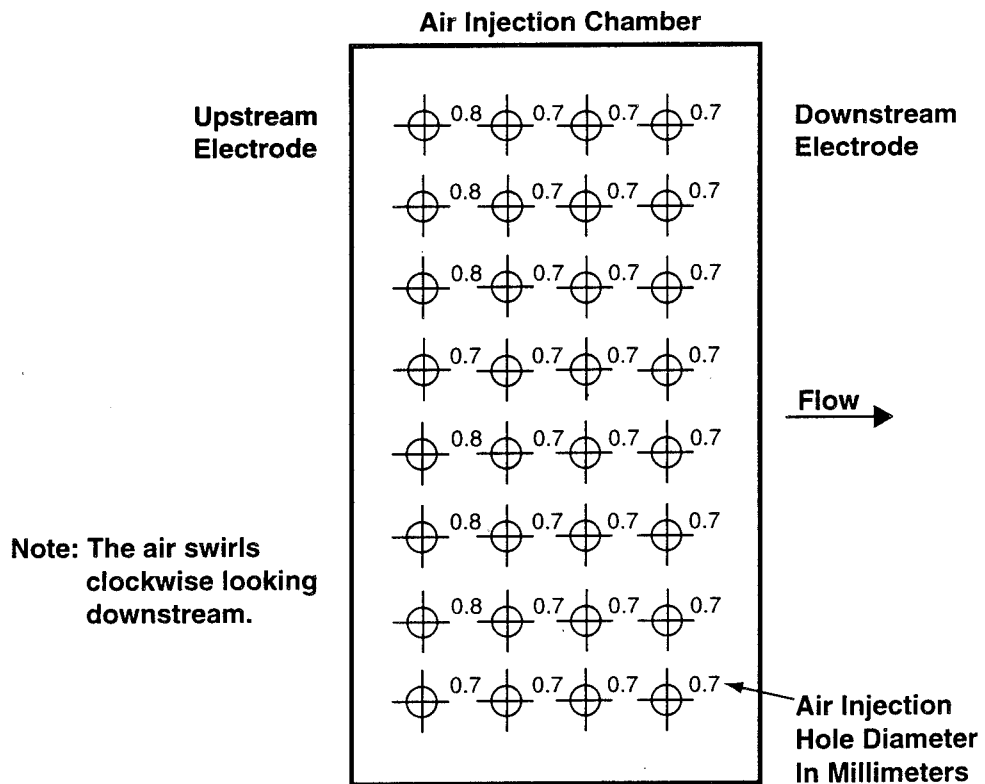


Figure 5. HP air injector locations and diameters.

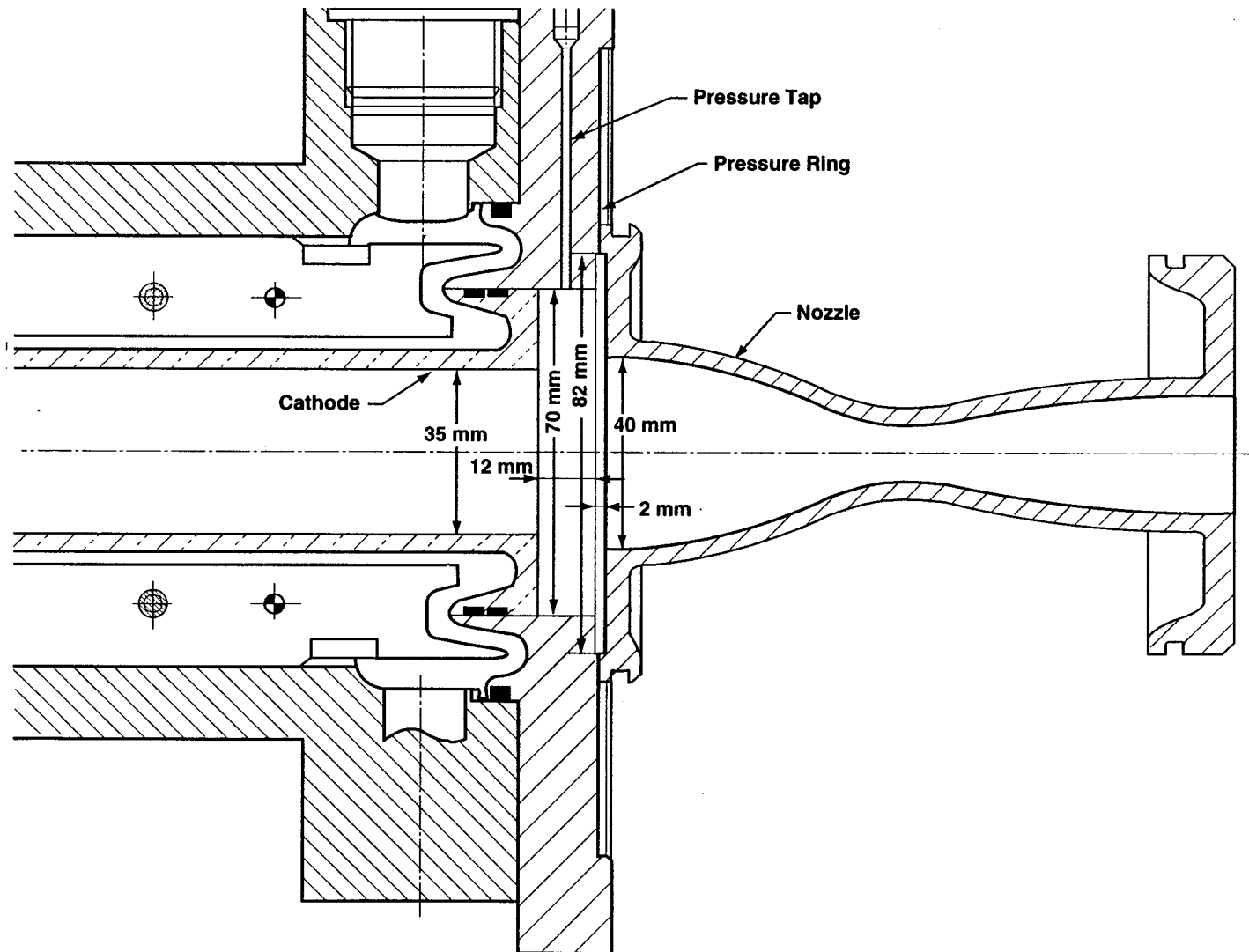


Figure 6. Details of the nozzle - pressure ring - cathode interfaces.

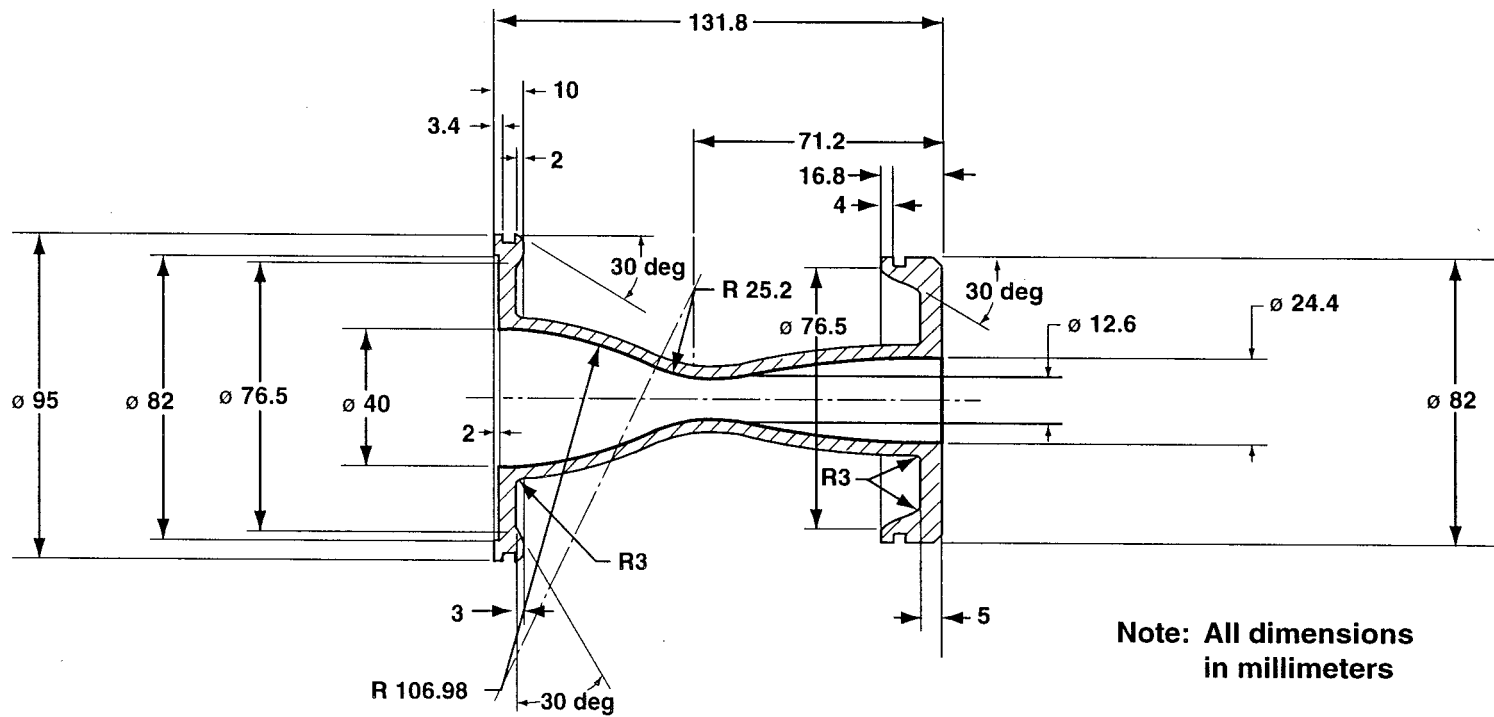
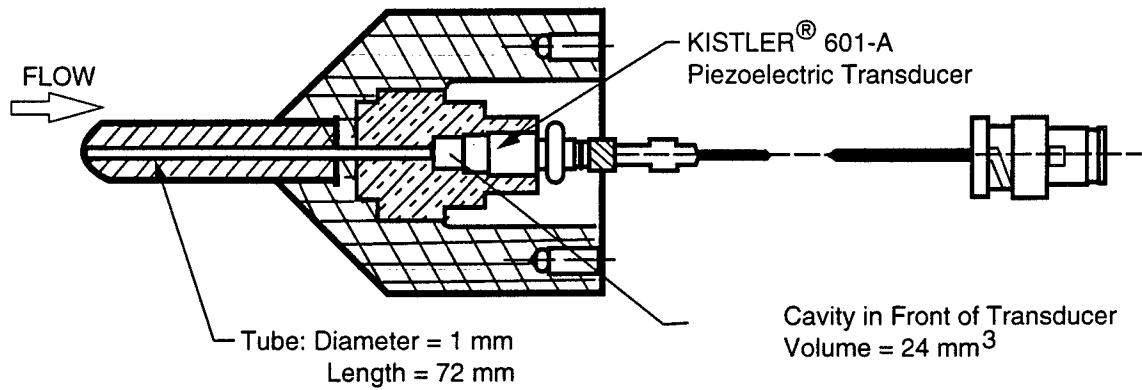
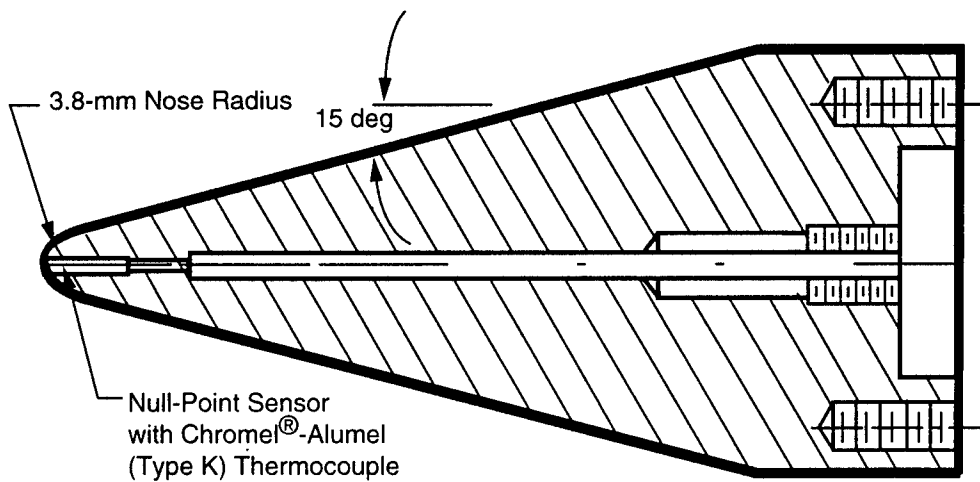


Figure 7. HP nozzle,  $A^* = 1.25 \text{ cm}^2$ .



**Figure 8. Pitot pressure probe.**



**Figure 9. Heat flux probe.**

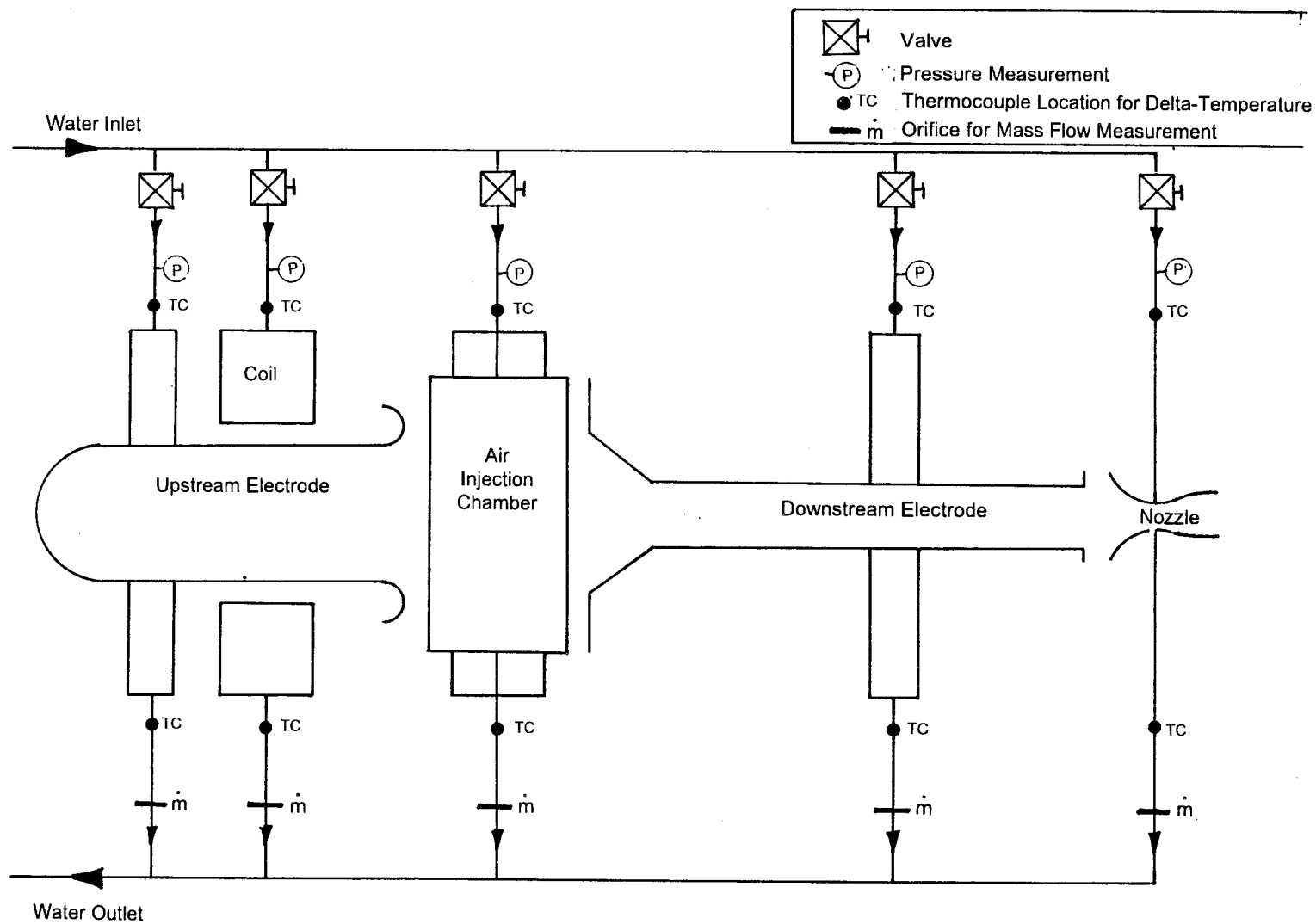


Figure 10. Schematic of HP cooling water system.

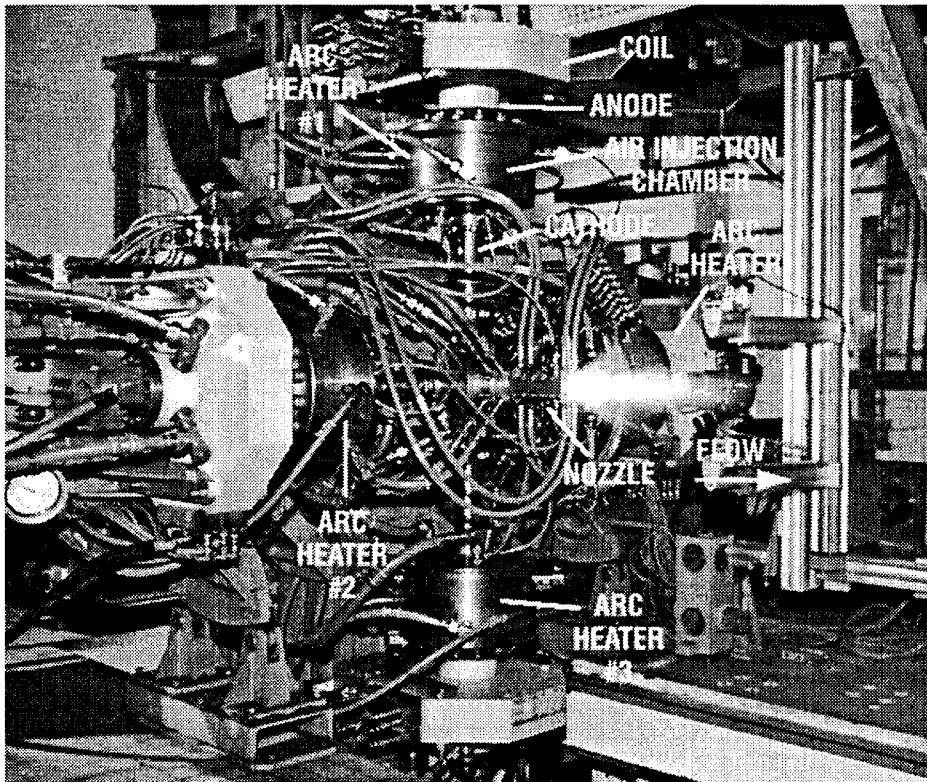
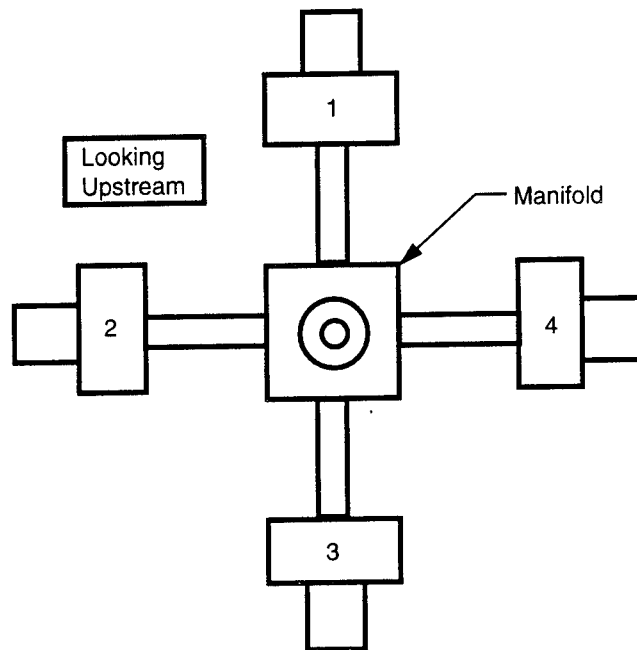
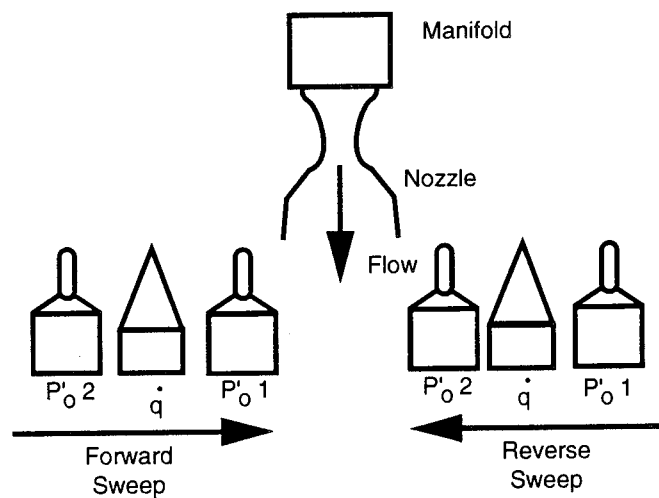


Figure 11. JP-200 arc heater facility.



**a. Heater locations**



**b. Probe sweep directions**

**Figure 12. JP-200 heater locations.**



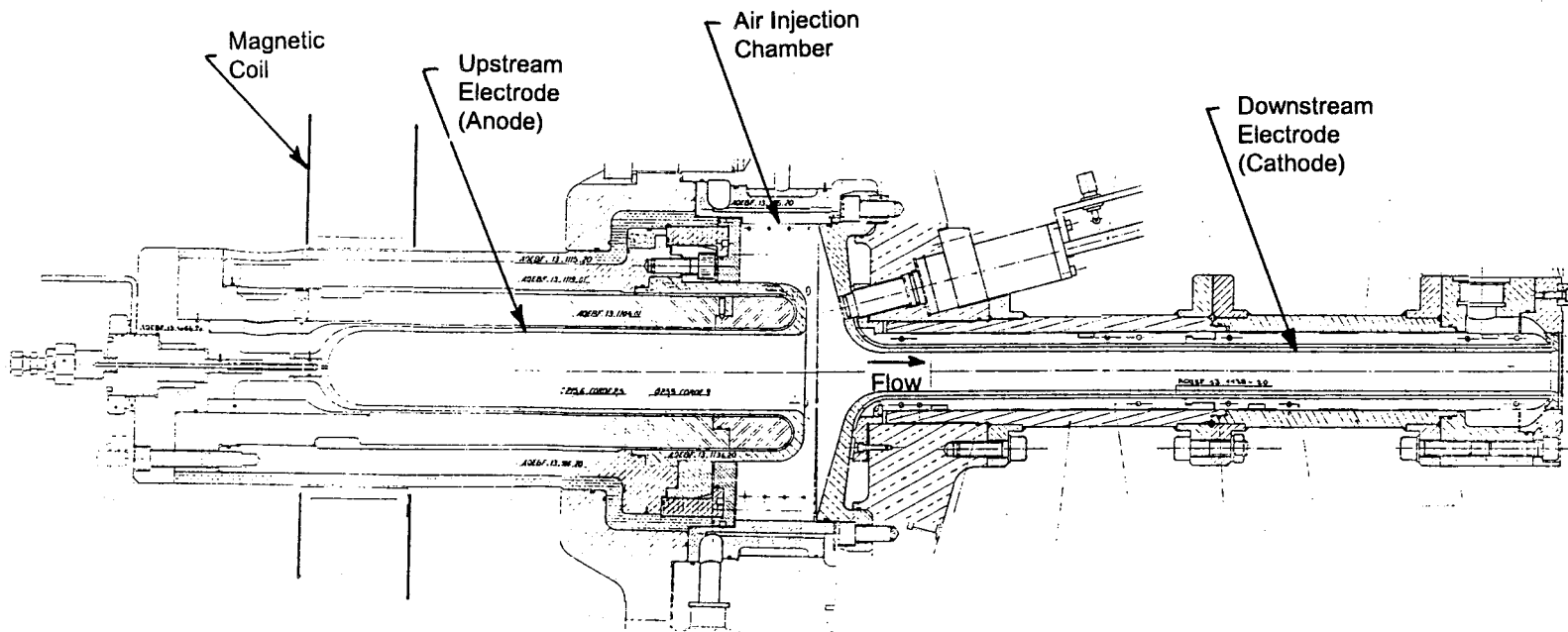
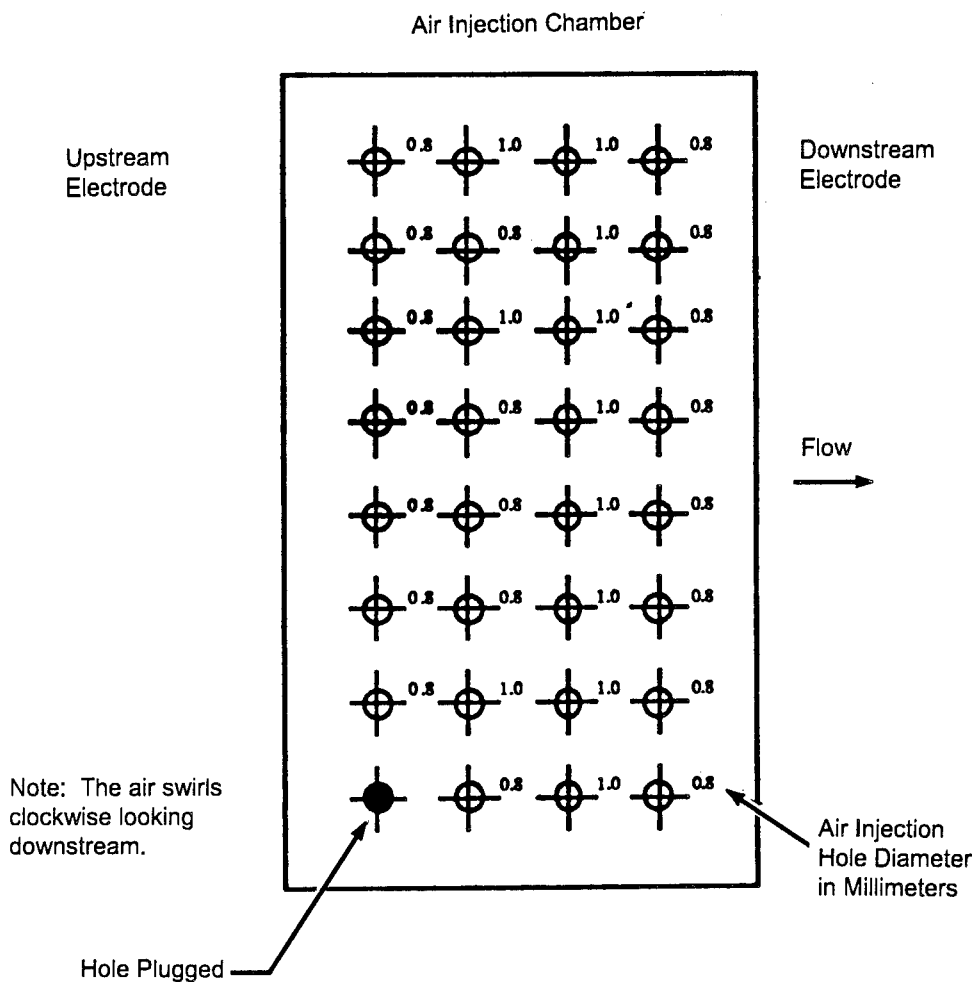


Figure 13. JP-200 arc heater.



**Figure 14. JP-200 air injector locations and diameters.**

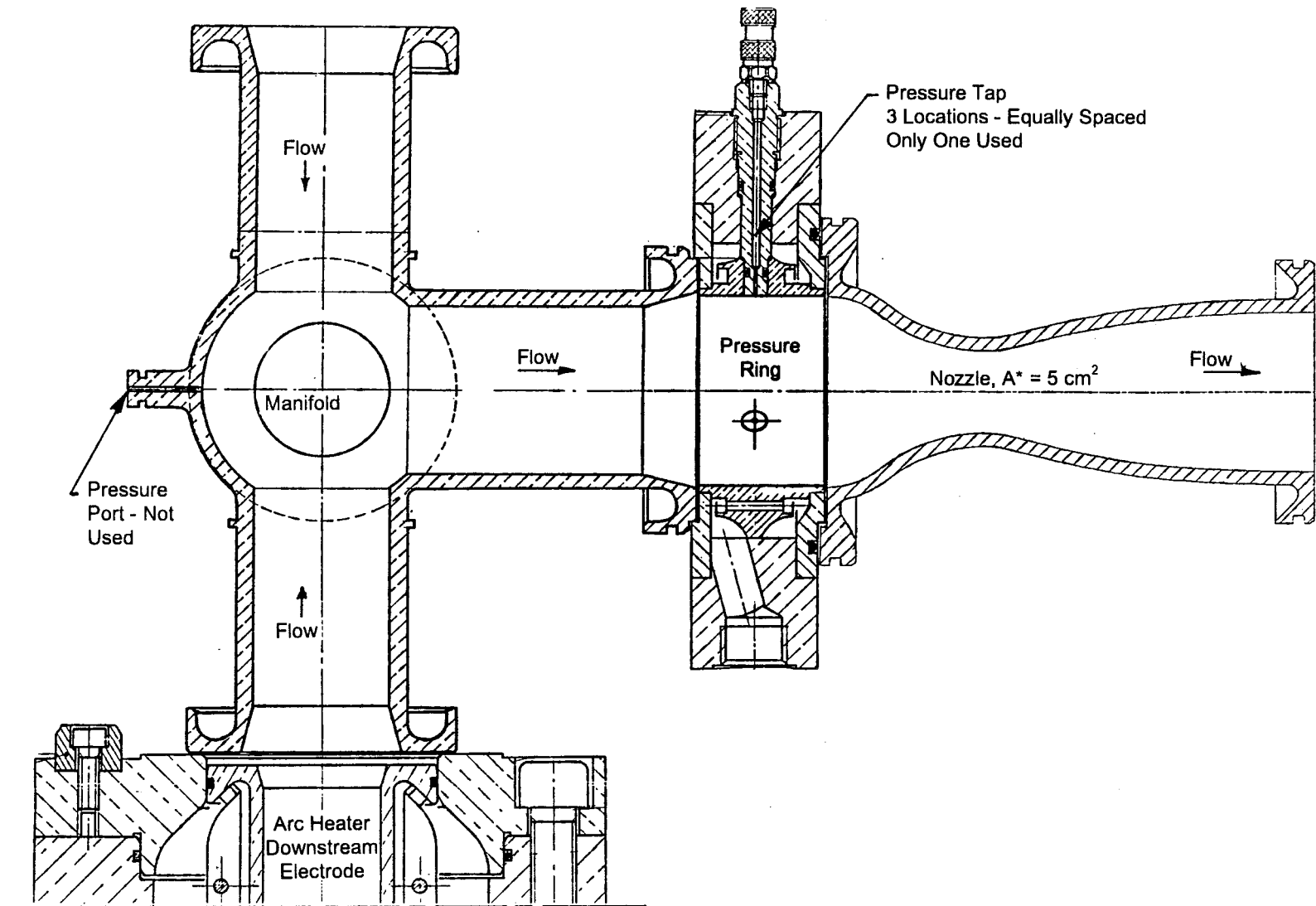
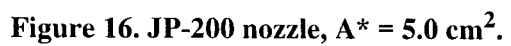
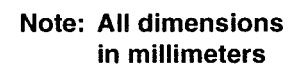
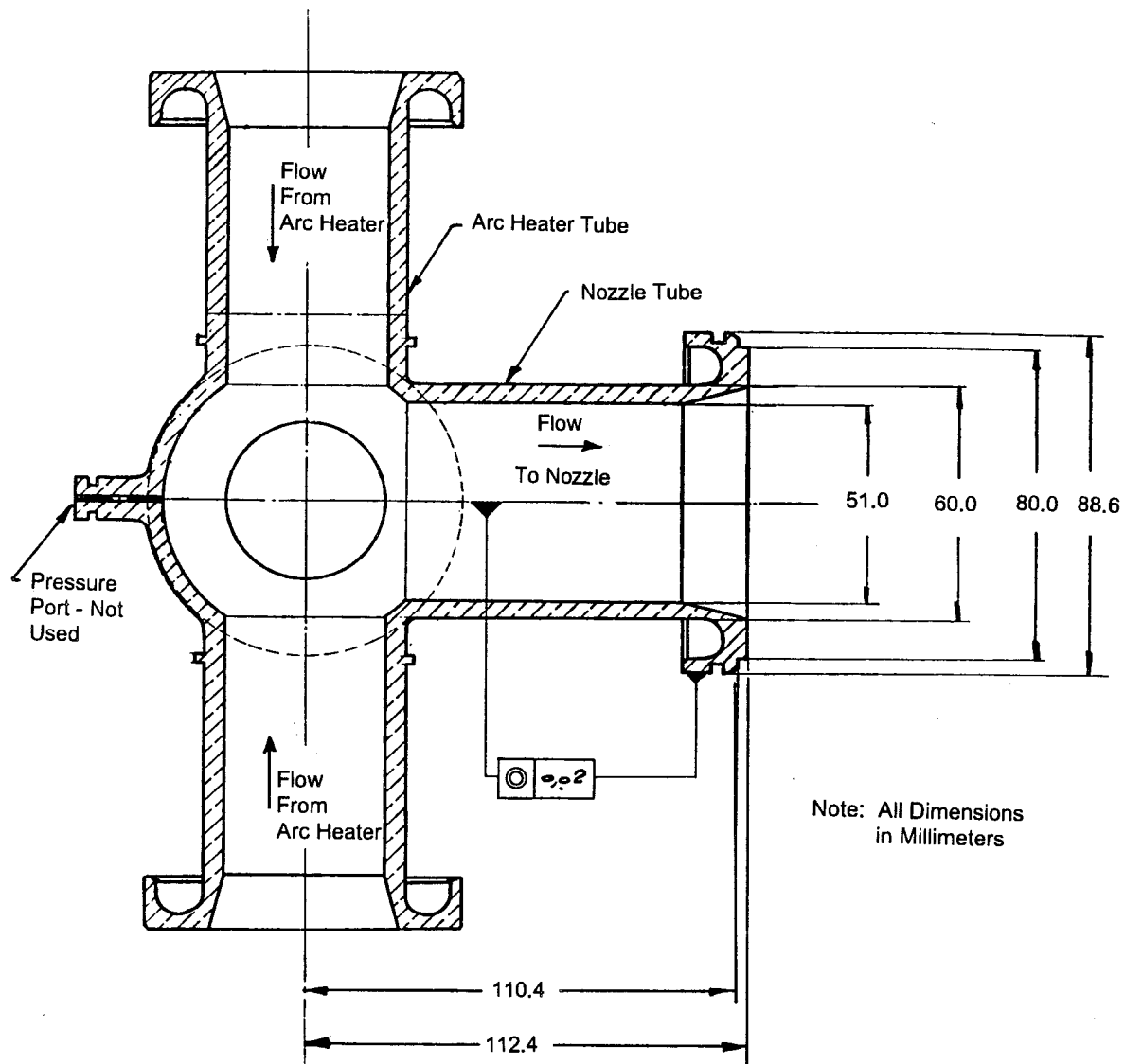


Figure 15. Assembly view of arc heater, manifold, pressure ring, and nozzle.

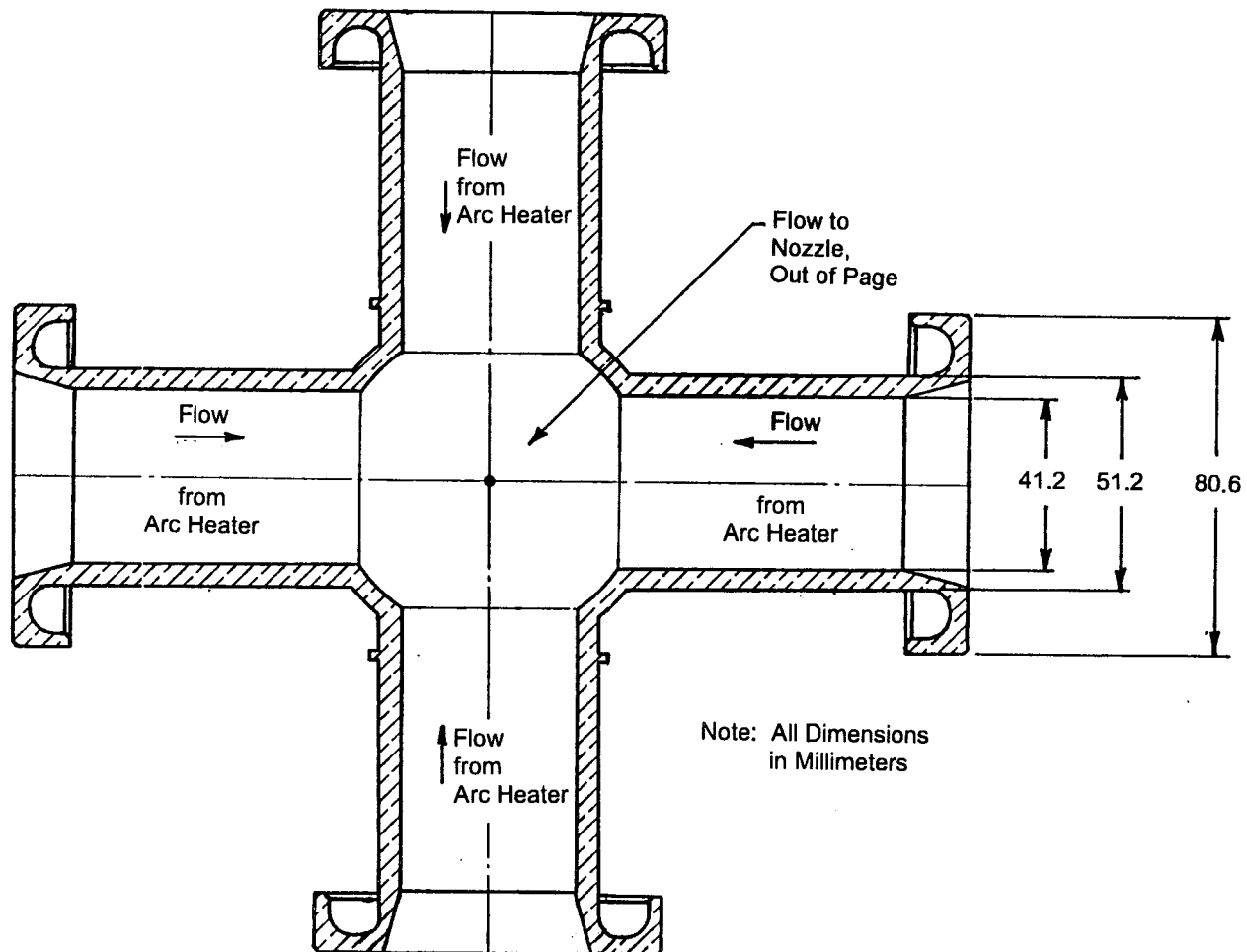




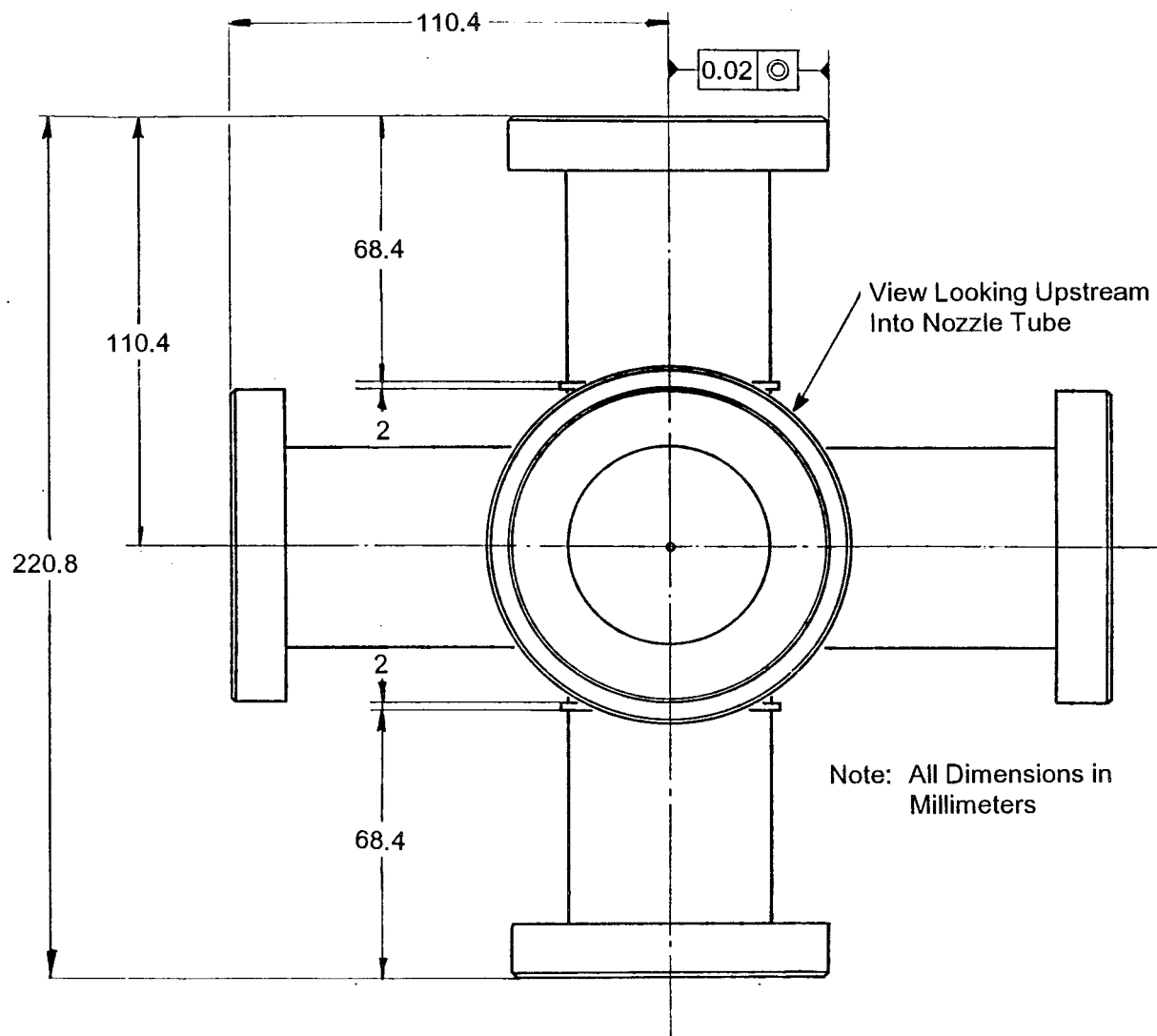
**Figure 17. JP-200 nozzle,  $A^* = 2.5 \text{ cm}^2$ .**



a. Side view-showing nozzle tube  
 Figure 18. Manifold liner dimensions.



b. Front view-showing the four arc heater tubes  
Figure 18. Continued.



c. Front view-showing external dimensions of the arc heater tubes  
Figure 18. Concluded.



Supply  
Tank

Return  
Tank

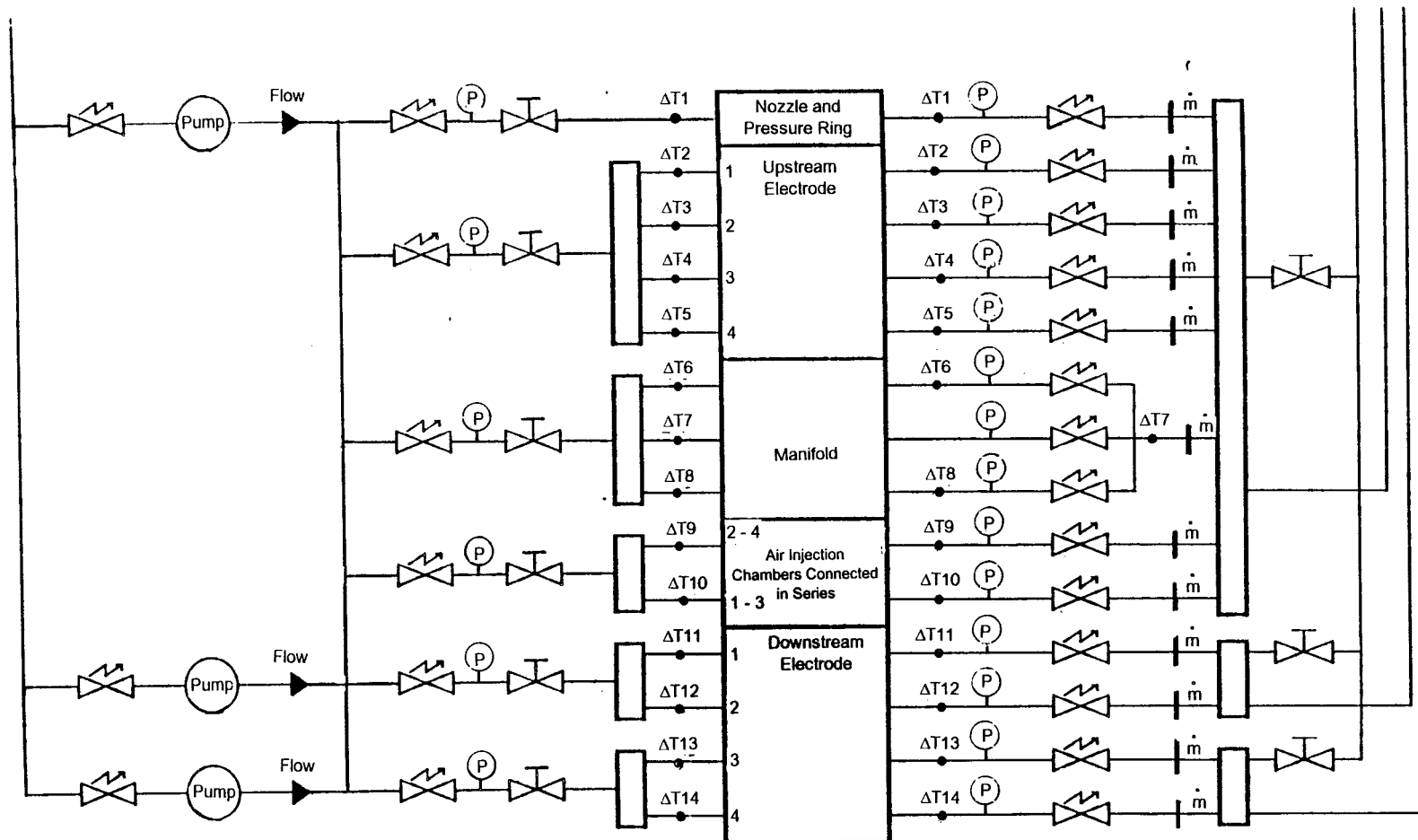


Figure 19. JP-200 Water cooling system for Runs 1506 and 1507.

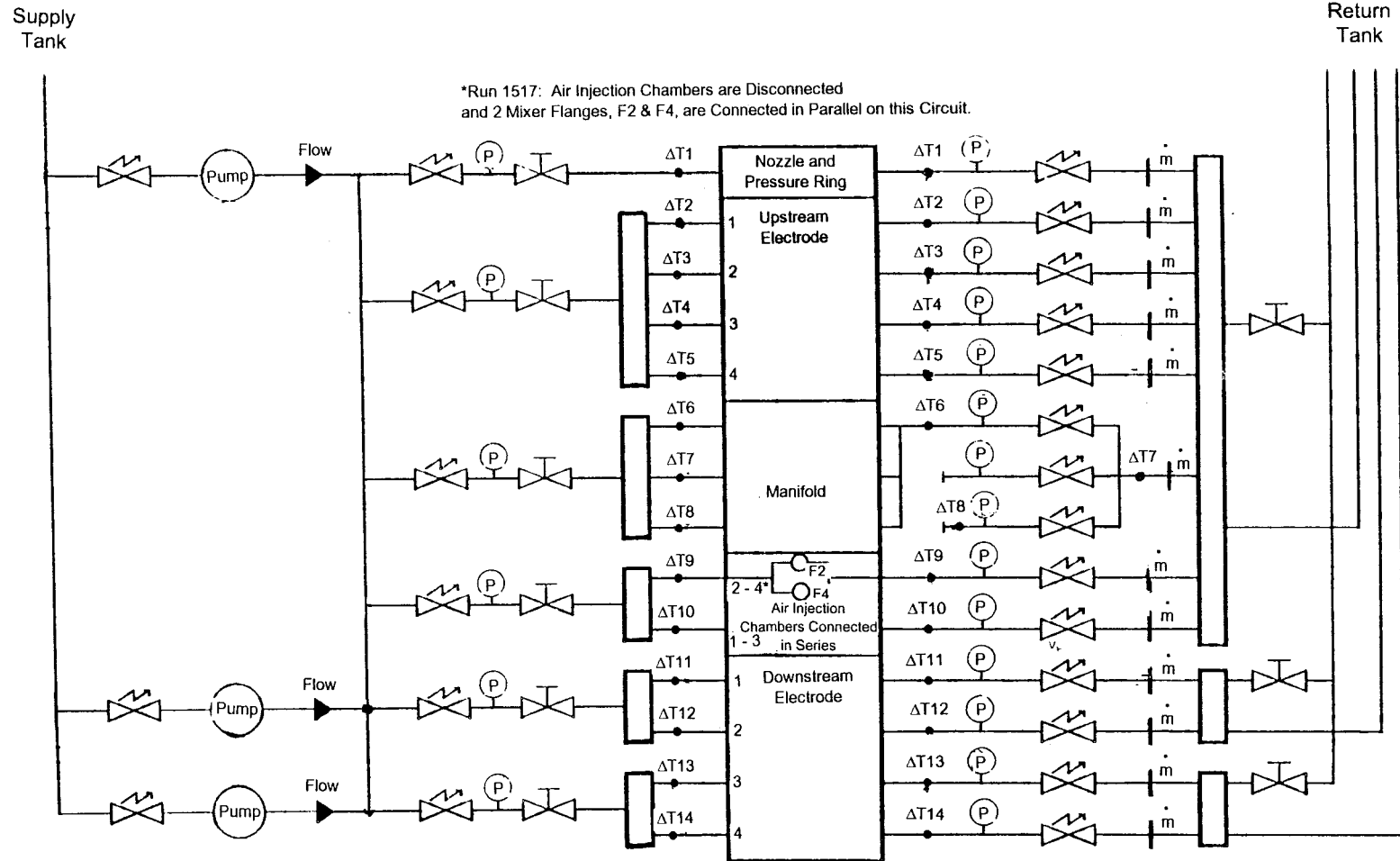


Figure 20. JP-200 Cooling water system for Runs 1508 through 1517.

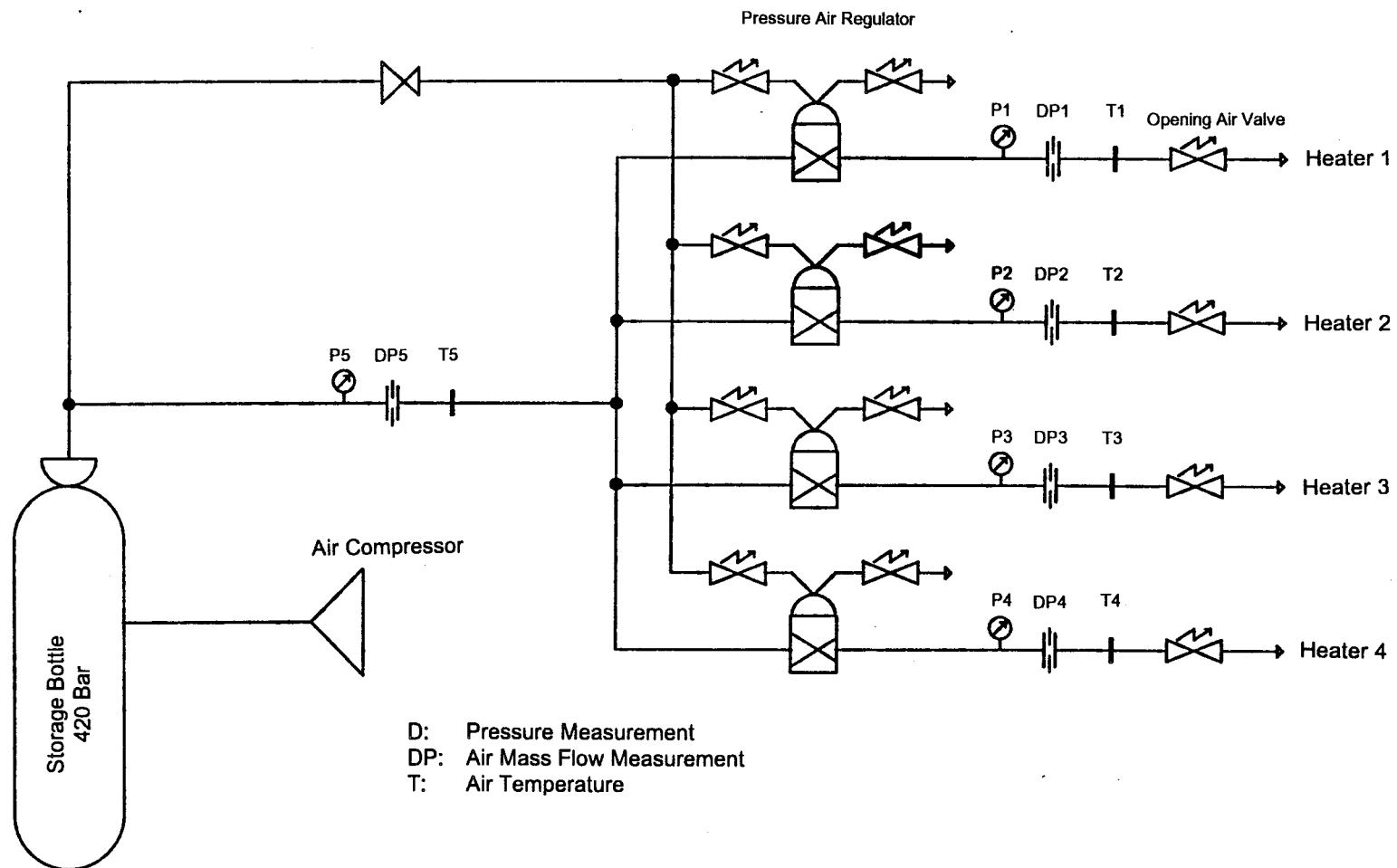
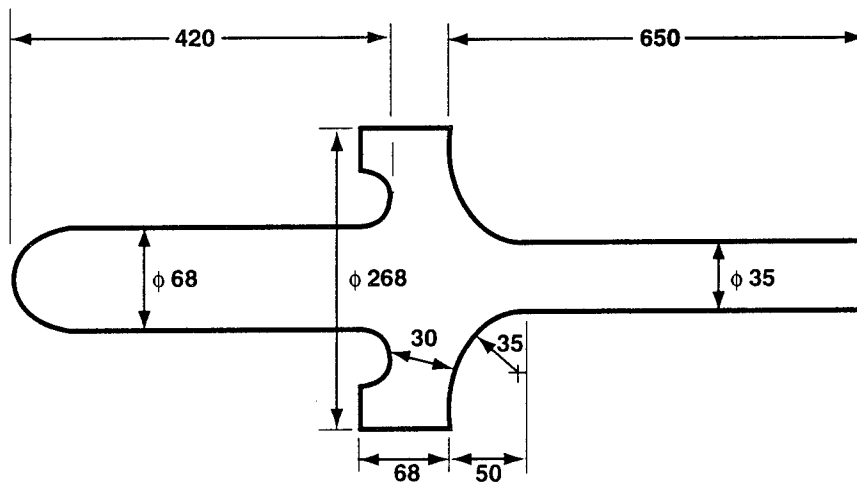
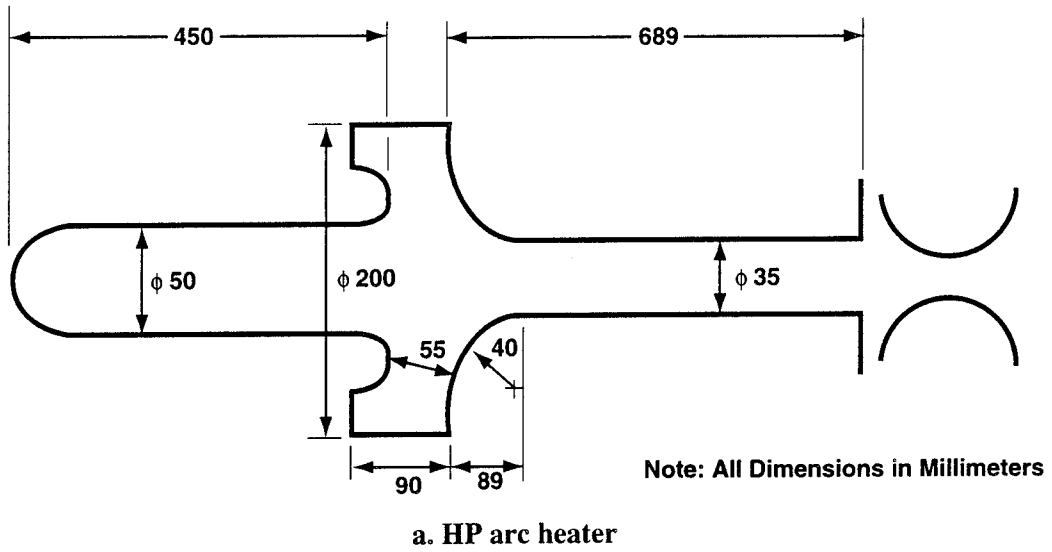


Figure 21. JP-200 high-pressure air system.



b. JP-200 arc heater (all four identical)  
Figure 22. Heater geometry comparison.

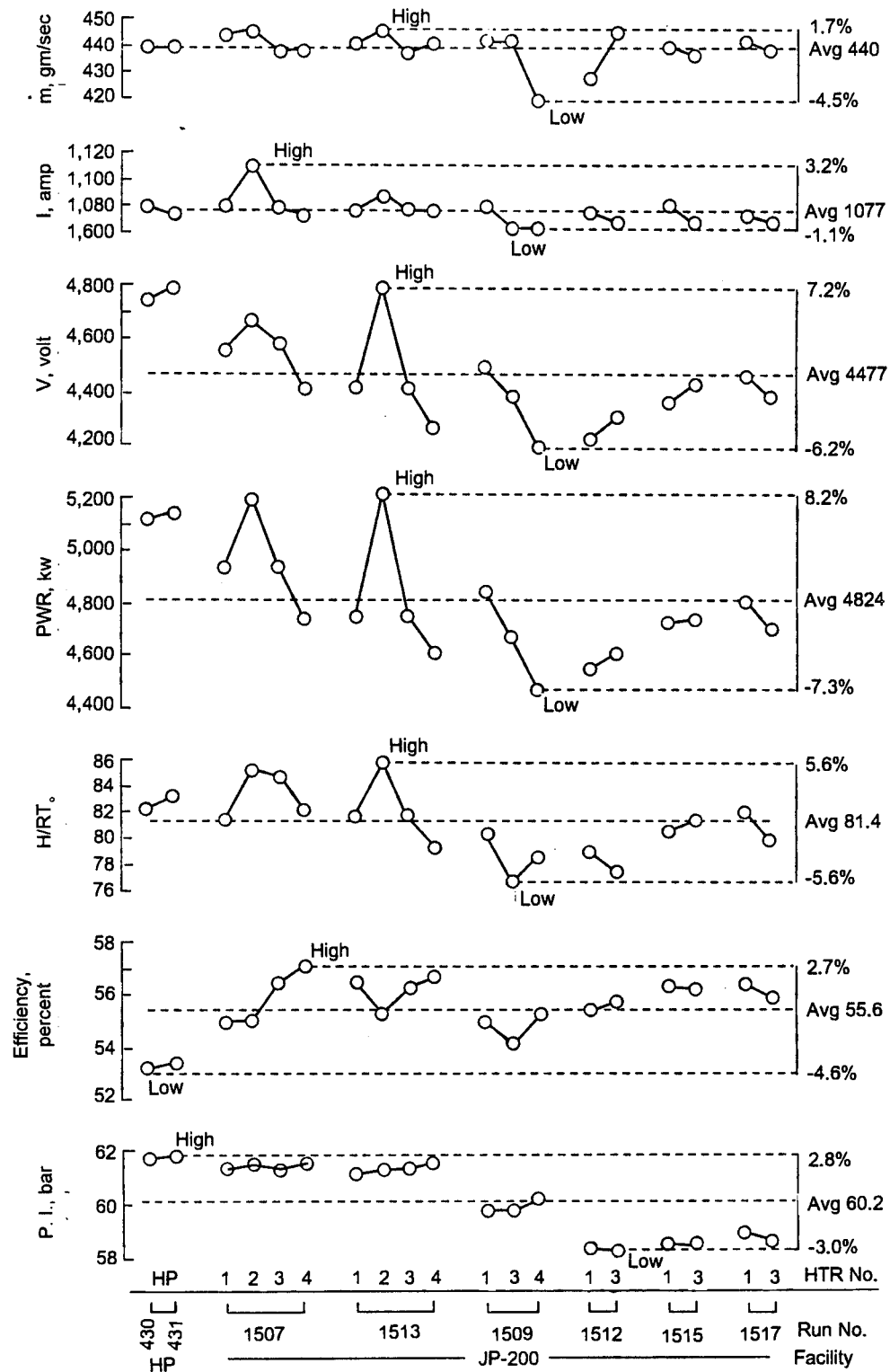


Figure 23. Individual arc heater performance at cathode exit.

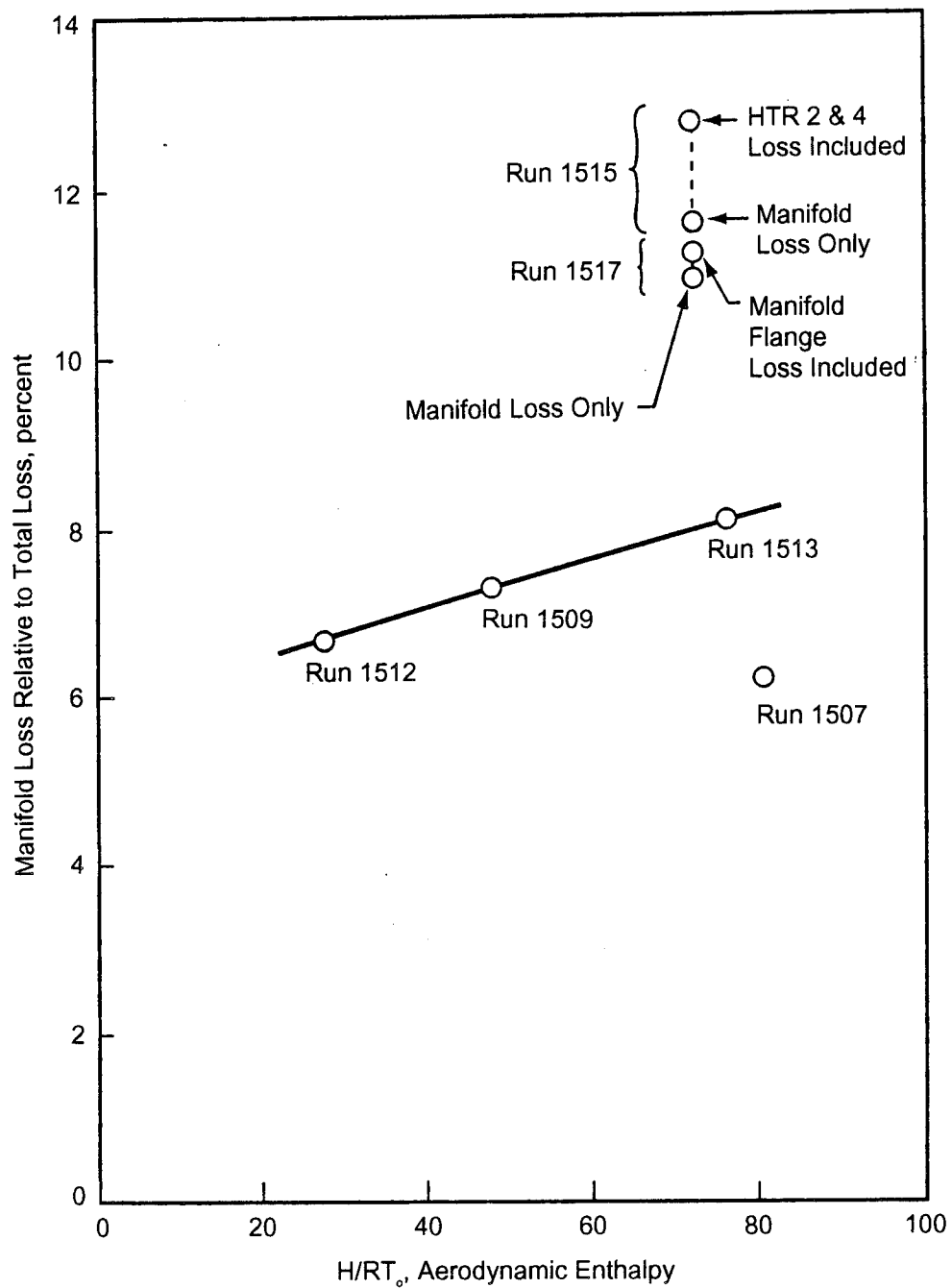


Figure 24. JP-200 manifold thermal loss relative to the total loss.

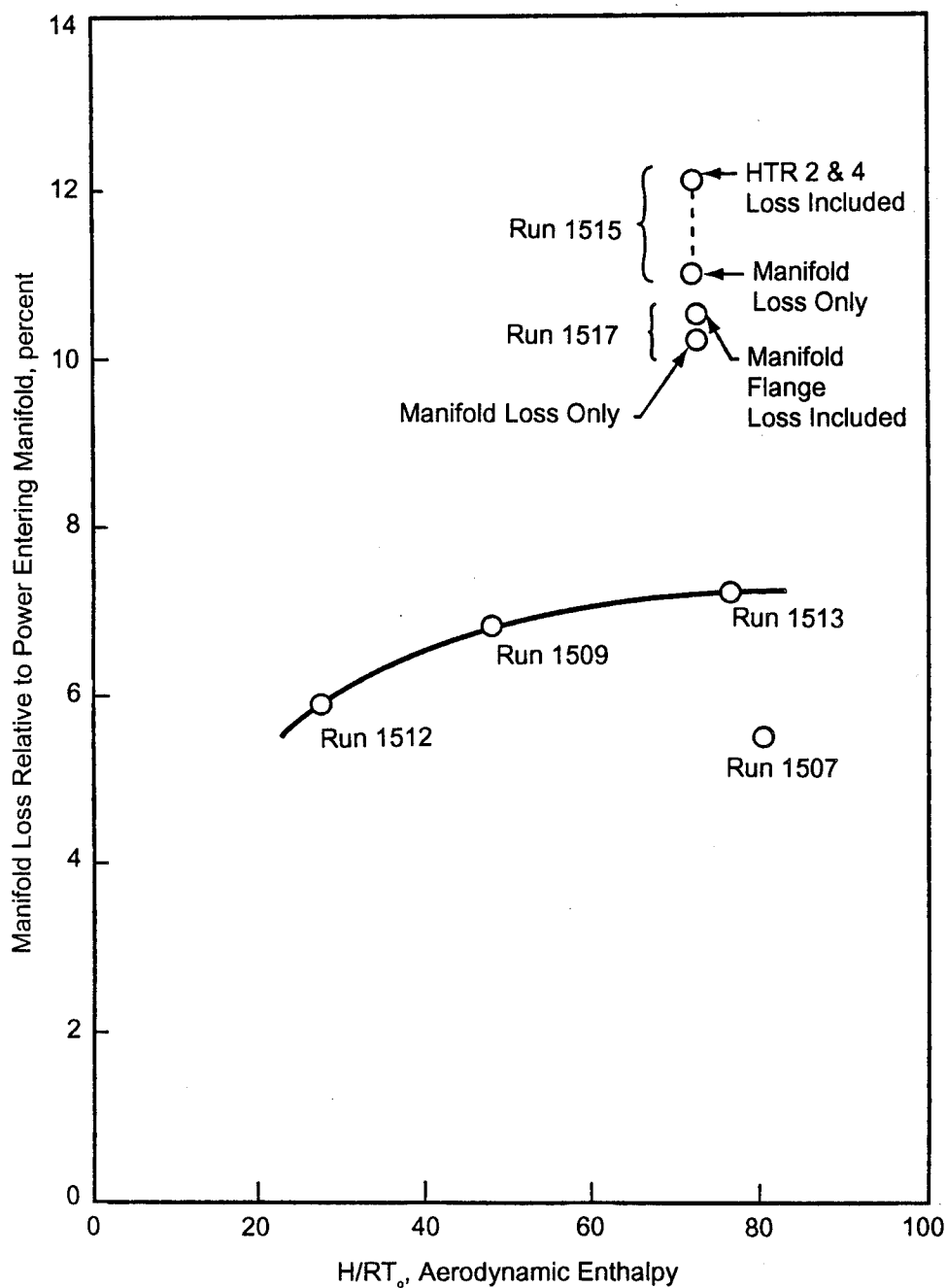


Figure 25. JP-200 manifold thermal loss relative to the power in the gas entering the manifold.

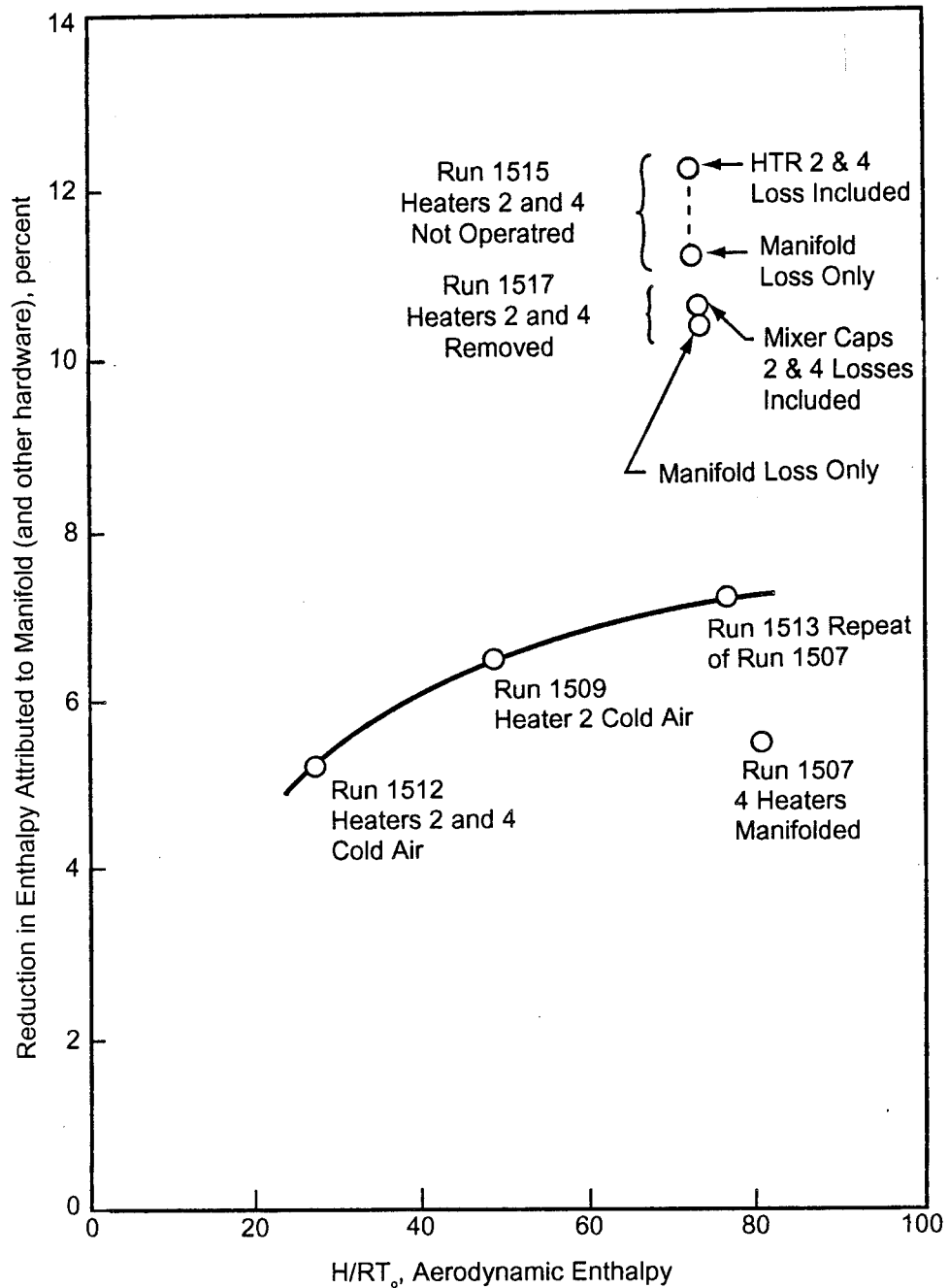


Figure 26. JP-200 percent reduction in enthalpy attributed to the manifold (and other related hardware).



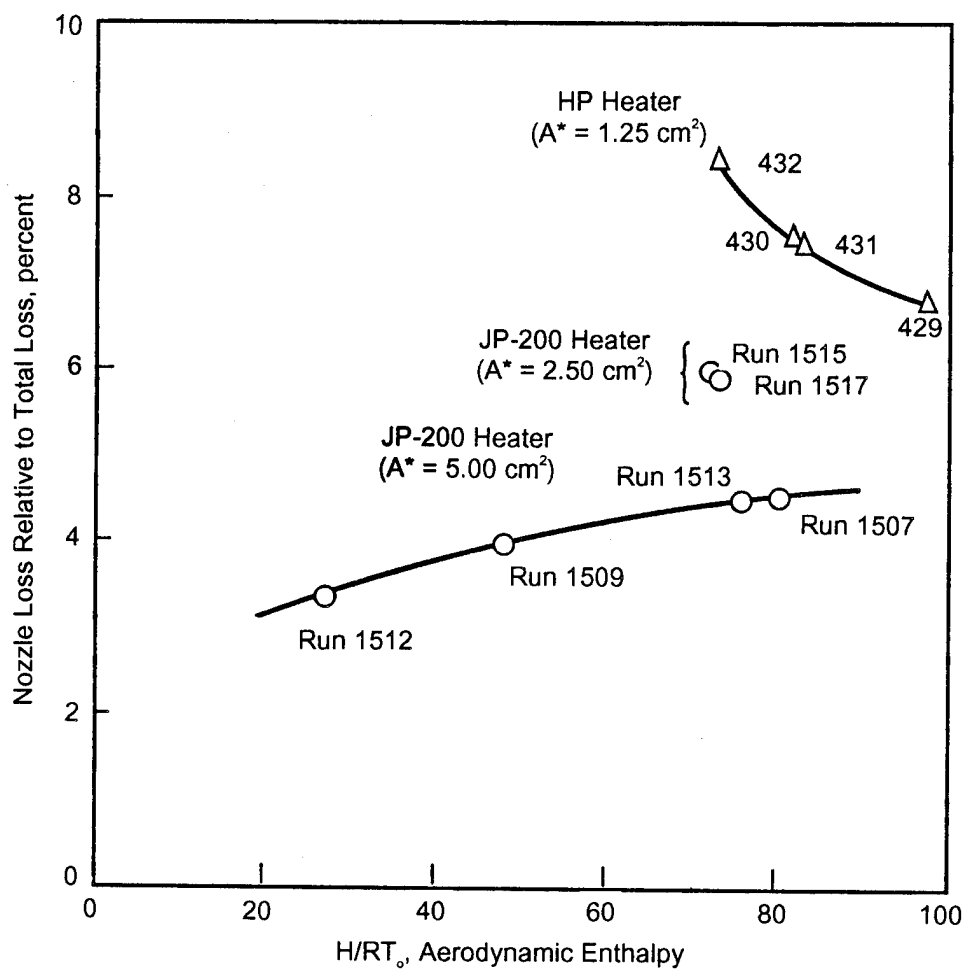


Figure 27. Nozzle thermal loss relative to the total loss.

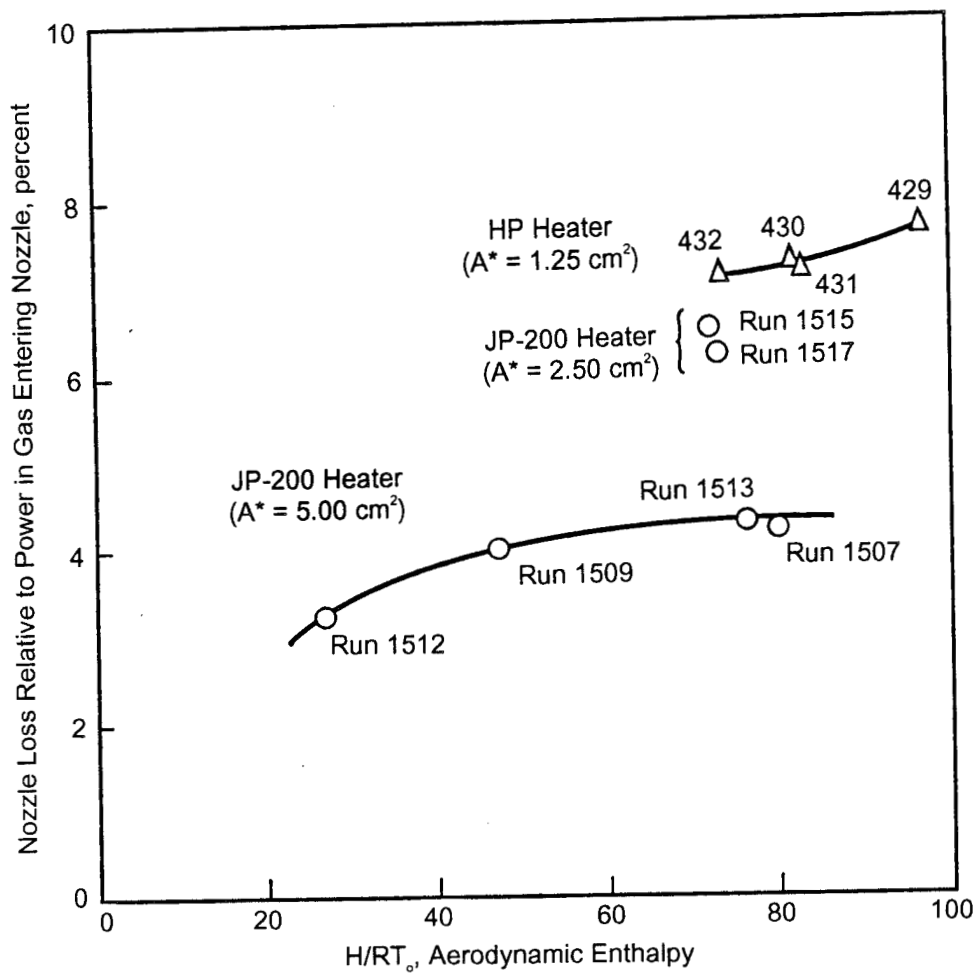


Figure 28. Nozzle thermal loss relative to the power in the gas entering the nozzle.

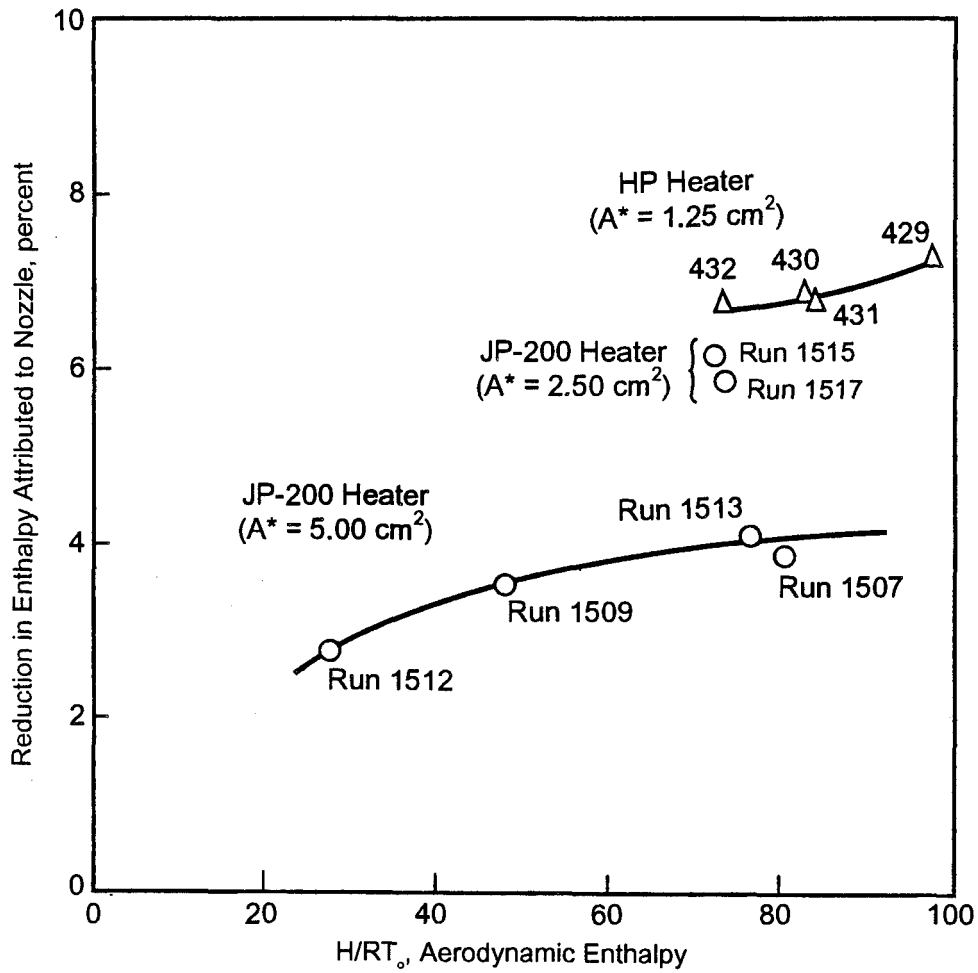


Figure 29. Percent reduction in enthalpy attributed to the nozzle.

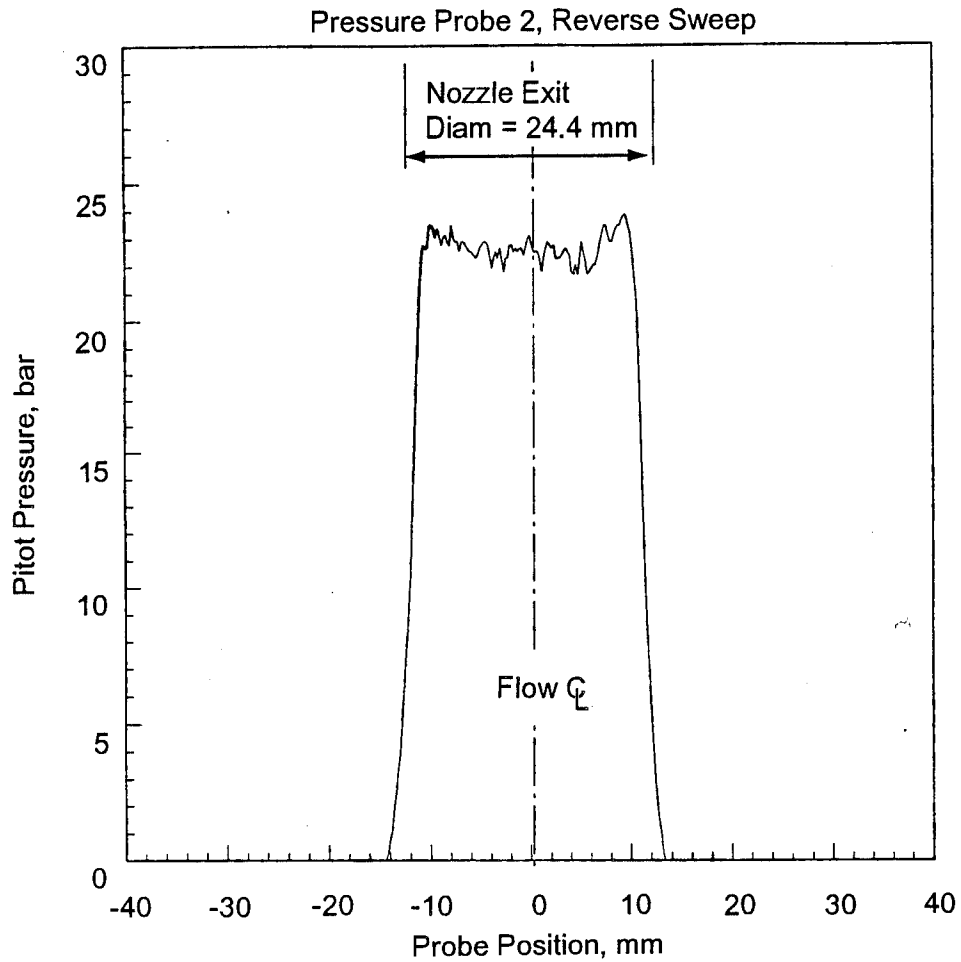


Figure 30. Pitot pressure probe data for HP Run 430.

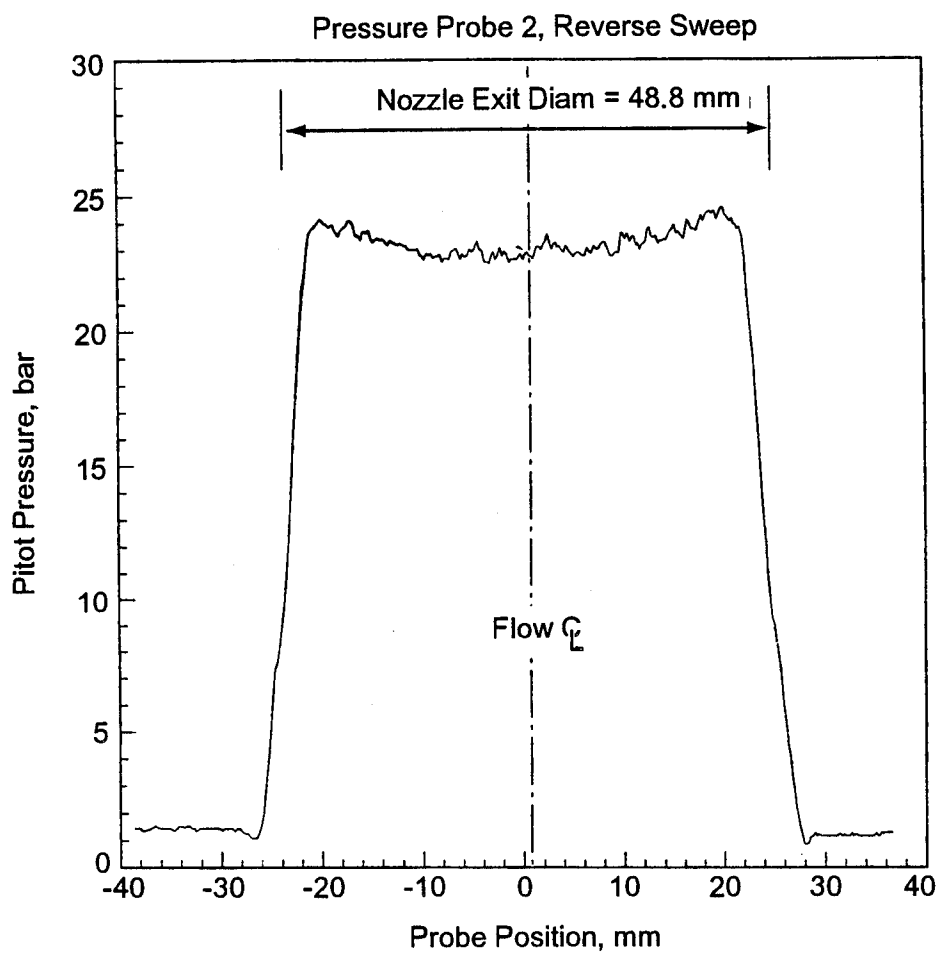


Figure 31. Pitot pressure probe data for JP-200 Run 1513.

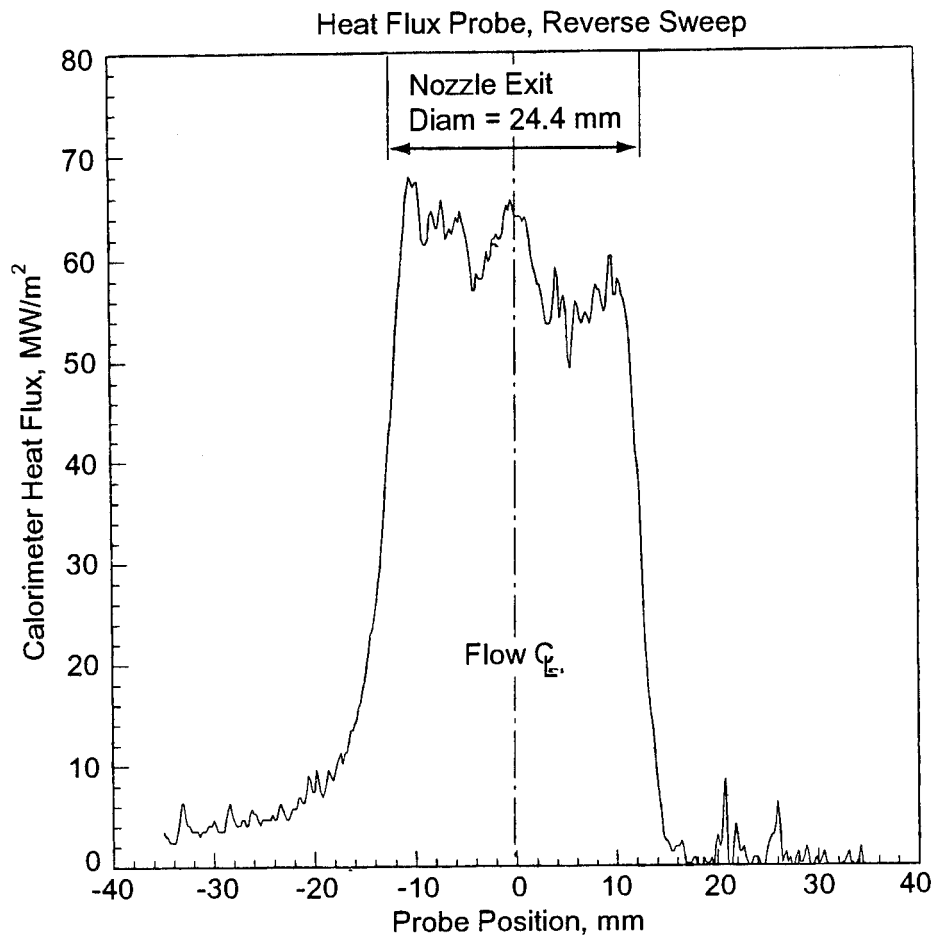


Figure 32. Heat flux probe data for HP Run 430.

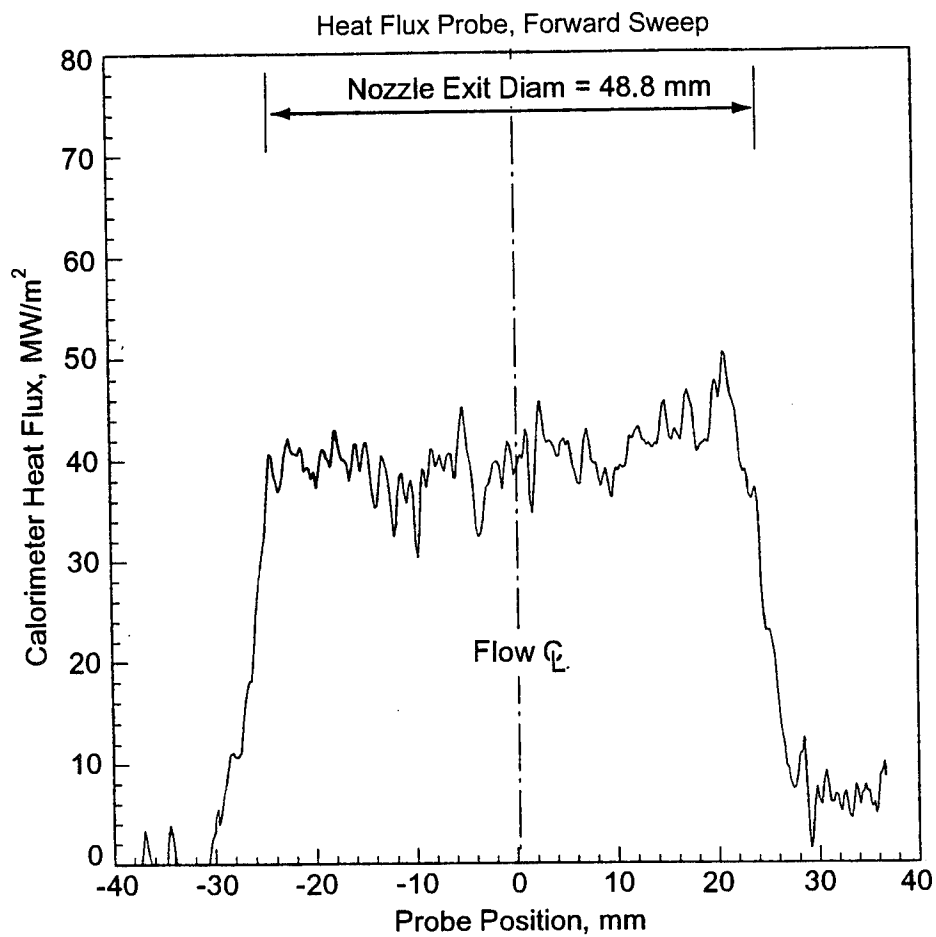
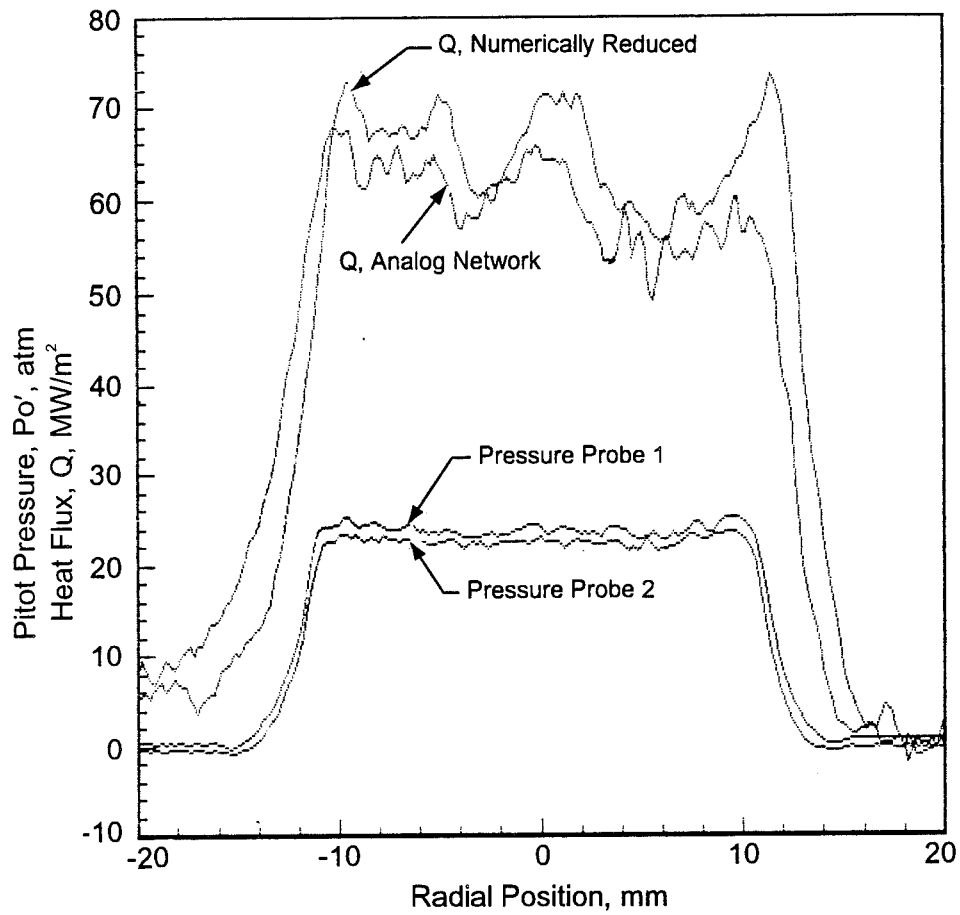


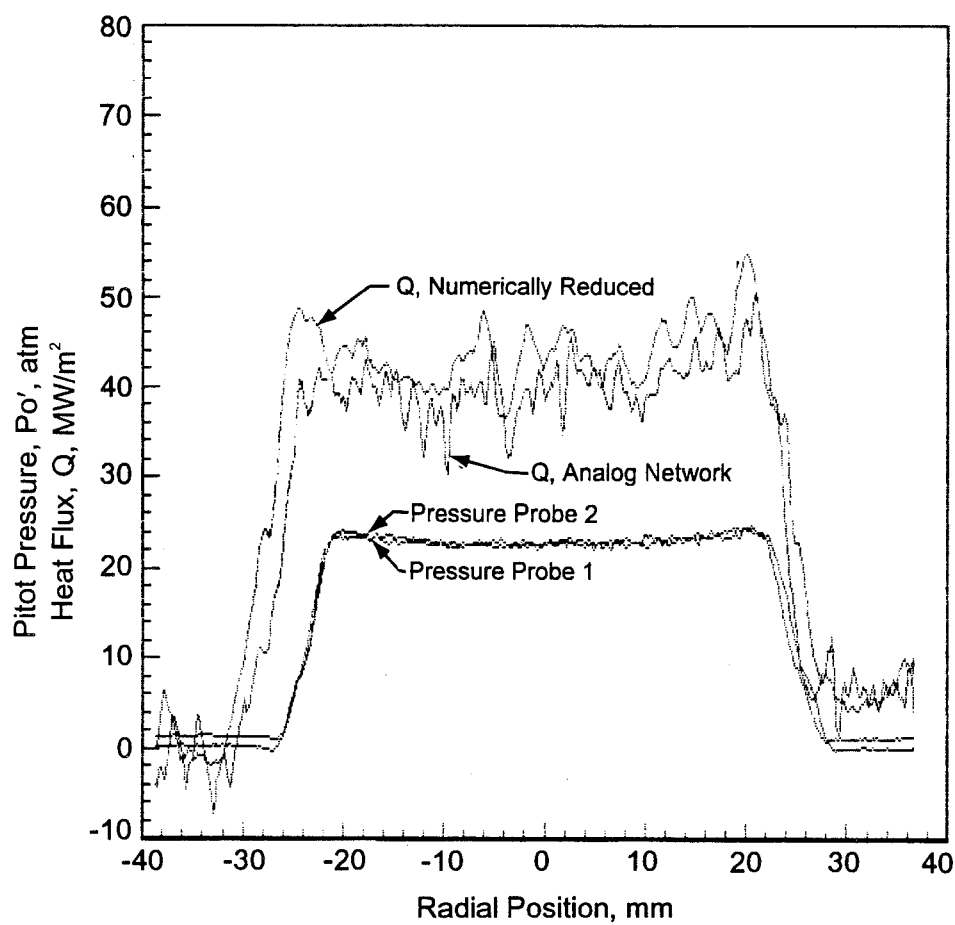
Figure 33. Heat flux probe data for JP-200 Run 1513.



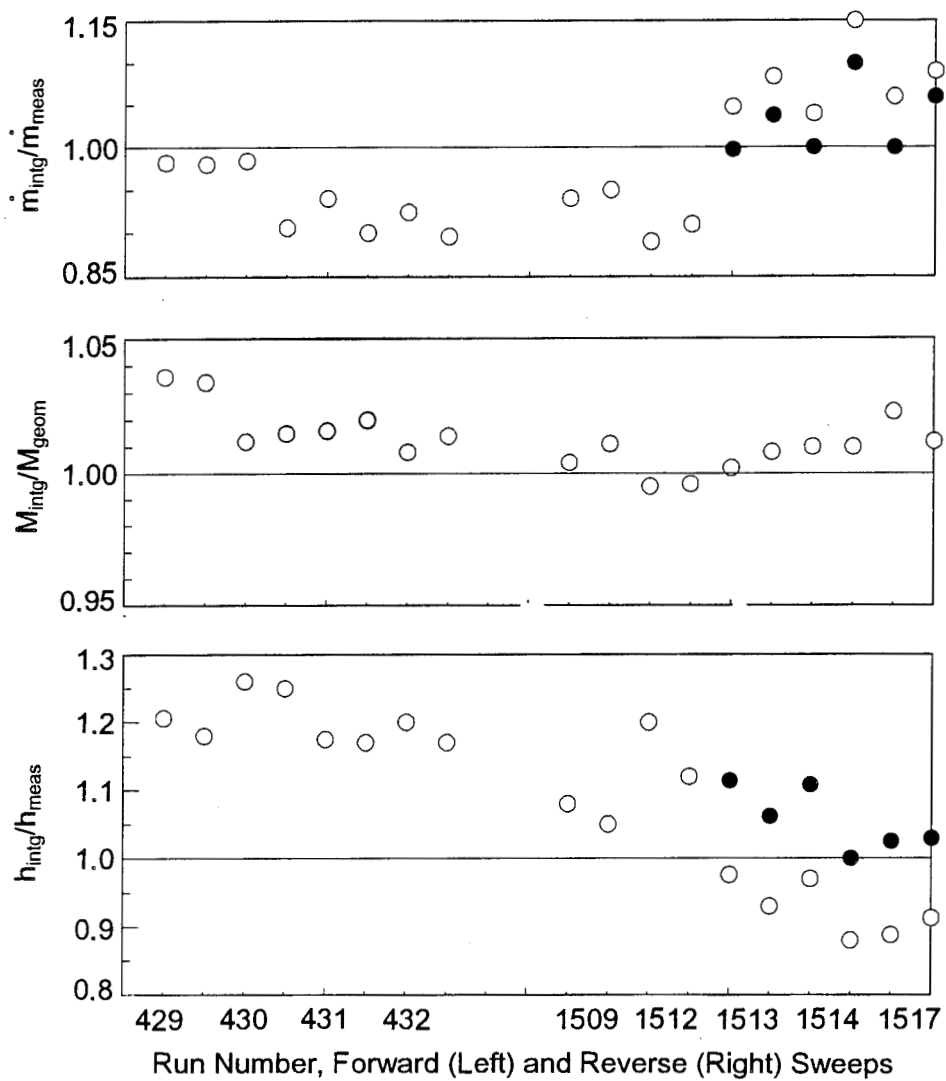
a. Run HP430, reverse sweep

Figure 34. Typical pressure and heat flux profiles.

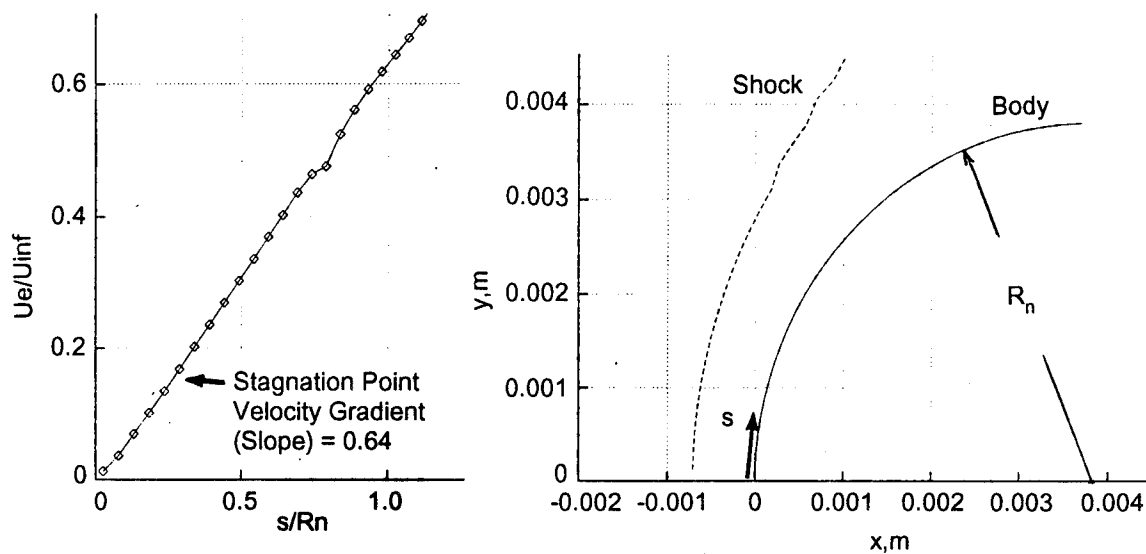




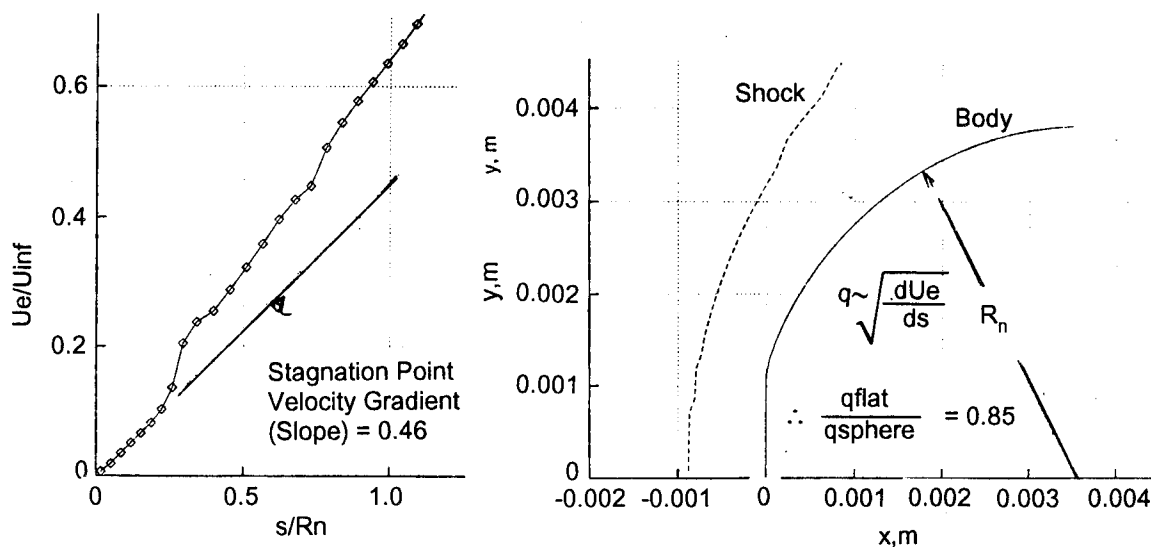
b. Run JP 1513, forward sweep  
Figure 34. Concluded.



**Figure 35.** Ratios of integrated probe data quantities to measured bulk data quantities (solid symbols include bluntness correction).

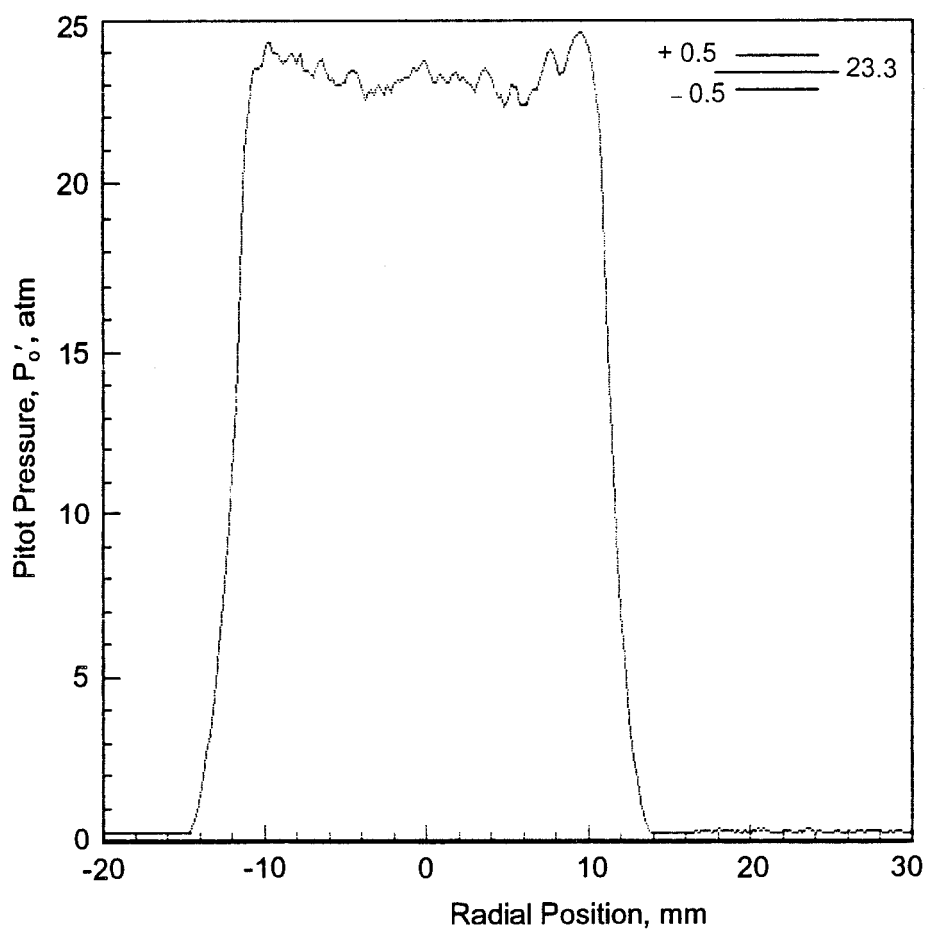


a. Hemisphere:  $(dU_e/U_{\infty}) / (d s/R_n) = 0.64$



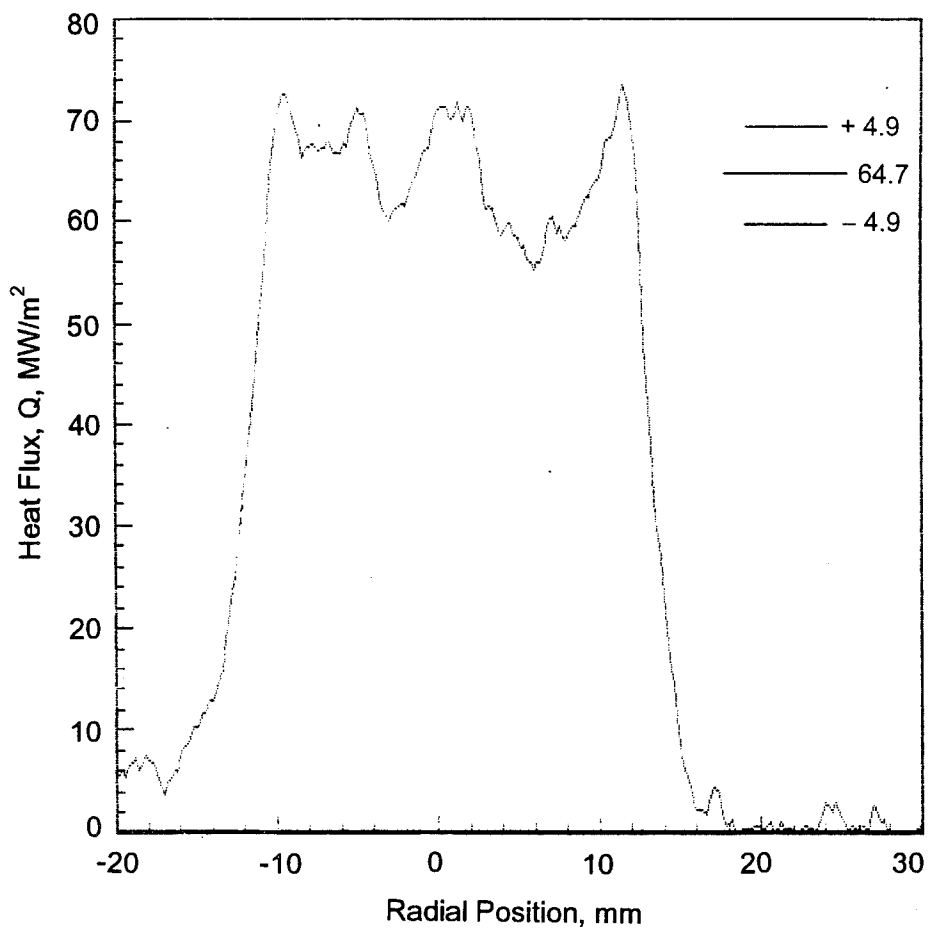
b. Flattened hemisphere:  $(dU_e/U_{\infty}) / (d s/R_n) = 0.46$

Figure 36. The effect of a flattened nose on stagnation point heat transfer.

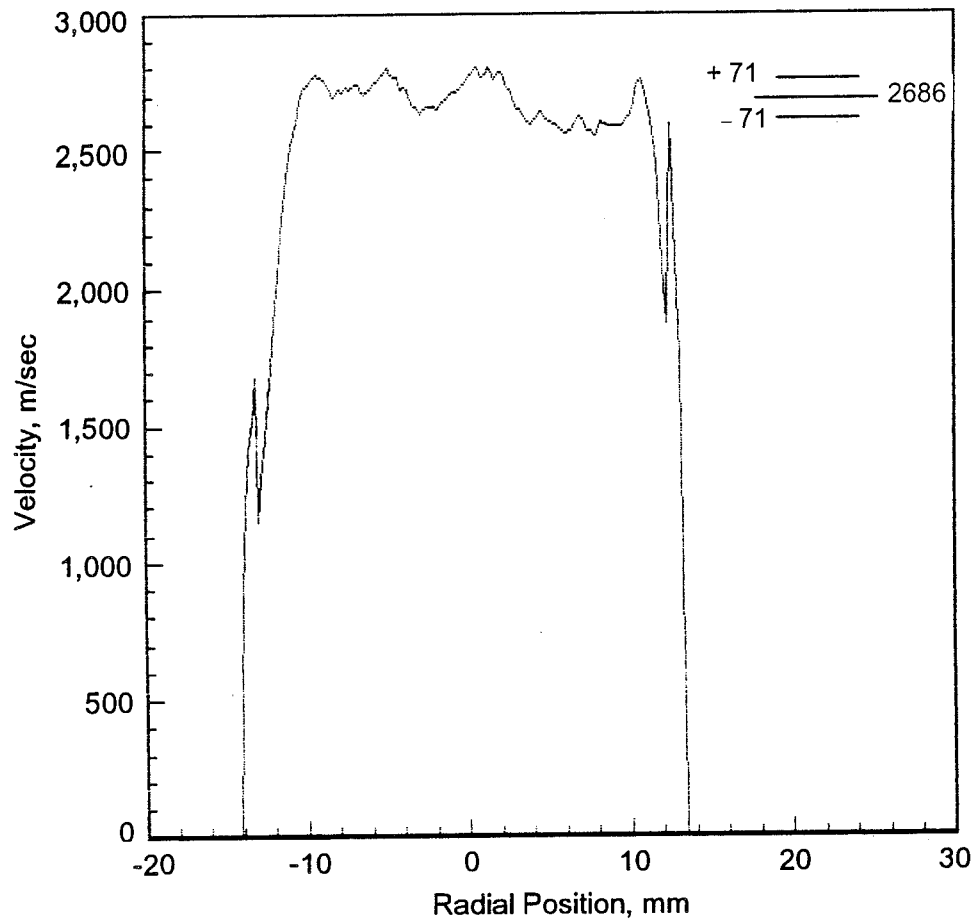


a. Pitot pressure (average of Probes 1 and 2)

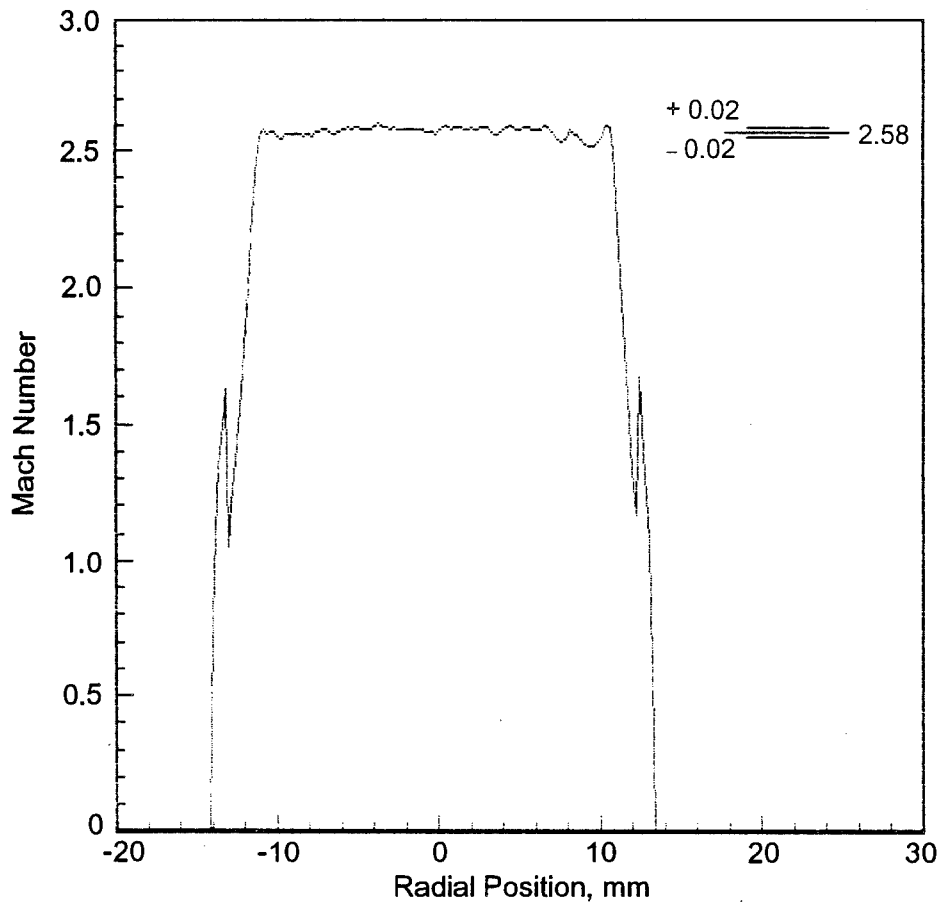
Figure 37. Profiles for Run HP430, reverse sweep; mean value  $\pm$  one standard deviation shown (computed over  $r = \pm 8$  mm).



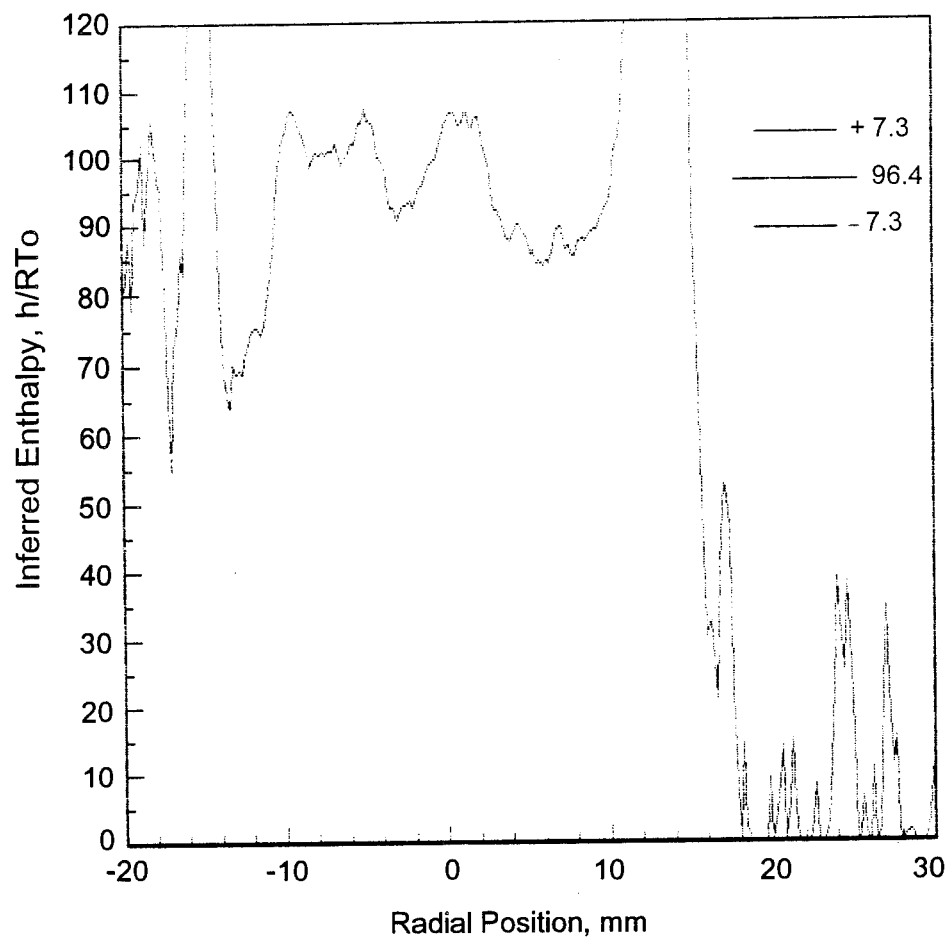
b. Heat flux  
Figure 37. Continued.



c. Velocity  
Figure 37. Continued.

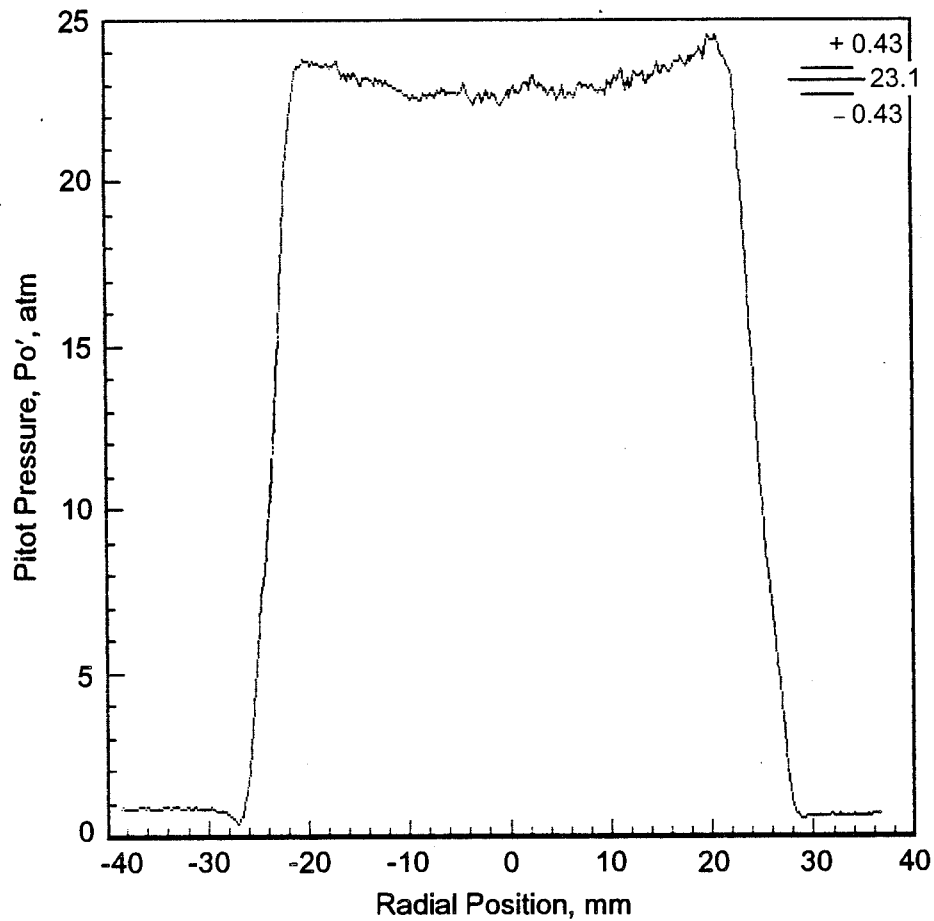


d. Mach number  
Figure 37. Continued.



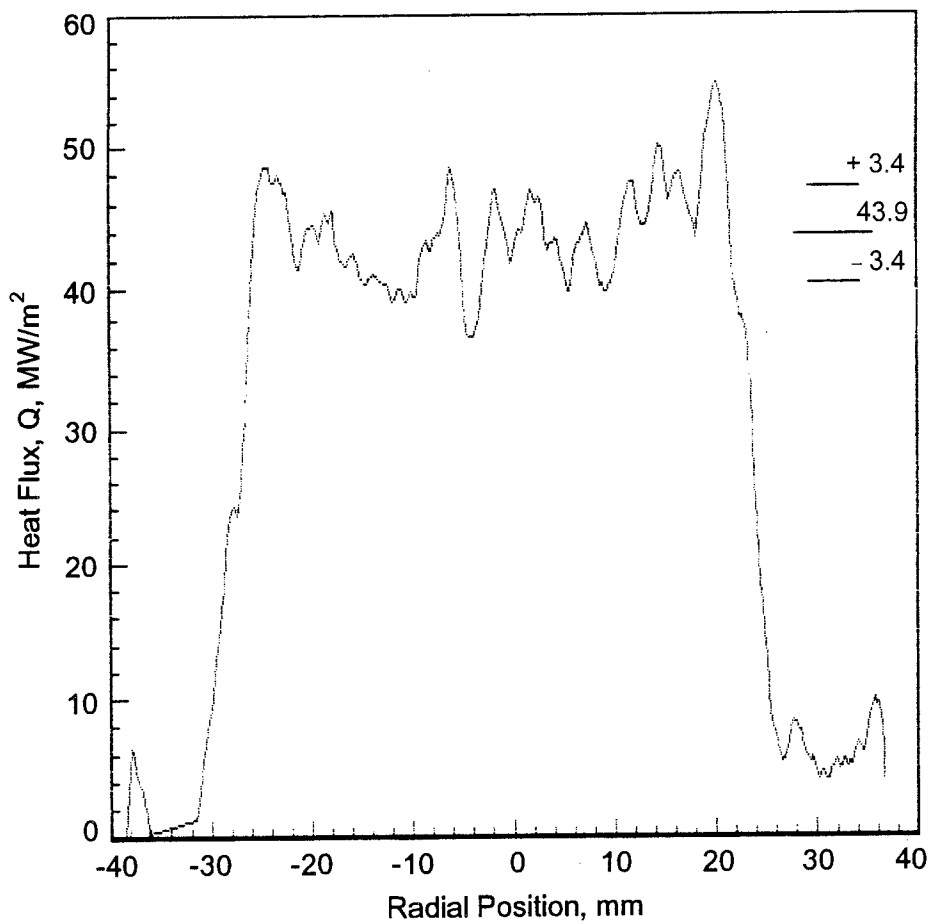
e. Inferred enthalpy  
Figure 37. Concluded.



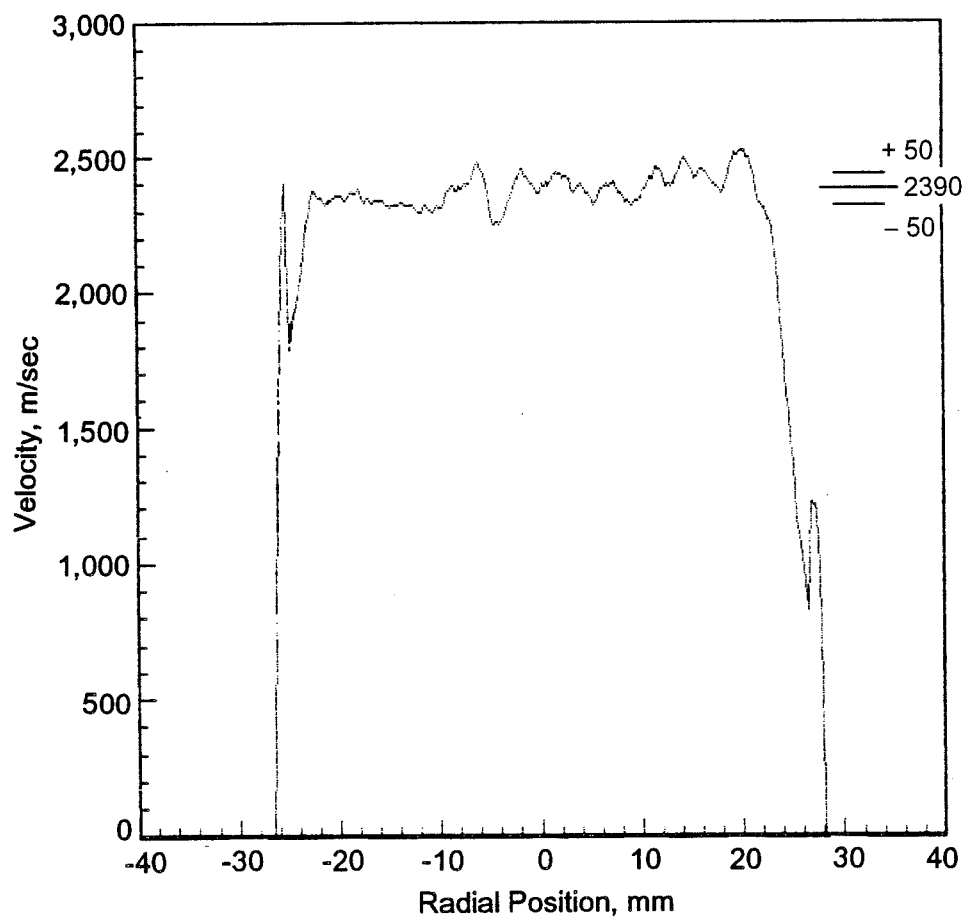


a. Pitot pressure (average of Probes 1 and 2)

Figure 38. Profiles for Run HP430, reverse sweep; mean value  $\pm$  one standard deviation shown (computed over  $r = \pm 20$  mm).

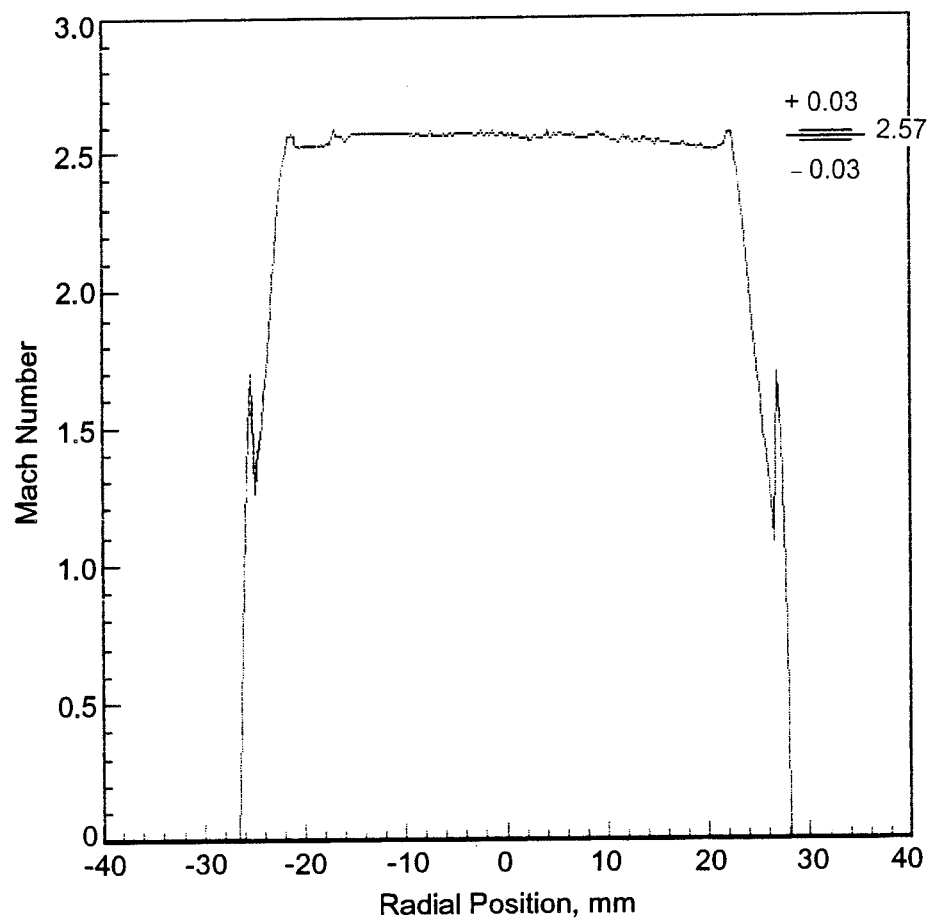


b. Heat flux  
Figure 38. Continued.

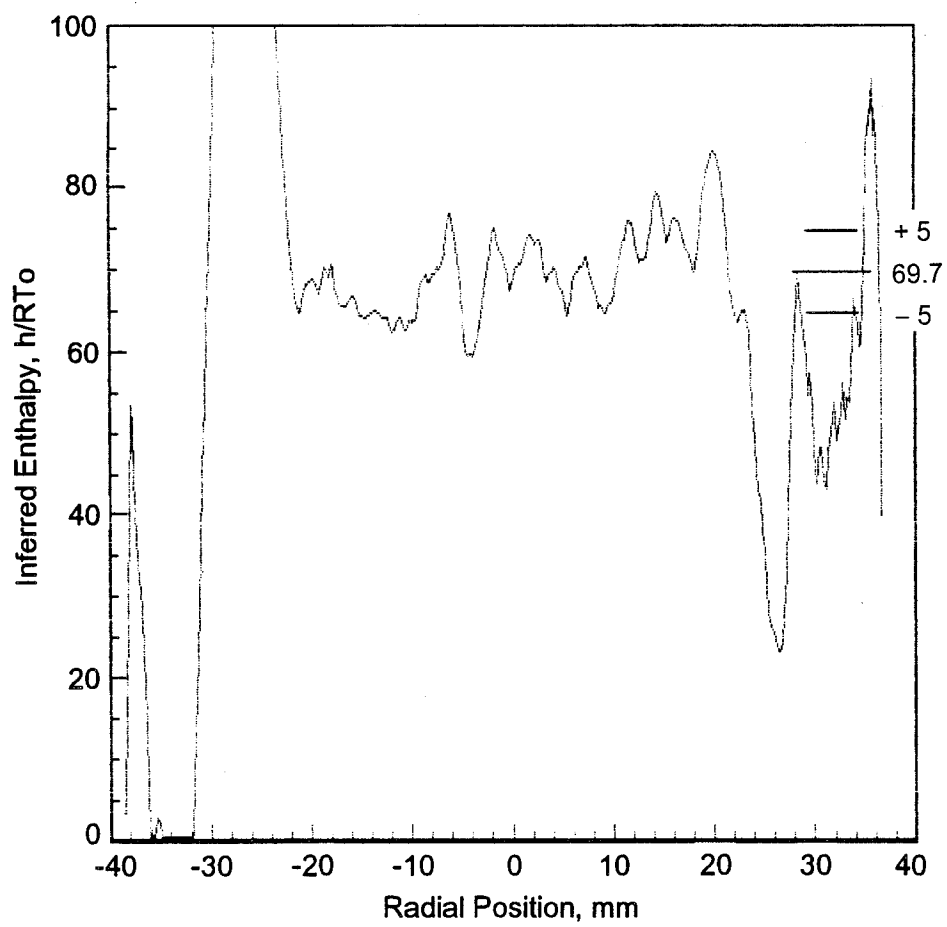


c. Velocity

Figure 38. Continued.



d. Mach number  
Figure 38. Continued.



e. Inferred enthalpy  
Figure 38. Concluded.

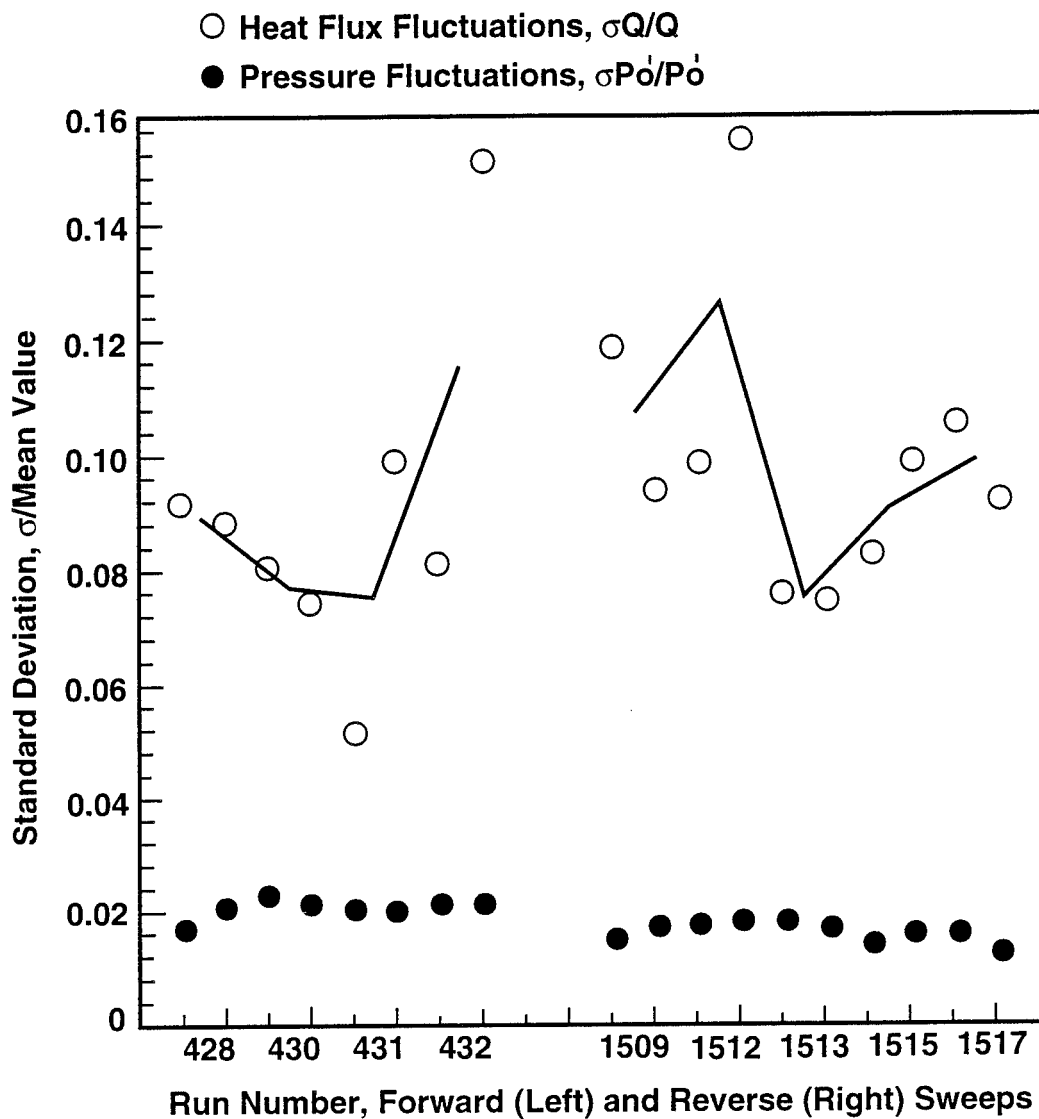


Figure 39. Standard deviation expressed as a fraction of the parameter; pressure,  $\sigma P_o'/P_o'$ , and heat flux,  $\sigma Q/Q$ .

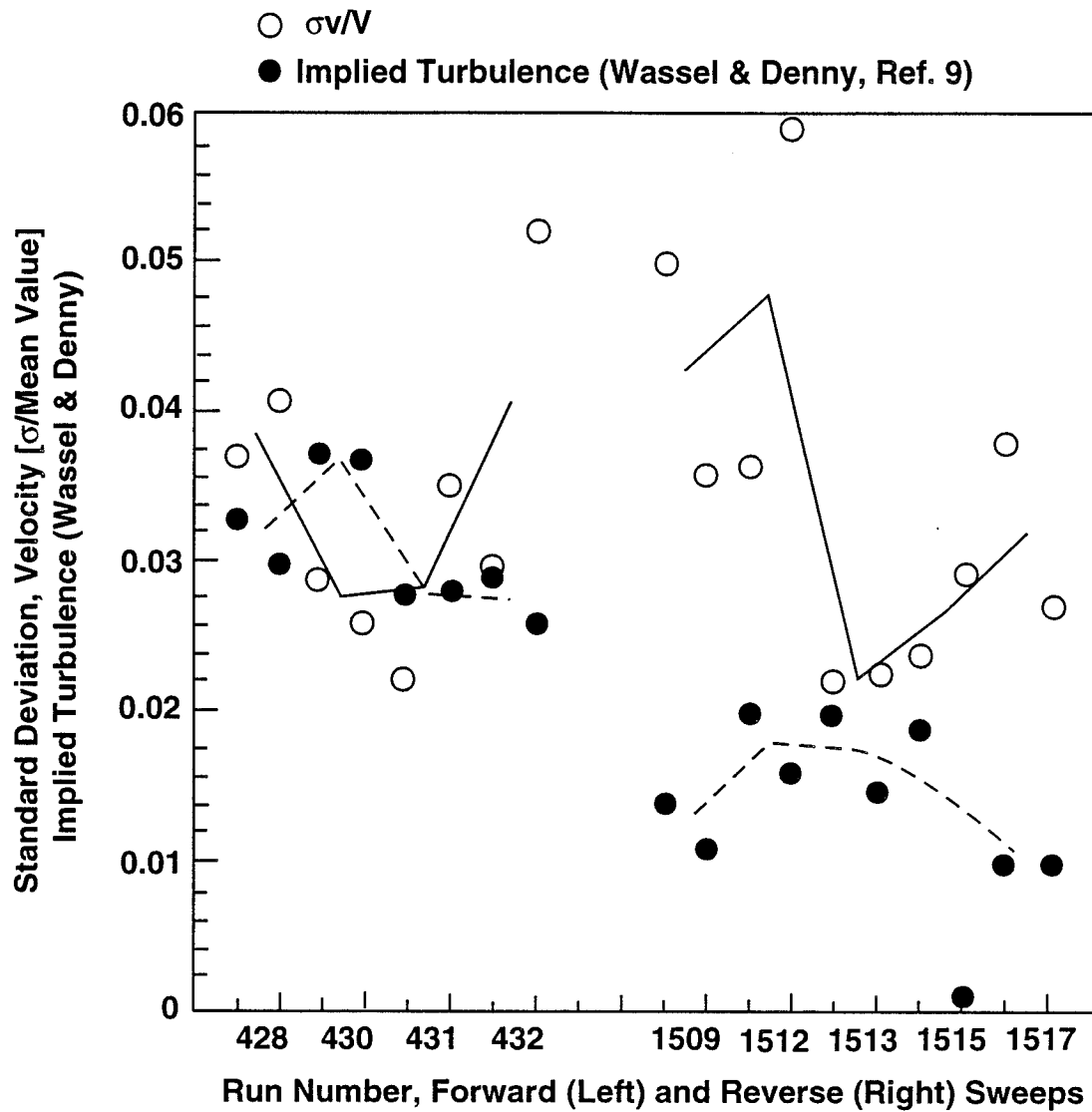


Figure 40. Velocity fluctuations (standard deviation) compared with the implied turbulence based on the measured enthalpy enhancement.

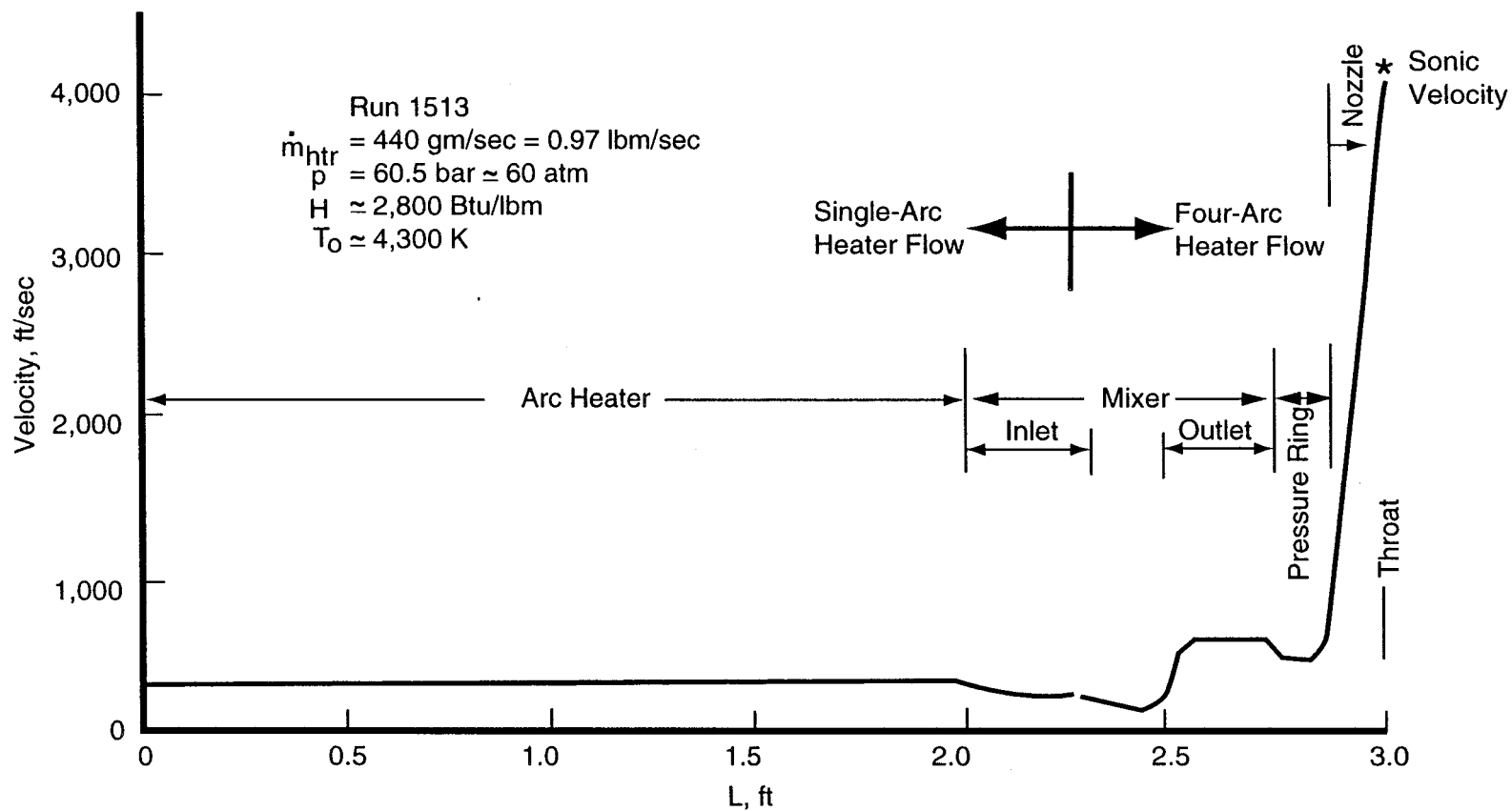
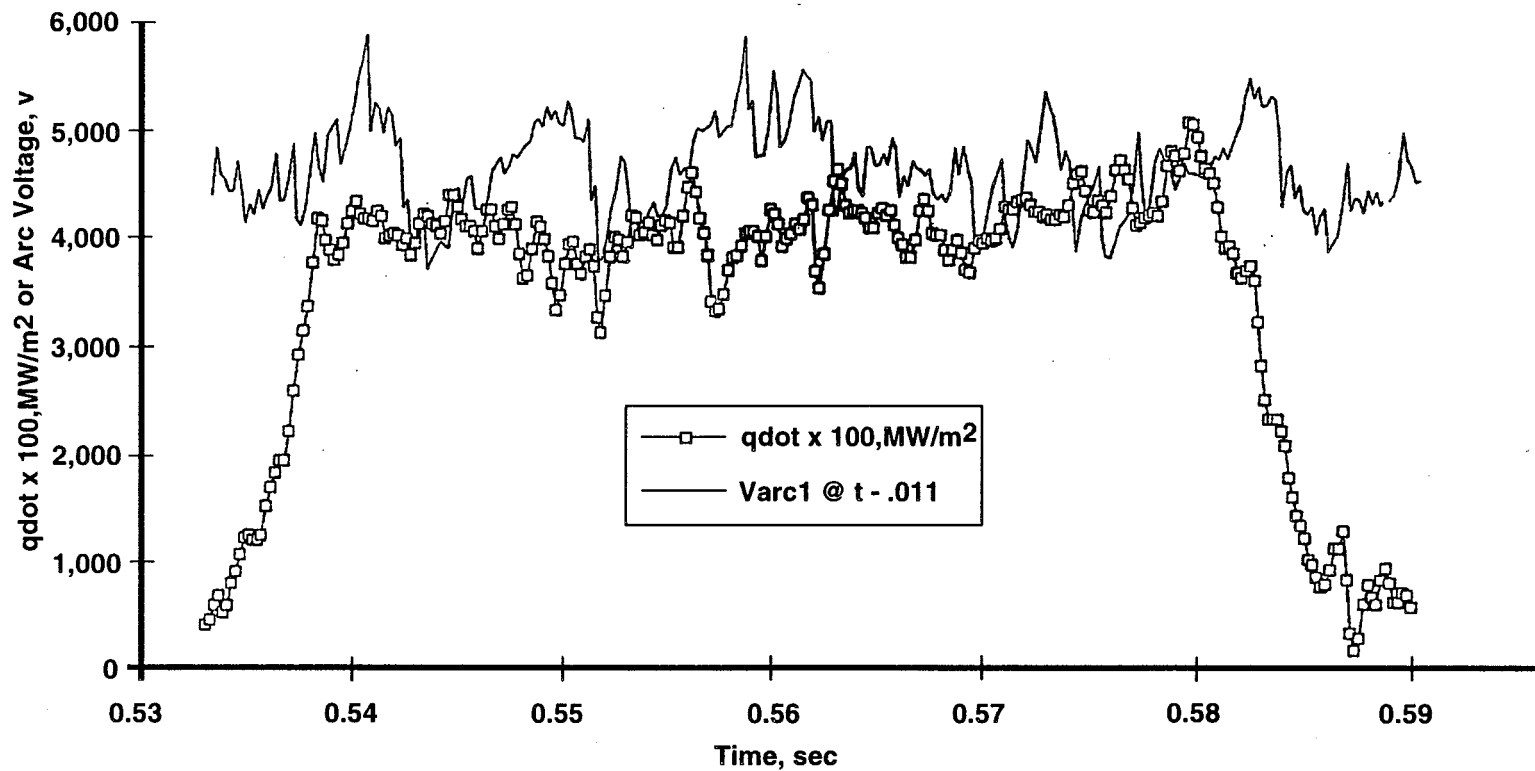
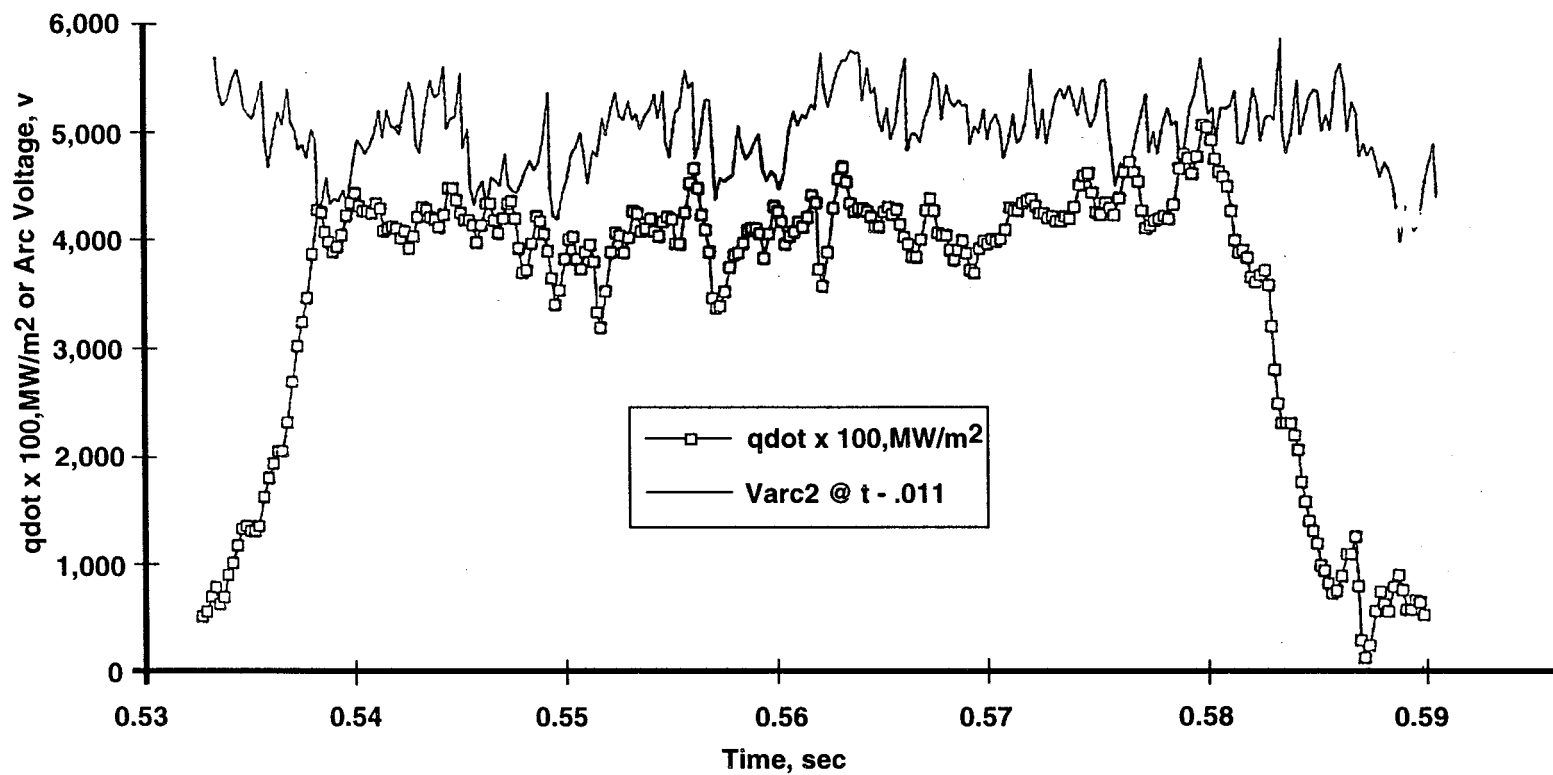


Figure 41. Velocity profile in the multi-arc configuration.

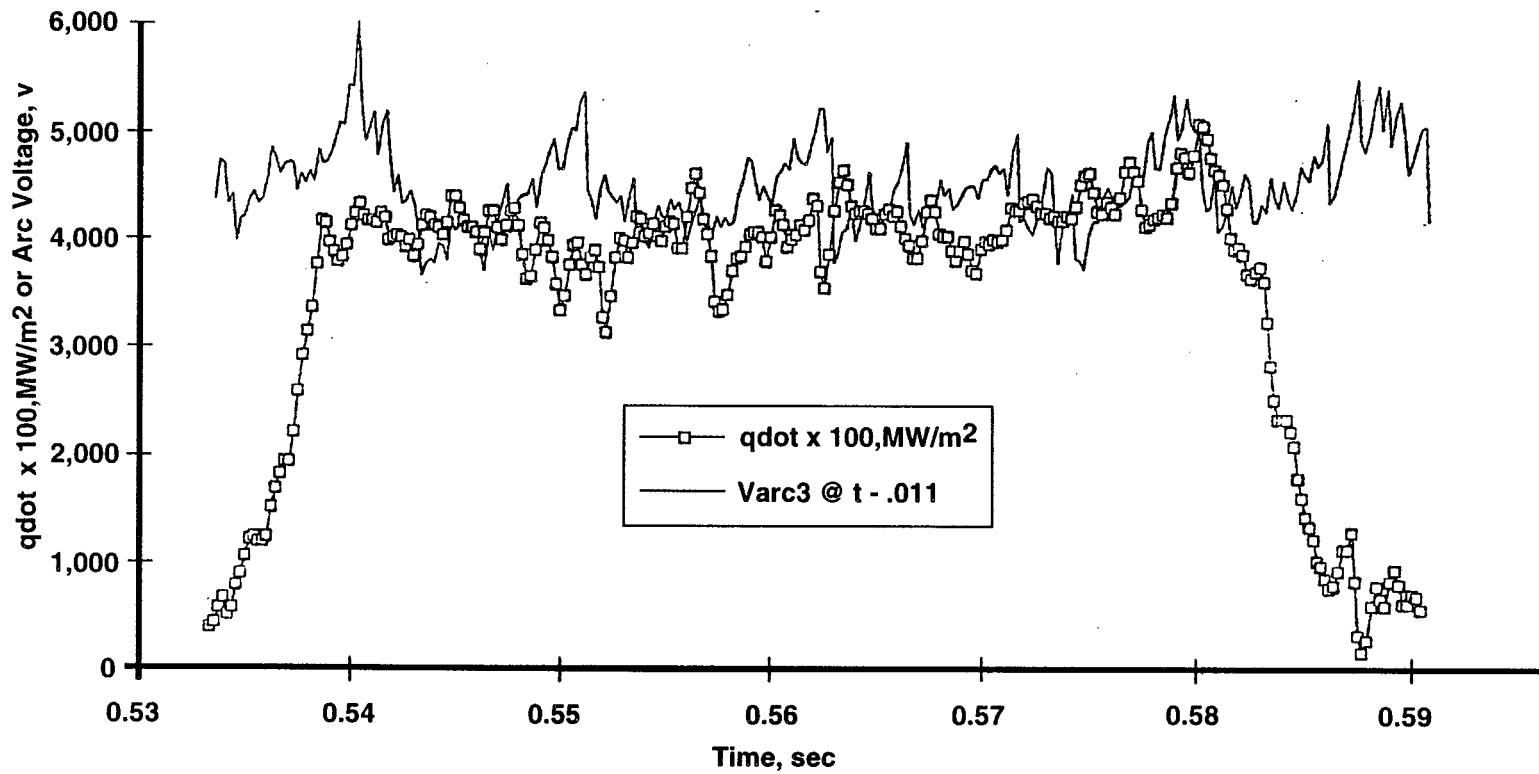




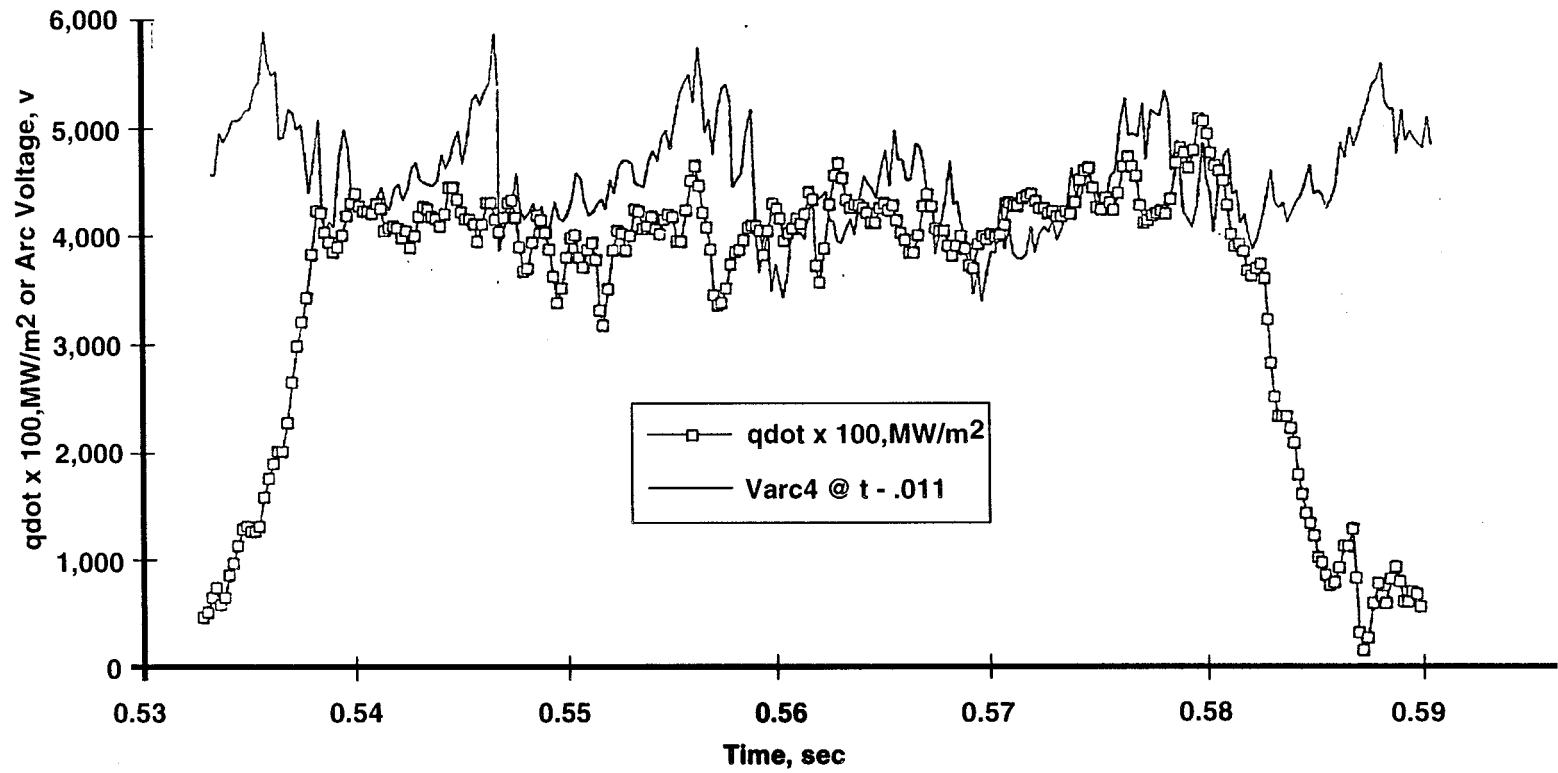
a. Run 1513, forward sweep, Varc 1 fluctuations  
Figure 42. Heat flux/voltage comparison.



b. Run 1513, forward sweep, Varc 2 fluctuations  
Figure 42. Continued.



c. Run 1513, forward sweep, Varc 3 fluctuations  
Figure 42. Continued.



d. Run 1513, forward sweep, Varc 4 fluctuations  
Figure 42. Concluded.

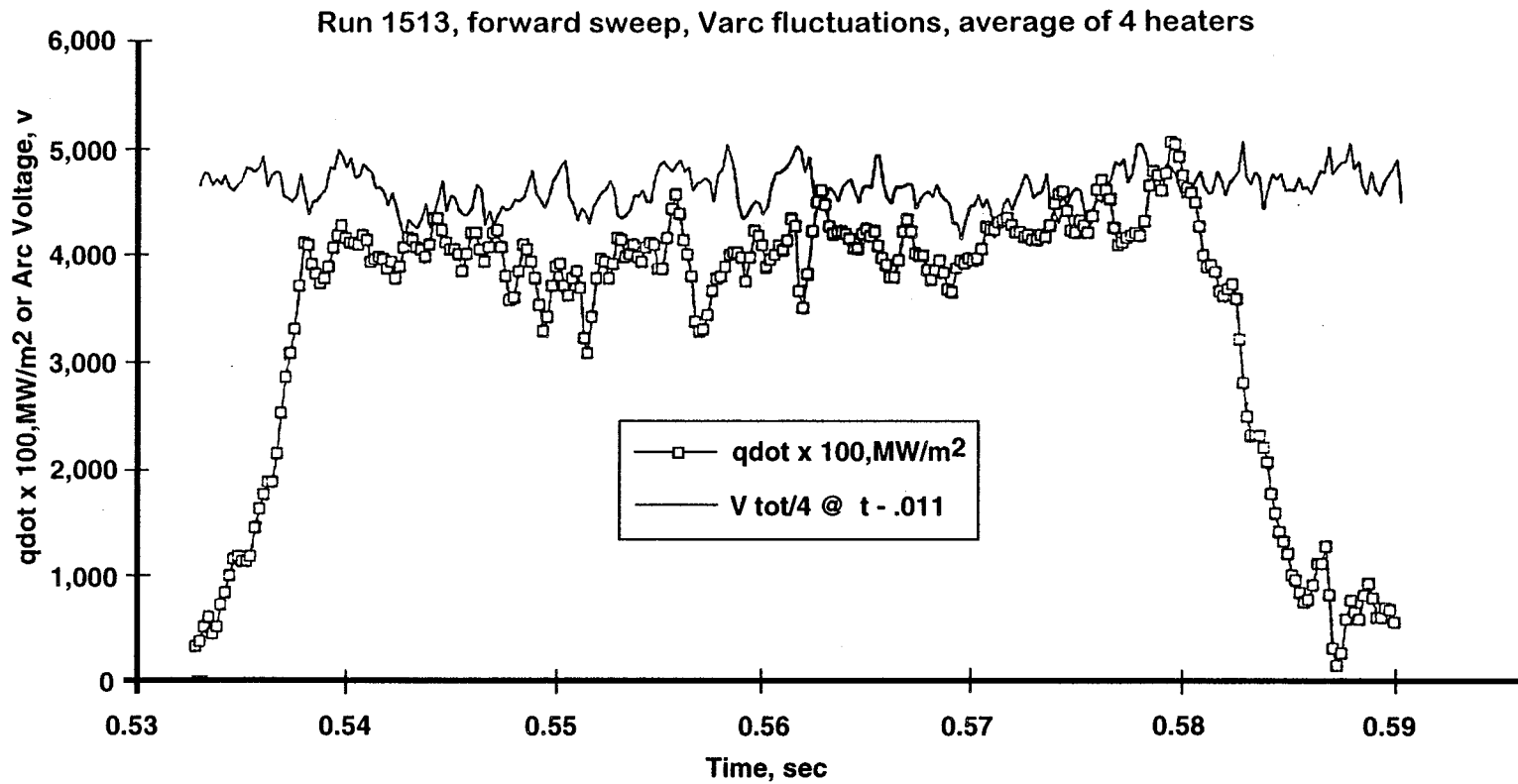


Figure 43. Heat flux/total voltage comparison.

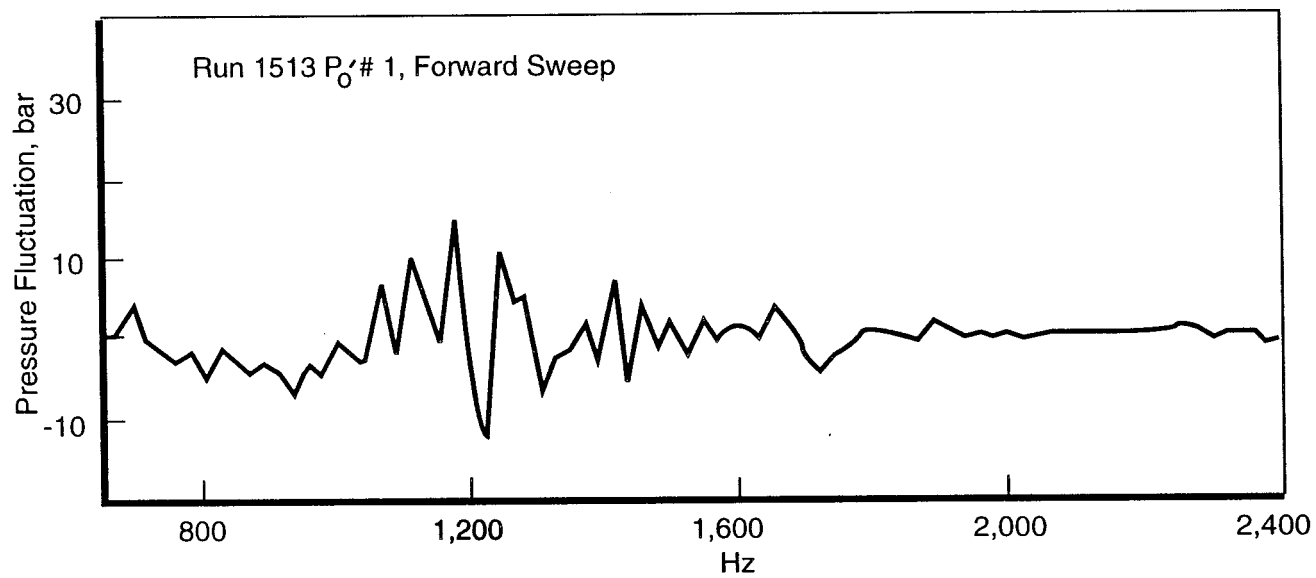


Figure 44. Fast fourier transform of pitot pressure data.

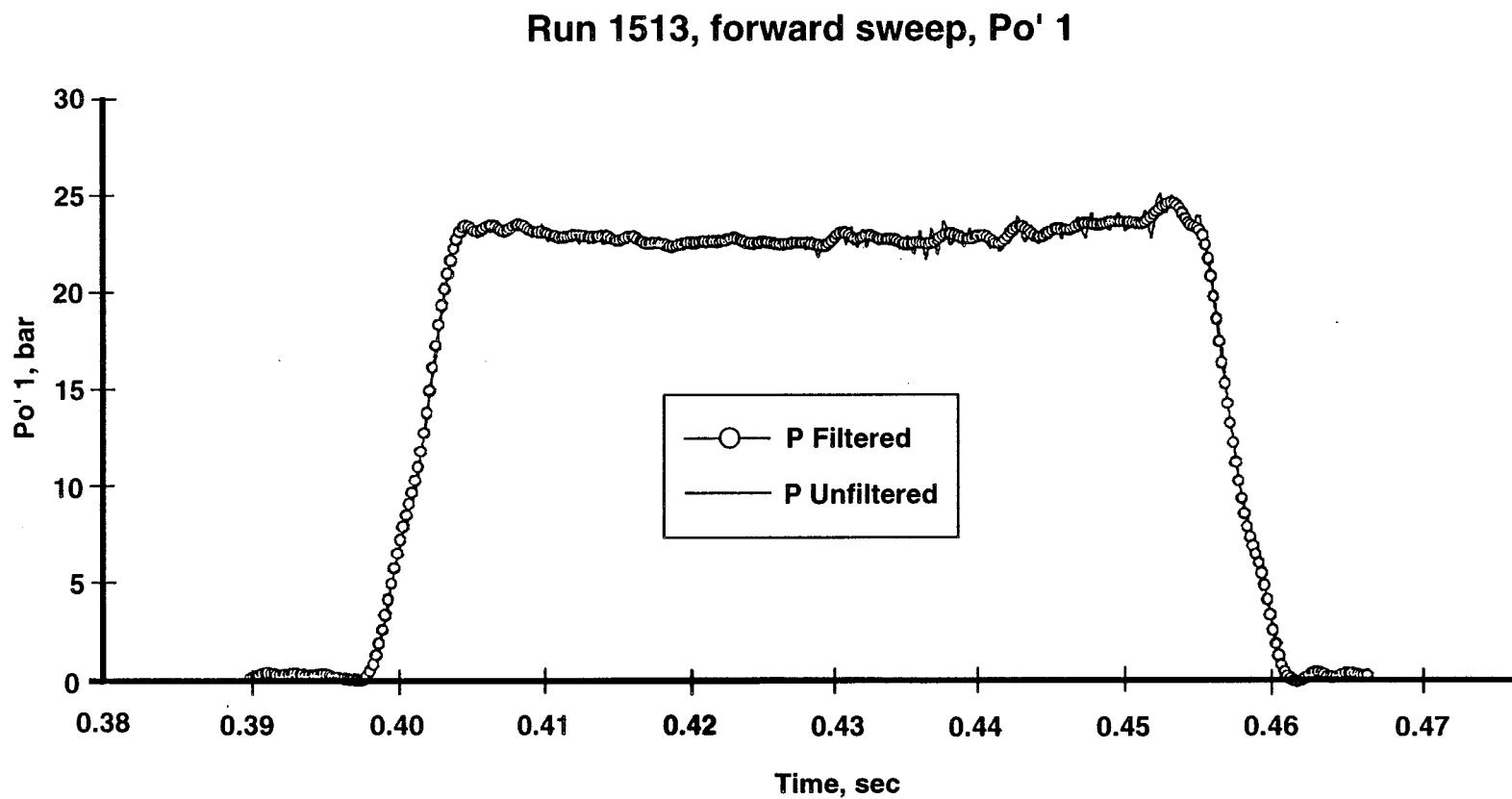
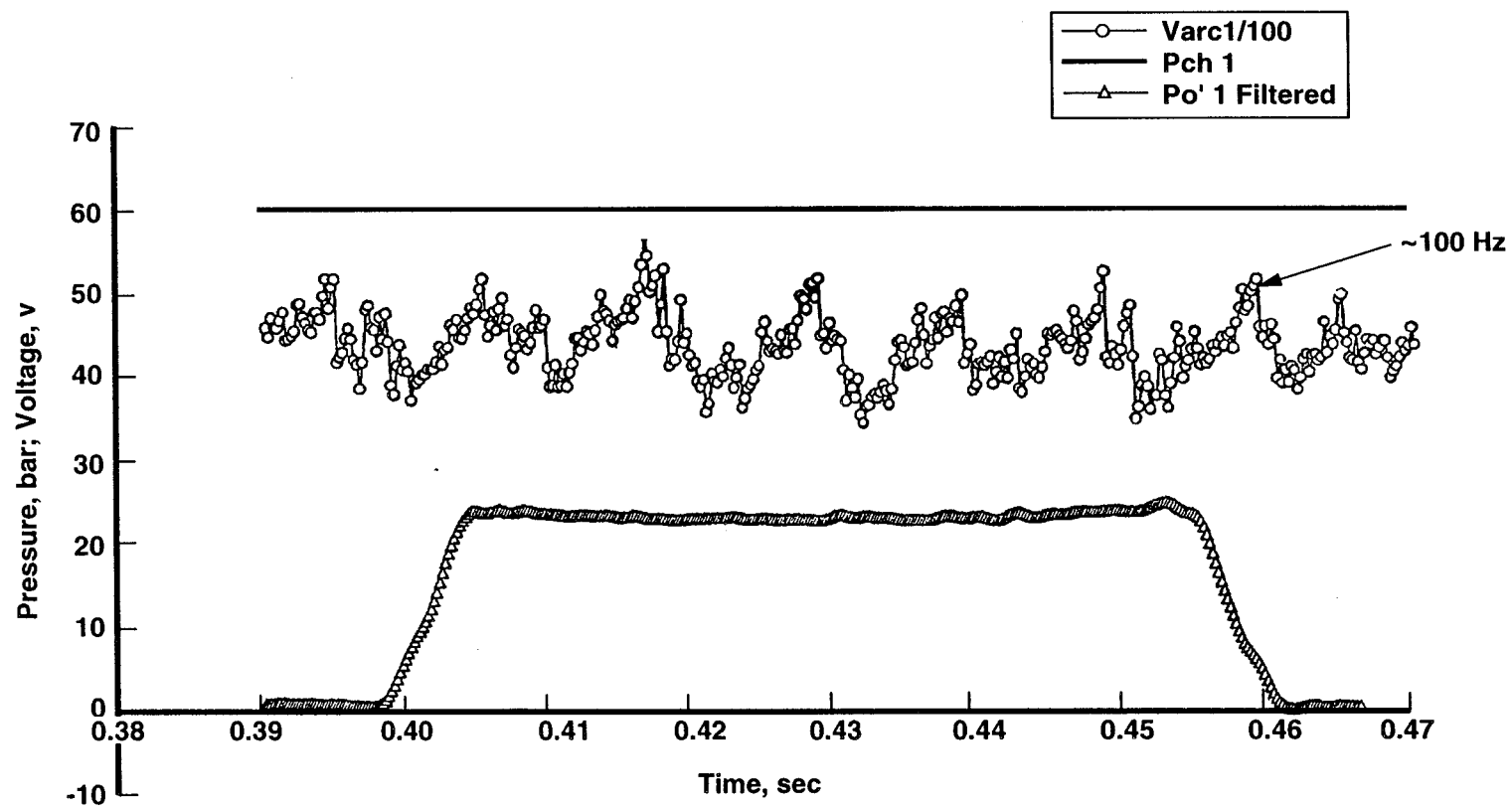


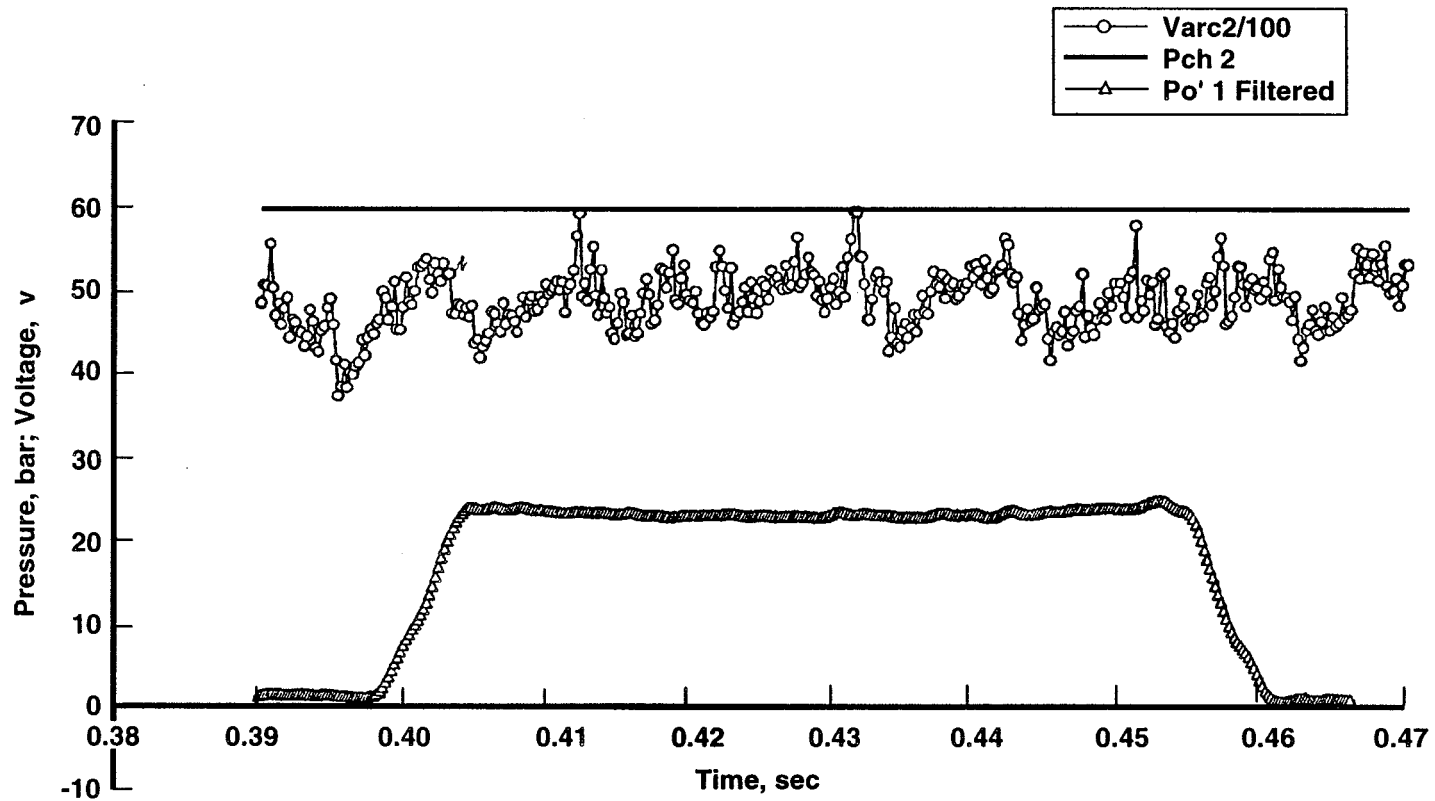
Figure 45. Pitot pressure signal processing.



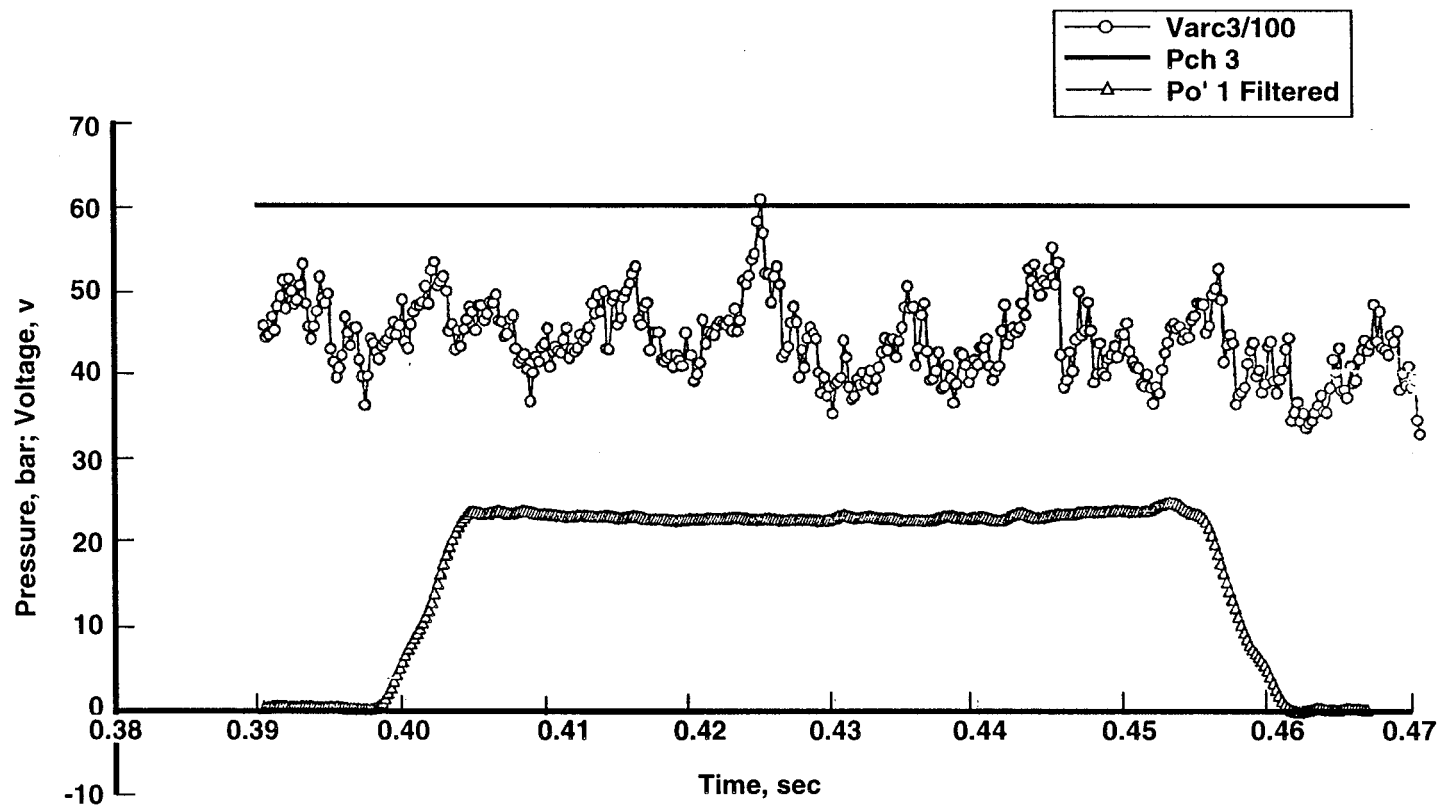
a. Run 1513, forward sweep, Varc 1

Figure 46. Pitot pressure/arc voltage comparison.

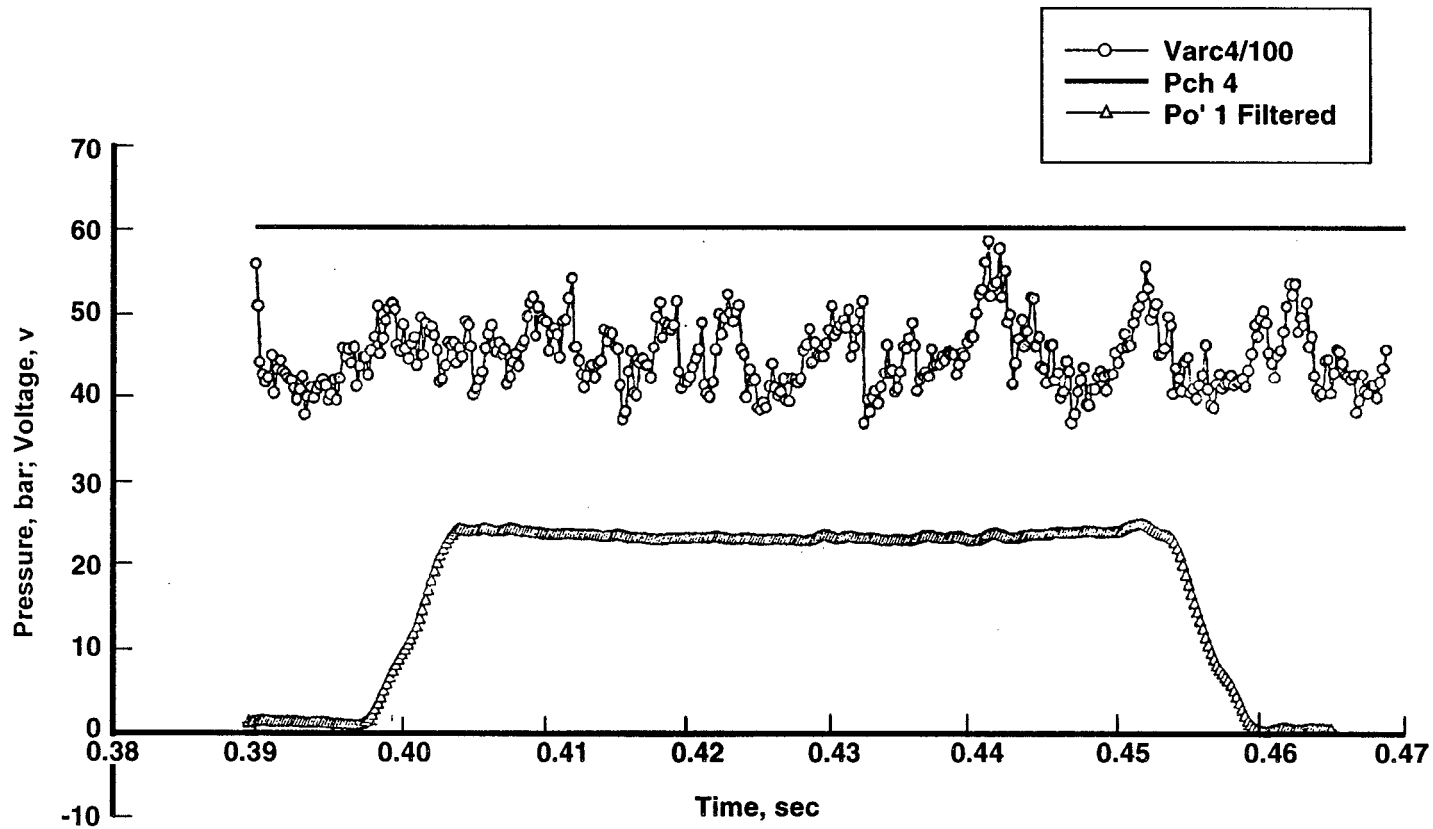




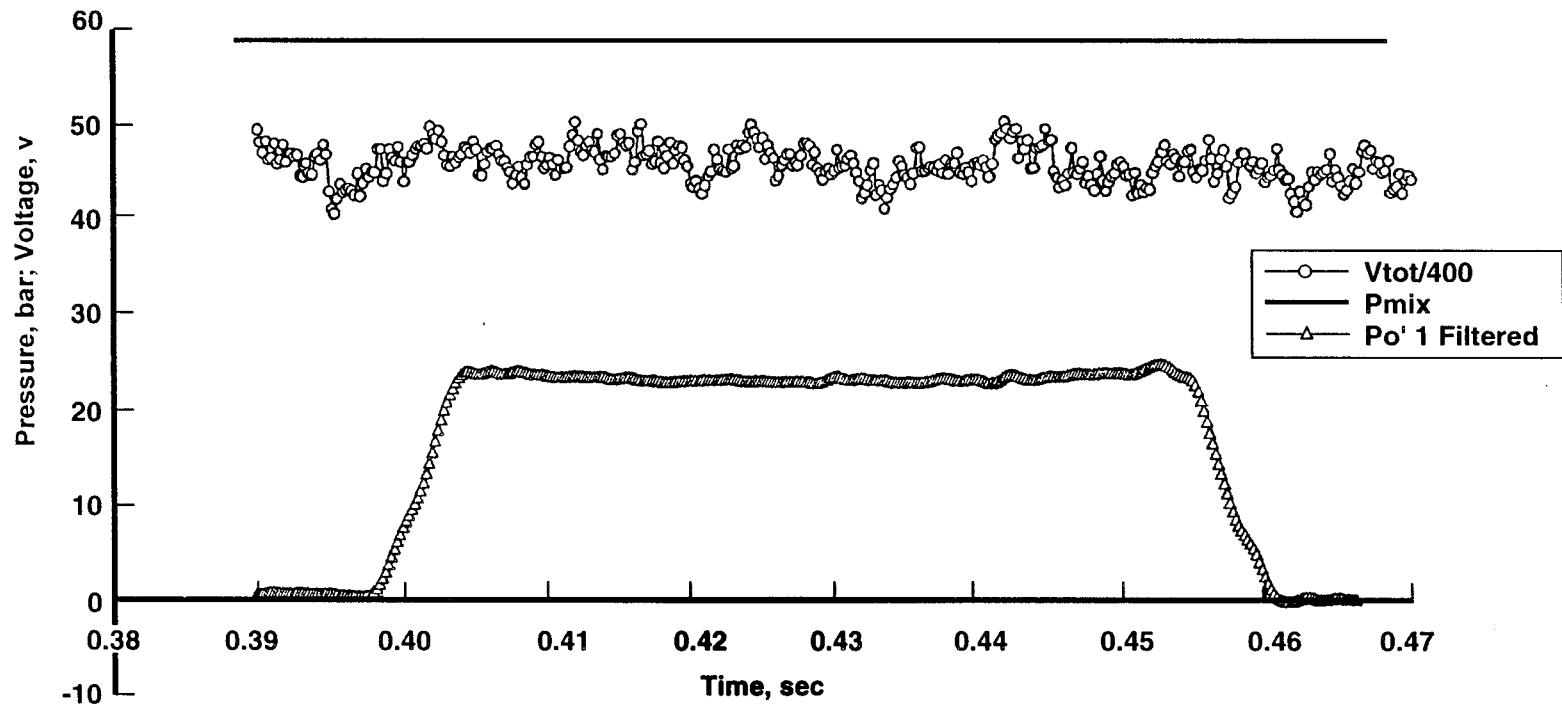
b. Run 1513, forward sweep, Varc 2  
Figure 46. Continued.



c. Run 1513, forward sweep, Varc 3  
Figure 46. Continued.



d. Run 1513 forward sweep, Varc 4  
Figure 46. Continued.



e. Run 1513, forward sweep, average of 4 heaters  
Figure 46. Concluded.

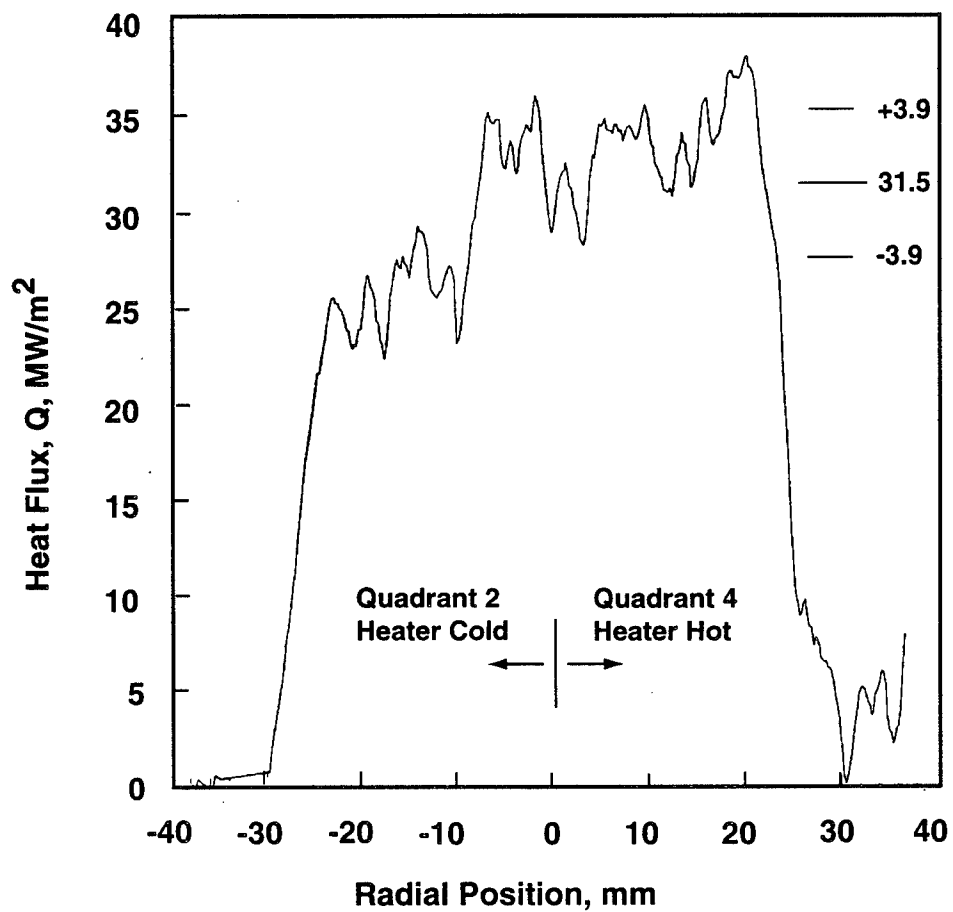


Figure 47. Heat flux profile, Run 1509, forward sweep; heaters 1,3,4 hot, heater 2 cold.

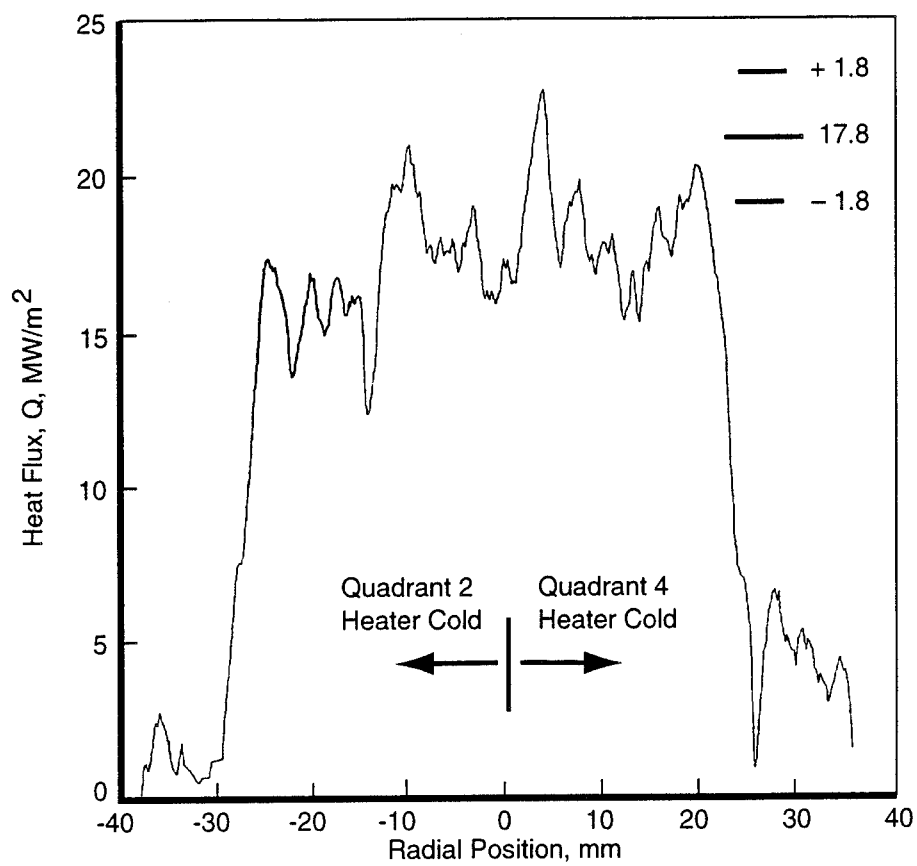
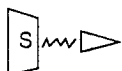


Figure 48. Heat flux profile, Run 1512, forward sweep; heaters 1,3 hot, heaters 2,4 cold.

**Table 1. HP Instrumentation**

PARAMETER	SCHEMATIC	HEATER ACQUISITION	
		SLOW SPEED	FAST SPEED
Uarc		Uarc	Uarc
Iarc		Iarc	
PL		PI	PI1
P SAT		P SAT	
Water Flow		DP (x5)	P SAT
		DT (x5)	
Air Flow		DPair	Tair
		Pair	
P Pitot 1 to 2			P Pitot (x2)
Heat Flux			TC flux
			Flux



= Amplifier/insulator SIEMENS



= Amplifier ANALOG DEVICES



= Voltage, current sensor (Hall principle)

Table 2. JP-200 Instrumentation

PARAMETER	SCHEMATIC	HEATER ACQUISITION		
		SLOW SPEED	FAST SPEED	
Uarc 1to 2		Uarc 1 to 3	Uarc 1 to 3	
Uarc 4		Uarc 4		
Iarc 1to 4		Iarc 1 to 4	Uarc 4	
PI 1 to 4		PI (x4)		
P SAT		P SAT	PI (x4)	
		DP (x12)		
Water Flow		DT (x12)	Tair (x4)	
Air Flow		DPair (x4)		
		Tair (x4)	Pair (x4)	
		Pair (x4)		
P Pitot 1 to 2		P Pitot (x2)	TC flux	
Heat Flux		Flux		
= Amplifier ANALOG DEVICES				
= Amplifier/insulator SIEMENS				



**Table 3. Surface Area of HP and JP-200 Arc Heater Facilities Exposed to Hot Gas****HP** (Swirl Chamber Surface Area Not Included, Since Cooling Losses are Minimal)

Anode =  $706.86 \text{ cm}^2$

Cathode (including pressure station) =  $827.17 \text{ cm}^2$

Nozzle (upstream of the throat) =  $98.46 \text{ cm}^2$

Ratio of Nozzle Surface Area to Total Area = 0.0603

**JP-200** (Swirl Chamber Surface Area Not Included, Since Cooling Losses are Minimal)

4 Anodes =  $3588.96 \text{ cm}^2$

4 Cathodes =  $2858.84 \text{ cm}^2$

Manifold =  $648.92 \text{ cm}^2$

Nozzle (upstream of the throat, including pressure station) =  $127.11 \text{ cm}^2$

Ratio of Nozzle of Surface Area to Total Area = 0.0176

**Table 4. HP and JP-200 Run Matrix**

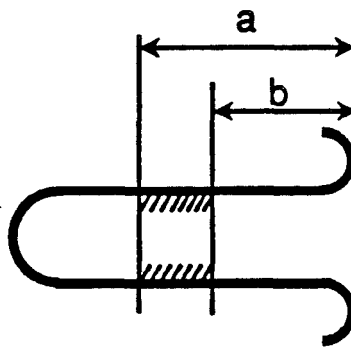
Date	Run Number	Run Time, sec	Number of Heaters Energized	Throat Area, $\text{cm}^2$	Heater Air Flow, gm/sec	Cold Air Flow, gm/sec	Reduced Enthalpy, H/RT	Configuration
6-2-94	<b>HP</b> 429	29	1	1.25	440	---	74	Single Heater
6-3-94	430*	30	1	1.25	440	---	74	Single Heater
6-6-94	431	30	1	1.25	440	---	74	Single Heater
6-6-94	432	30	1	1.25	440	---	74	Single Heater
10-4-94	<b>JP-200</b> 1506	12.4	4	5.0	$4 \times 440$	---	74	4 Heaters Hot
10-5-94	1507	35	4	5.0	$4 \times 440$	---	74	4 Heaters Hot
10-6-94	1508	15	3	5.0	$3 \times 440$	810	48	Cold Air Heater 2
10-10-94	1509*	35	3	5.0	$3 \times 440$	810	48	Cold Air Heater 2
10-11-94	1510	15	2	5.0	$2 \times 440$	$2 \times 905$	27	Cold Air Heaters 2 & 4
10-11-94	1511	15	2	5.0	$2 \times 440$	$2 \times 905$	27	Cold Air Heaters 2 & 4
10-12-94	1512*	40	2	5.0	$2 \times 440$	$2 \times 905$	27	Cold Air Heaters 2 & 4
10-12-94	1513*	40	4	5.0	$4 \times 440$	---	74	4 Heaters Hot
10-13-94	1514	15	2	2.5	$2 \times 440$	---	74	Heaters 2 & 4 Inactive
10-14-94	1515*	40	2	2.5	$2 \times 440$	---	74	Heaters 2 & 4 Inactive
10-18-94	1516	14.9	2	2.5	$2 \times 440$	---	74	Heaters 2 & 4 Removed
10-19-94	1517*	40	2	2.5	$2 \times 440$	---	74	Heaters 2 & 4 Removed

\* Matrix Runs

Note: All runs to be performed at a nominal chamber pressure of 60 bar.

**Table 5. Anode Arc Attachment Locations**

Heater Number	a, mm	b, mm
Heater 1	195	145
Heater 2	210	160
Heater 3	195	140
Heater 4	185	130
HP Heater	200	160

**Table 6. Electrode Mass Loss**

Electrode	Diameter, mm	Electrode Total Run Time, sec	Total Mass Loss, gm	Mass Loss Rate, gm/hr	Mass Loss Ratio Cu to Air, ppm
<b>JP-200, HEATER 1</b>					
Upstream (Anode)	68	394	68	621	391
Downstream (Cathode)	35	394	89	813	512
<b>HP</b>					
Upstream (Anode)	50	192	61	1,144	722
Downstream (Cathode)	35	192	59	1,106	698

**Table 7. Analysis of Individual Arc Heater Performance (at end of cathode)**

Run No.	Heater No.	P. I., bar	ṁ, gm/sec	I, amp	V, volts	Power, kw	Loss, kw	H/RT <sub>o</sub>	Efficiency, percent	Percent Dev. From Mean Value, Each Run			
										ṁ	PWR	H/RT <sub>o</sub>	EFF
430	HP	61.8	440	1079	4747	5122	2403 <sup>H</sup>	82.48	53.08 <sup>L</sup>	-	-	-	-
(22 to 29 sec)													
431	HP	61.9 <sup>H</sup>	440	1074	4794	5148	2400	83.32	53.38	-	-	-	-
(22 to 29 sec)													
1507	JP200												
	1	61.39	444.5	1080	4572	4938	2223.5	81.56	54.97	0.5	-0.4	-2.4	-1.6
	2	61.48	445.8	1112 <sup>H</sup>	4675	5199	2338.5	85.49	55.02	0.8	4.9	2.3	-1.5
	3	61.40	439.3	1078	4593	4951	2154.5	84.85	56.48	-0.6	-0.1	1.6	1.1
	4	61.79	439.0	1073	4414	4736	2031.5	82.24	57.11 <sup>H</sup>	-0.7	-4.4	-1.5	2.2
(30 to 36 sec)													
Run Total			1768.6			19824	8748.0						
Run Average		61.52	442.2	1086	4564	4956	2187	83.53*	55.87*				
1513	1	60.31	440.6	1078	4425	4770	2069.1	81.85	56.62	-0.3	-1.5	-0.6	0.6
	2	60.40	447.1 <sup>H</sup>	1087	4800 <sup>H</sup>	5218 <sup>H</sup>	2332.3	85.97 <sup>H</sup>	55.30	1.2	7.8	4.4	-1.7
	3	60.54	438.8	1078	4425	4770	2077.2	81.94	56.45	-0.7	-1.5	-0.5	0.3
	4	60.81	440.4	1078	4275	4608	1990.1 <sup>L</sup>	79.49	56.81	-0.3	-4.8	-3.4	1.0
(31 to 37 sec)													
Run Total			1766.9			19366	8468.7						
Run Average		60.52	441.7	1080	4481	4842	2117	82.33*	56.27*				
1509	1	60.02	442.5	1080	4500	4860	2190.5	80.62	54.93	1.7	4.0	2.3	0.2
	3	59.88	442.5	1065 <sup>L</sup>	4400	4686	2148.2	76.84 <sup>L</sup>	54.16	1.7	0.3	-2.5	-1.2
	4	60.32	420 <sup>L</sup>	1065 <sup>L</sup>	4200 <sup>L</sup>	4473 <sup>L</sup>	1992.7	79.00	55.45	-3.4	-4.3	0.2	1.1
(30 to 36 sec)													
Run Total			1305.0			14019	6331.4						
Run Average		60.07	435.0	1070	4367	4673	2110.5	78.81*	54.84*				
1512	1	58.49	429.1	1077	4230	4556	2021.2	79.02	55.64	-1.9	-0.7	1.0	-0.2
	3	58.42 <sup>L</sup>	445.9	1069	4320	4618	2037.6	77.49	55.88	1.9	0.7	-1.0	0.2
(36.42 sec)													
Run Total			875.0			9174	4058.8						
Run Average		58.46	437.5	1073	4275	4587	2029.4	78.23*	55.75*				
1515	1	58.60	440.5	1081	4375	4729	2059.1	80.98	56.46	0.3	-0.3	-0.4	0.1
	3	58.70	438.0	1069	4450	4757	2078.0	81.68	56.32	-0.3	0.3	0.4	-0.1
(31 to 37 sec)													
Run Total			878.5			9486	4137.1						
Run Average		58.65	439.3	1075	4413	4743	2068.6	81.33*	56.39*				
1517	1	59.1	442.1	1076	4475	4815	2088.7	82.32	56.62	0.3	1.2	1.4	0.6
	3	58.9	439.6	1069	4400	4704	2069.9	80.10	56.00	-0.3	-1.2	-1.4	-0.6
(31 to 37 sec)													
Run Total			881.7			9519	4158.6						
Run Average		59.9	440.9	1073	4438	4760	2079.3	81.21*	56.31*				
<b>ALL RUNS</b>													
Heater Avg		60.22	439.8	1077	4477	4824	2142.4	81.38	55.61				
H-High		61.9	447.1	1112	4800	5218	2403	85.97	57.11				
% Above Avg		2.79	1.66	3.25	7.21	8.17	12.16	5.64	2.70				
L-Low		58.42	420	1065	4200	4473	1990.1	76.84	53.08				
% Below Avg		-2.99	-4.50	-1.11	-6.19	-7.28	-7.11	-5.58	-4.55				

\* Based on total power, total loss, and total mass flow for all arc heaters for that run.

**Table 8. JP200 Manifold Performance and Thermal Efficiency**

Run No.	JP200 Configuration of Arc Heaters	P. Sat, bar	H/RT <sub>0</sub> Aero.	Thermal Loss, kw		Manifold Loss, percent of Total	PWR to Gas Before Manifold, kw	Manifold Loss, percent of PWR to Gas Before Manifold	H/RT <sub>0</sub> Calorimetric		Enthalpy Reduction Caused by Manifold (and other related hardware), percent
				Total	Manifold (and other related hardware)				Total	Manifold Excluded (and other related hardware)	
1507	1, 2, 3, 4 Hot	60.4	80	9797	607.6	6.2	11,076	5.5	76.00	80.37	5.4
1513	1, 2, 3, 4 Hot	59.4	76	9685	781.5	8.1	10,897	7.2	73.58	79.20	7.1
1509	1, 3, 4 Hot 2 Cold	58.9	47.5	7142	523.5	7.3	7688	6.8	45.15	48.28	6.5
1512	1, 3 Hot 2, 4 Cold	57.1	27	4510	303.3	6.7	5115	5.9	25.92	27.34	5.2
1515	1, 3 Hot 2, 4 Inactive	58.1	72	5094	590.9 (649.8)*	11.6 (12.8)*	5349	11.0 (12.1)*	67.49	76.04 (76.89)*	11.2 (12.2)*
1517	1, 3 Hot 2, 4 Removed	58.7	73	5022	554.6 (563.2)**	11.0 (11.2)**	5360	10.3 (10.5)**	68.78	76.77 (76.90)**	10.4 (10.6)**

Note: Nominal condition for arc heaters operating hot for all runs: I = 1,075 amp and mass flow = 440 gm/sec

\* Thermal losses from arc heaters 2 and 4 included with manifold loss.

\*\* Thermal losses from flanges 2 and 4 included with manifold loss.

**Table 9. Nozzle Performance and Thermal Efficiency**

Run No.	Configuration of Arc Heaters	P. Sat, bar	H/RT <sub>o</sub> Aero.	Thermal Loss, kw		Nozzle Loss, percent of Total	PWR to Gas Before Nozzle, kw	Manifold Loss, percent of PWR to Gas Before Nozzle	H/RT <sub>o</sub> Calorimetric		Enthalpy Reduction Caused by Nozzle, percent
				Total	Nozzle				Total	Nozzle Loss Excluded	
HP											
429	1,446 amp	65.1	97	3591	248	6.9	3236	7.7	90.05	97.19	7.3
430	1,079 amp	61.5	82	2599	196	7.5	2719	7.2	76.82	82.48	6.9
431	1,074 amp	61.6	83	2595	195	7.5	2748	7.1	77.69	83.32	6.8
432	863 amp	58.7	73	2093	177	8.5	2443	7.2	69.26	74.35	6.8
JP200											
1507	1, 2, 3, 4 Hot	60.4	80	9797	441	4.5	10,468	4.2	76.00	79.17	4.0
1513	1, 2, 3, 4 Hot	59.4	76	9685	434.5	4.5	10,116	4.3	73.58	76.71	4.1
1509	1, 3, 4 Hot 2 Cold Air	58.9	47.5	7142	284.8	4.0	7162	4.0	45.15	46.85	3.6
1512	1, 3 Hot 2, 4 Cold Air	57.1	27	4510	153.5	3.4	4818	3.2	25.92	26.64	2.7
1515	1, 3 Hot 2, 4 Inactive	58.1	72	5094	307	6.0	4699	6.5	67.49	71.93	6.2
1517	1, 3 Hot 2, 4 Removed	58.7	73	5022	300	6.0	4797	6.3	68.78	73.10	5.9

Note: Nominal condition for arc heaters operating hot for all runs, except where noted: I = 1075 amp (except HP Runs 429 and 432) and mass flow = 440 gm/sec.

**Table 10. Overall Arc Heater Performance and Thermal Loss**

Run No.	Configuration of Arc Heaters  HP	P. Sat, bar	H/RT <sub>0</sub> Aero.	H/RT <sub>0</sub> Calorimetric				ṁ Total, gm/sec	Total Power, kw	Losses, kw			
				Total	Nozzle Loss Excluded	Manifold Loss, Excluded (and other related hardware)	Nozzle and Manifold Loss Excluded (and other related hardware)			Total	Nozzle	Manifold	Other Related Hardware
429	1,446 amp	65.1	97	90.05	97.19	---	---	441	6578	3591	248	---	---
430	1,079 amp	61.5	82	76.82	82.48	---	---	440	5122	2599	196	---	---
431	1,074 amp	61.6	83	77.69	83.32	---	---	440	5148	2595	195	---	---
432	863 amp	58.7	73	69.26	74.35	---	---	441	4359	2093	177	---	---
<b>JP200</b>													
1507	1, 2, 3, 4 Hot	60.4	80	76.00	79.17	80.37	83.53	1,769	19,824	9797	441	607.6	---
1513	1, 2, 3, 4 Hot	59.4	76	73.58	76.71	79.20	82.33	1,767	19,366	9685	434.5	781.5	---
1509	1, 3, 4 Hot 2 Cold Air	58.9	47.5	45.15	46.85	48.28	49.99	2,123	14,019	7142	284.8	523.5	---
1512	1, 3 Hot 2, 4 Cold Air	57.1	27	25.92	26.64	27.34	28.07	2,702	9174	4510	153.5	303.3	---
1515	1, 3 Hot 2, 4 Inactive	58.1	72	67.49	71.93	76.04 (76.89)	80.47 (81.33)	878.5	9486	5094	307	590.9	--- (58.9)
1517	1, 3 Hot 2, 4 Removed	58.7	73	68.78	73.10	76.66 (76.90)	81.09 (81.21)	881.7	9519	5022	300	554.6	--- (8.6)

Note: Nominal condition for arc heaters operating hot: I = 1075 amp (except HP Runs 429 and 432) and mass flow = 440 gm/sec.

## Appendix A. Surface Area of HP and JP200 Arc Heater Facilities Exposed to Hot Gas

**HP** (Swirl Chamber Surface Area Not Included, Since Cooling Losses are Minimal)

$$\text{ANODE} \quad A_s \cong \pi DL = \pi (5 \text{ cm}) (45 \text{ cm}) = 706.86 \text{ cm}^2$$

$$\text{CATHODE} \quad A_s \cong \pi (3.5) (68.9) + \pi (7) (1.2) + \frac{\pi}{4} (7^2 - 3.5^2) + \frac{\pi}{4} (8.2^2 - 7^2) = 827.17 \text{ cm}^2$$

(Incl Pr. Sta.)

$$\text{NOZZLE} \quad A_s \cong \pi (8.2) (0.2) + \frac{\pi}{4} (8.2^2 - 4^2) + \pi (3.9) (1) + \pi (3.75) (1) + \pi (3.4) (1) + \pi (2.8) (1) + \pi (2.0) (1) + \pi (1.3) (0.8) = 98.46 \text{ cm}^2$$

(Upstr. of Throat)

$$\text{Ratio of Nozzle Surface Area to Total Area} = \frac{98.46}{706.86 + 827.17 + 98.46} = 0.0603$$

### JP200

$$4 \text{ ANODES} \quad A_s \cong 4\pi (6.8) (42) = 897.24 \text{ cm}^2 \times 4 = 3588.96 \text{ cm}^2$$

$$4 \text{ CATHODES} \quad A_s \cong 4\pi (3.5) (65) = 714.71 \text{ cm}^2 \times 4 = 2858.84 \text{ cm}^2$$

$$\text{MANIFOLD} \quad A_s \cong A_{\text{SPHERE}} + 4A_{\text{A.H. TUBES}} + A_{\text{NOZ TUBE}} = 80.25 + 427.06 + 141.61 = 648.92 \text{ cm}^2$$

$$\text{NOZZLE} \quad A_s \cong \frac{\text{PR. MEAS. STA.}}{\text{NOZZLE INSIDE SURFACE CONTOUR TO THROAT}} \pi (5.8) (3.8) + \pi (5.65) (1) + \pi (4.75) (1) + \pi (3.5) (1) + \pi (2.75) (1) + \pi (2.53) (0.7) = 127.11 \text{ cm}^2$$

(Upstr. of Throat, Incl Pr. Sta.)

$$\text{Ratio of Nozzle Surface Area to Total Area} = \frac{127.11}{3588.96 + 2858.84 + 648.92 + 127.11} = 0.0176$$

NOTE: Surface area of swirl chamber(s) not included because thermal losses are negligible.